

Department of Electronic and Electrical Engineering
University College London
Torrington Place, London

Doctor of Philosophy Thesis

July 1993

**An Investigation of the Second Order Nonlinear Optical Properties
of Self Assembled Organic Materials.**

M. Stanley

Optical and Display Science Division
DRA
St Andrews Road, Malvern, Worcestershire

Supervisors

Prof. G. Parry
Dr S.E. Day
Dr D.G. McDonnell

Crown Copyright © 1993

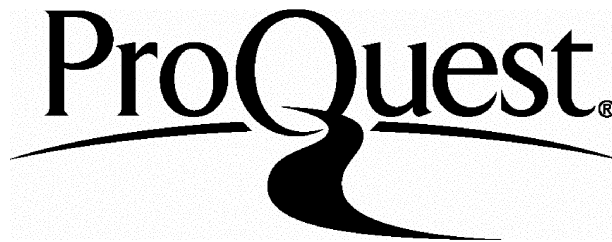
ProQuest Number: 10046185

All rights reserved

INFORMATION TO ALL USERS

The quality of this reproduction is dependent upon the quality of the copy submitted.

In the unlikely event that the author did not send a complete manuscript and there are missing pages, these will be noted. Also, if material had to be removed, a note will indicate the deletion.



ProQuest 10046185

Published by ProQuest LLC(2016). Copyright of the Dissertation is held by the Author.

All rights reserved.

This work is protected against unauthorized copying under Title 17, United States Code.
Microform Edition © ProQuest LLC.

ProQuest LLC
789 East Eisenhower Parkway
P.O. Box 1346
Ann Arbor, MI 48106-1346

To Alexandria Catherine Victoria

*This is the patent age of new inventions
For killing bodies and for saving souls,
All propagated with the best intentions'*

BYRON

Acknowledgements.

This work was completed at the Defence Research Agency (DRA), formally Royal Signals and Radar Establishment (RSRE), Malvern, funded by the Ministry of Defence.

This thesis could not have been completed without the help of many people. The guidance, insight and support of my supervisors to this project, Drs Sally Day and Damien McDonnell at DRA, and Prof. Gareth Parry at UCL, have been invaluable. The combination of their expertise in the fields of physics, chemistry and electronic engineering was essential, and demonstrated how the different subjects can combine and produce something greater than their constituent parts.

Many colleagues at DRA have contributed in some way to this work. I would like to acknowledge Dr Cliff Jones, Mike Towler, Dr Amarjit Samra, and Marie Anderson for their discussions and assistance. I must also mention Bob Bannister, and his team, for the cell fabrication.

I wish to thank Mike Griffith and Mike Worboys at GEC Marconi Research centre for their collaborative work with the polymers, and to Merck (UK) for the synthesis of the polymer, and supply of other liquid crystals and data used in this study. Thanks must also go to Prof. John Goodby, and Simon Cross at Hull University for the synthesis of new ferroelectric liquid crystal materials, and Dr David Dunmur at Sheffield University for his molecular modelling expertise and facilities.

Finally, I must also thank Victoria and Alexandria for their tremendous support, understanding, and patience whilst this thesis was written. I also thank my parents for the support and encouragement they have given me throughout my long education.

Abstract.

The requirement for efficient second order nonlinear optical materials which are easy to produce and form into devices is paramount for the successful application of nonlinear optics to optical data storage and signal processing. Mature technologies such as lithium niobate are making some progress, but the immense potential of organic materials cannot be ignored. The combination of molecular engineering and computer modelling can control many parameters including absorption bands, dipole moments and conformation of the molecules, to tailor their properties to the specific application.

The self assembling nature of liquid crystal materials has been suggested to offer several potential benefits for the engineering of useful bulk materials for nonlinear optical applications. This thesis describes the investigation and exploitation of self assembled systems, both in monomeric and polymeric form, for such applications, and critically assesses the benefits and drawbacks of these materials. Two cases have been studied in detail. The first is the use of poled nematic liquid crystal side chain polymers for use in electro-optic and second harmonic generation applications. The second is an investigation into the inherent non-centrosymmetry of chiral smectic C liquid crystals.

The potential advantages of using poled liquid crystal side chain polymers over amorphous polymers are a five times theoretical improvement in the nonlinear coefficient and improved orientational stability to increase device lifetimes. In practice the improvement in the nonlinear coefficient was found not significant, and cross-linking the polymer whilst being poled offers even greater stability, even at elevated temperatures. A simple experiment was developed to monitor the electro-optic coefficient of the polymer as the material was poled. The form of the response gave insight into the reorientation mechanisms both in poling and relaxing after the poling field had been removed.

Ferroelectric liquid crystals can form a noncentrosymmetric symmetry if their helix can be suppressed using surface alignments and/or electric fields. The second order nonlinear coefficients of these materials have been measured using second harmonic generation (SHG). Commercial materials had relatively small coefficients, but molecular engineering has developed new materials with improved nonlinear coefficients by over one order of magnitude, and is continuing to improve. A standard material was used to investigate a number of potential device alignment configurations. SHG was also used to measure liquid crystal material parameters for application in display technologies.

Presentations

Stanley M., McDonnell D.G. & Day S.E., "Dynamics of Poling Side chain Polymers.", poster presentation at *Organic Materials for Nonlinear Optics III*, Oxford, UK, 1992. and to be published in the book of proceedings of the same name.

Stanley M., "Dynamics of Poling Side chain Polymers.", invited oral presentaion, Rank Prize Funds symposium on *Polymeric Materials for Electro-Optic Devices*, Broadway, UK, 1992.

Stanley M., "Non-Display Applications of Liquid Crystals.", invited oral presentation, SIRA forum on *Liquid Crystal Component Applications*, Chislehurst, UK, 1993.

Contents.

Acknowledgements	i
Abstract	ii
Presentations	iii
Contents	iii
1. Introduction	1
1.1 Applications of Nonlinear Optical Materials	3
1.2 Liquid Crystal Materials and Devices	5
1.3 Polymers and Polymeric Liquid Crystals	10
1.4 Overview of the Dissertation	11
2. Nonlinear Optical Materials for Electro-Optic Devices	13
2.1 Theory of Nonlinear Optics	13
2.2 Nonlinear Optics at the Molecular Level	15
2.3 From Molecules to Bulk properties	18
2.4 Classes of Bulk Nonlinear Organic Materials	19
2.4.1 Organic Crystals	19
2.4.2 Side Chain Polymers and Poling	20
2.4.3 Liquid Crystals	21
2.4.4 Langmuir Blodgett Films	22
2.5 The Linear Electro-Optic Effect	22
2.6 Second Harmonic Generation	24
2.7 Requirements for Nonlinear Optical Materials	24
2.8 Nonlinear Optical Devices	25
2.8.1 Through-Plane Electro-Optic Modulators	26
2.8.2 Transverse Electro-Optic Modulators	27
2.8.3 Bandwidth Limits	28
2.8.4 Waveguide Modulators	29
2.8.5 Waveguides in Poled Polymers	29
2.8.6 Second Harmonic Generation Devices	30
2.9 Comparison of Materials for Electro-Optic and SHG Applications	31
2.9.1 Inorganic Crystals	31
2.9.2 Organic Crystals	34
2.9.3 Poled Polymeric Materials	35
2.9.4 Ferroelectric Liquid Crystals	36

2.10	Overview of Electro-Optic Materials	36
3	Dynamics of Poling Side Chain Polymers	38
3.1	Measurement of the Induced Nonlinear Optical Coefficients	38
3.2	Preparation and Evaluation of Nonlinear Optical Copolymers	40
3.3	Preparation of Thin Film Samples	41
3.4	Measurement of Refractive Indices	42
3.4.1	Measurement of n_o	42
3.4.2	Measurement of n_e	44
3.5	The Experimental Arrangement to Measure r_{eff}	45
3.6	Dispersion in the Electro-Optic Coefficient	46
3.7	Dependence of the Nonlinear Coefficient with Poling Voltage	48
3.8	Dynamic Measurements of Poling Processes	49
3.9	Results of the Dynamic Measurements	51
3.9.1	Above the Glass Transition	52
3.9.2	Below the Glass Transition	53
3.9.3	Poling Efficiency as a Function of Temperature	54
3.10	Fast Amplitude Modulation	55
3.11	Limitations to the Poling Technique	56
3.12	Discussions and further Work	58
4	Second Harmonic Generation in Liquid Crystals	60
4.1	Theory of Second harmonic Generation	61
4.1.1	Phase Matching	62
4.2	Materials and Device Requirements for Second harmonic Generation	64
4.3	Ferroelectric Liquid Crystals	65
4.3.1	Alignment of Ferroelectric Liquid Crystals	68
4.4	Experiment to Measure SHG Efficiency	71
4.4.1	Maker Fringes	74
4.5	Investigation of a Standard FLC Material- SCE13(*)	77
4.5.1	Analysis of SCE13* using Homeotropic Cells	77
4.5.2	Molecular and Bulk Coefficients	82
4.6	Novel FLC Materials with High Nonlinear Optical Coefficients	88
4.7	Evaluation of New Materials for Nonlinear Optics	90
5	Using SHG as a Measurement Probe in Liquid Crystals	95
5.1	Measurement of Smectic C Refractive Indices and Optical Baxiality	96
5.2	The Critical Unwinding Field and the B_3 elastic Constant	101

5.2.1	Derivation of the Critical Unwinding Field	101
5.2.2	Measurement of the Critical Unwinding Field	103
5.3	Uniform Planar FLC Alignment Geometry	107
5.4	Other SHG Probe Measurements	112
5.5	Summary of Chapter	113
6.	Conclusions	115
	References	118
	Appendices	
	A	122
	B	127

1 Introduction.

The increasing amount of information which is transferred from person to person, or computer to computer via a communications network has stretched electronics to its limits. The use of digital technology to send audio and video information is increasingly becoming limited by the bandwidth of the electrical networks which carry the information, typically 10^9 Hz maximum. As an example, the new high definition TV (HDTV) systems based upon images composed of more than 10^6 pixels with colour and grey scale approach this limit with a single channel of information. The need for a new communications media has driven developments in optical fibre technology to meet such requirements. Success in developing ultra-low loss optical fibres together with compact and efficient light sources and detectors has resulted in rapid application of this new technology.

Optical communication systems offer several advantages over electronic systems. The high frequency of light radiation offers a potential carrier bandwidth of greater than 10^{12} Hz. This increases the network capacity by several orders of magnitude, giving spare capacity for future requirements. The low losses achieved in optical fibres has surpassed electrical cables and even coaxial cable, allowing larger distances between source and detection, with fewer amplification stages. Their robustness and immunity from atmospheric and electrical interference has reduced maintenance, making them very competitive in cost to alternative technologies. More recent developments such as soliton propagation over huge distances and wavelength multiplexing to increase capacity mean that optical communication systems will continue to develop in the future.

Simple passive optical devices such as Y splitters have been fabricated in optical fibres and waveguides. However, there is a requirement for discrete, active optical elements for efficient optical switching and modulation. These devices include amplitude, polarisation and phase modulators, active optical routing, polarisation control and frequency shifting. The materials used in these devices require efficient nonlinear optical properties which can modify the temporal and spatial properties of the light at very high speeds using electrical or optical control. Nonlinear optical materials offer a number of properties which can enhance the capability of both optical communication systems and data storage devices. Materials currently available to produce these devices are inadequate in several respects, including: voltage of operation, bandwidth, insertion losses, cost and processability. An ideal specification is shown in table 1.1. One of the most successful materials used to date is the inorganic crystal lithium niobate (LiNbO_3) [Donaldson, (1991)]. Despite much development, it is still far from ideal for large scale exploitation of opto-electronics, which is clearly demonstrated by its limited applications.

This thesis will address the development and assessment of materials for two applications: electro-optic modulation, and second harmonic generation devices. These two applications can have quite different material requirements for optimum device performance. Electro-optical modulators are useful for a wide range of applications: they are required in waveguide geometries for communication systems, and are also needed in large configurations as fast shutters. These may modulate light

emerging from lasers, or provide ways of gating radiation incident on detectors. If the shutter is subdivided into pixels, then the device forms a spatial light modulator for use in parallel optical signal processing.

Nonlinear coefficient magnitude: $> 50 \text{ pmV}^{-1}$

$V_{\pi}L < 1 \text{ Vcm}$

Modulation bandwidth: $> 100 \text{ GHz}$

Propagation loss: $< 0.2 \text{ dBcm}^{-1}$

Unit cost: $< \text{£}100$

Compatible with other optical materials

Chemical and temperature stability

Low dielectric and optical coefficients

Table 1.1

An optical modulator is a simple way of superimposing information onto the light to be carried to the detector. Information may be carried in a light wave as amplitude, frequency or phase modulation. Modulators can be used in a range of device geometries, although the most common is optical waveguides for communications systems. It is desirable to carry out signal routing and processing whilst the information is in its optical form, thus removing the requirement to convert the optical signal to an electrical form and then back again. This would allow the optical system to be used to its full potential. Electrical signal routing and processing is becoming the slow link in modern communication systems due to the bandwidth limitation of electronic devices (a few GHz). Using optical signal processing devices, all-optical communication systems may offer increased bandwidth capabilities, lower power consumption and higher signal interference immunity. At present such devices are controlled electrically, however direct optical control may be needed in the future. Controlling light with light requires a new class of nonlinear material with large third order nonlinear effects [Shen, (1984)]. Such devices would remove the need for electronic control and its associated limitations, and allow the optical system to work at its full potential. However, this thesis will be limited to second order nonlinear optical effects and devices, and their application to current problems and requirements.

The second property of nonlinear optical materials was studied is that of frequency doubling, or second harmonic generation (SHG). Nonlinear optical processes within the material can be used to convert light to different frequencies. The most efficient conversion is to a wavelength half of the value of the incident light, with conversion efficiencies over 80% having been demonstrated [Ou et al., (1992)] in the laboratory. The inorganic material potassium dihydrogen phosphate (KDP) is often used in commercial devices with efficiencies of about 30%. This material has many problems including the

fact that it is hydroscopic, and so degrades when exposed to any form of humidity, and is very difficult to grow and polish in high quality. Consequently it is expensive.

There are several applications for devices which change the wavelength of light. The first is to obtain small and efficient laser sources in the blue and green region of the visible spectrum. Efficiencies greater than 30% are required with materials which are cheap, stable and easy to produce. This would enhance the very large market of optical data storage (e.g. compact disks), which has a limit to the density of information which can be stored which is related to the size of the spot which the reading (and writing) laser beam can be focused. Since the size of the focused spot of light is proportional to the wavelength of light, halving the wavelength would allow up to four times the information to be stored on the same size disk. Such frequency doubling devices would need to compliment semiconductor lasers in terms of size, cost and optical power requirements. For example a device would be mm^2 in size, cost less than £100 and only require 10's of mW of optical power for efficient conversion. This goal is the primary motivation for many electronics companies to research into nonlinear optics, as existing commercial materials do not meet this specification.

Second harmonic generation is not the only frequency shift which can be achieved, as optical parametric oscillators (OPO's) can shift radiation to shorter wavelengths (e.g. far IR to near IR) and provide tunability of laser radiation over a wide wavelength range e.g. from 0.65 to 3.0 μm [Milomi & Eberly, (1988)] using a combination of temperature tuning of the crystal and different pump wavelengths. Nonlinear optical devices can produce sources of laser radiation at wavelengths where no known lasers operate. These have applications in many fields of research, particularly spectroscopy. Replacement of delicate dye lasers with solid state lasers may take tuneable lasers out of research laboratories and into commercial applications.

There are many other applications for nonlinear optical materials: optical logic devices for optical computing, optical information storage, optical limiters and tuneable filters. Many of these can be fulfilled by present nonlinear optical materials, although better materials would be desirable. However, there are applications such as dynamic holography to produce 3-d displays which need better materials before such devices can be developed. Second harmonic generation has also potential as a selective optical probe to measure material and device properties. This has initially been reported in the field of liquid crystals [Shen, (1984)], but may also have application in other fields. There will be, of course, many other applications which have yet to emerge from this rapidly expanding field of nonlinear optics.

1.1 Nonlinear Optical Materials.

New materials are required which are simple and cheap to produce and process into devices, have large nonlinear coefficients, and low optical losses. These problems are common to almost all crystalline optical materials. There is considerable interest in developing new classes of materials, e.g.

polymers, for nonlinear optical applications which will allow simplified device preparation and improve the performance, resulting in more versatile devices and lower operating voltages.

The inorganic crystal lithium niobate has already been discussed as the benchmark for electro-optic applications. The material has been developed over many years, and has been used successfully to produce modulators and waveguide devices. It has an electro-optic coefficient $r_{33} = 30.8 \text{ pmV}^{-1}$, or more significantly, requires a voltage of approximately 1 kV to induce a π phase delay. Much of the development work in this material has involved research into the crystal growth to reduce the time and cost involved in producing crystals of the required optical quality. However, this material is still inadequate for large scale implementation of optical signal processing, due to the difficulty and expense of growing and polishing crystalline materials, and its moderate nonlinear coefficients.

An alternative inorganic crystalline material for nonlinear optics is based upon the material gallium arsenide (GaAs) [Dorn et al., (1992)]. The principal attraction of this material is that a complete optical system can be defined within one material - the semiconductor laser source, waveguides, electro-optic modulators, and photo detectors. The processing technology is available, as are large high quality crystals, and there would be few additional processing steps to produce such an 'optical chip'. However, this system would operate at wavelengths of approximately $0.8 \mu\text{m}$, and so is unsuitable for application in telecommunication systems, which centre on wavelengths of 1.3 and $1.5 \mu\text{m}$ for minimum optical fibre losses. Other limitations of this material are that it has a relatively low nonlinear coefficient, and the proximity of a large absorption band close to the operating wavelength results in high optical losses for such a system.

Organic materials are also promising materials for successful exploitation of nonlinear optics. Molecular engineering has resulted in molecules with very large molecular nonlinear coefficients (hyperpolarisabilities) [Tweig et al, (1983)]. This has been achieved using the highly delocalised π electron systems found particularly with carbon-carbon double bonds and benzene ring structures, and has led to enhancement of the nonlinear optical coefficients compared to inorganic crystals such as lithium niobate. These molecules have been developed into bulk nonlinear optical materials as both crystals and polymers. Organic crystals have exhibited very large nonlinear coefficients [Beirlein, (1990)], but are difficult to grow and process, and it can be difficult to predict which crystal structure they will adopt. Many crystal symmetries obey inversion symmetry and do not exhibit bulk second order nonlinear optical effects. The simplicity of processing and flexibility in molecular design has made polymeric materials very attractive for nonlinear optics. There are a number of additional benefits of organic systems which include:

- i. limited tuning of refractive indices through established molecular engineering processes.
- ii. potential ease of fabrication using polymeric materials in place of large crystals.
- iii. compatibility with both semiconductor materials and glass optical fibres.

In combination these benefits are beginning to challenge the established inorganic materials such as lithium niobate in waveguide applications. However, despite their great potential, there are still many problems with organic materials which have to be solved before these materials will become widely

available for applications, including improved efficiency, reducing optical losses, and cost. A particular problem associated with polymeric materials is the requirement to induce the required noncentrosymmetry by poling. This induced order slowly relaxes over a period of days or months, reducing the induced nonlinear coefficient and the overall efficiency of potential devices. This problem may be overcome by the natural self ordering ability of liquid crystal materials, and will be investigated in this study.

1.2 Liquid Crystal Materials and Devices.

Liquid crystal devices are probably the most successful type of electro-optic device yet developed. Here, the nonlinear effect originates in the reorientation of molecules in response to applied electric fields. The optical effect is very large - a phase delay of π radians can be induced with less than 5 volts. However, the effects are relatively slow, with an upper bandwidth limit of approximately 10^6 Hz, and so have limited use in optical communications systems. They have, however, found great success as low power, light weight, low cost displays and shutters for low complexity applications such as calculators and watches, and are now being developed for complex i.e. video and computer displays. They are also one of the most promising technologies for spatial light modulators for optical signal processing applications. Technically, they are not nonlinear optical materials in the same sense as lithium niobate, although they can exhibit a refractive index which is dependent on an applied electric or magnetic field. This is due to the molecules reorienting themselves in response to the applied field as opposed to electrons or ions being polarised within the material.

Liquid crystal materials are anisotropic materials which exhibit a combination of liquid and crystalline properties. Materials which form these phases generally comprise of long thin rod-shaped molecules (mesogens), which as they are cooled may spontaneously condense into one, two or three dimensionally ordered systems, reducing the degree of disorder in each case. It is envisaged that these materials may have beneficial properties in the field of nonlinear optics, based upon two points. The first is the high level of understanding and control in molecular engineering of such anisotropic molecules, and the second is their ability to spontaneously form well-ordered bulk materials without the need for growing crystalline materials. The asymmetric nature of the nonlinear optical molecules is very similar to that of liquid crystal molecules, suggesting that the combination of large nonlinear coefficients and liquid crystallinity is achievable in the same molecules. In addition, some of the liquid crystal molecules spontaneously form noncentrosymmetric alignments, particularly the chiral smectic C phase, thus achieving the requirement of noncentrosymmetry in liquid crystal materials for second order nonlinear optics.

The simplest phase is the nematic phase, where on average molecules order along a single axis called the director \mathbf{n} , as shown in figure 1.1a. This phase is symmetric because molecules have no preference as to which way they align - up or down. The molecular co-ordinate system used to describe

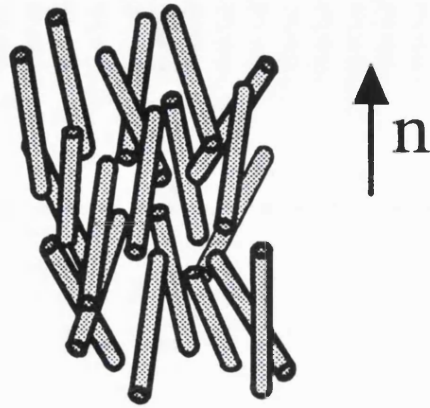


Figure 1.1a Nematic phase, N .

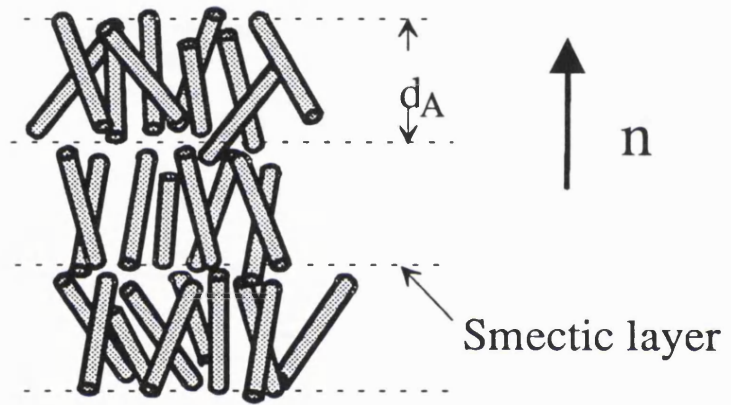


Figure 1.1b Smectic A phase, S_A .

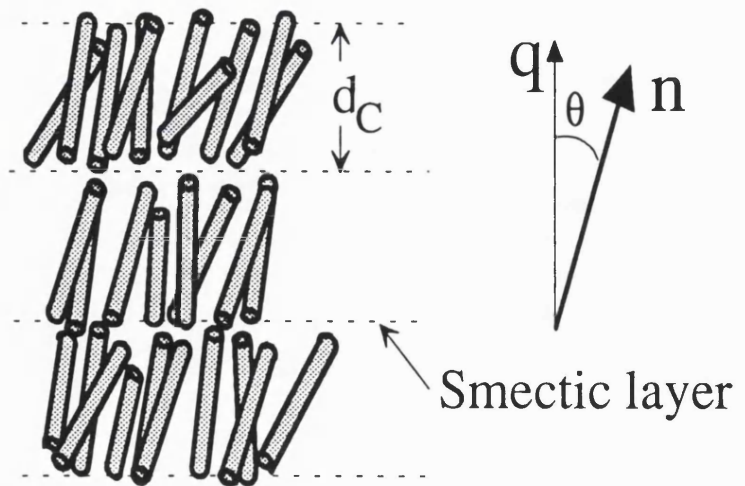


Figure 1.1c Smectic C phase, S_C .

Figure 1.1. Liquid Crystal Phases.

the nematic phase (x,y,z) is related to the laboratory frame (X,Y,Z) by the Euler angles (ξ, η, ζ) is shown in figure 1.2. An order parameter S describes the probability of the long axis of a molecule aligning with the director. This can be described as the statistical average of the Legendre polynomial P_2

$$S = \langle P_2 \rangle = \frac{1}{2} \langle 3\cos^2\xi - 1 \rangle \quad 1.1$$

where ξ is the angle between the long molecular axis and the director, and P_2 is averaged over all possible molecular directions.

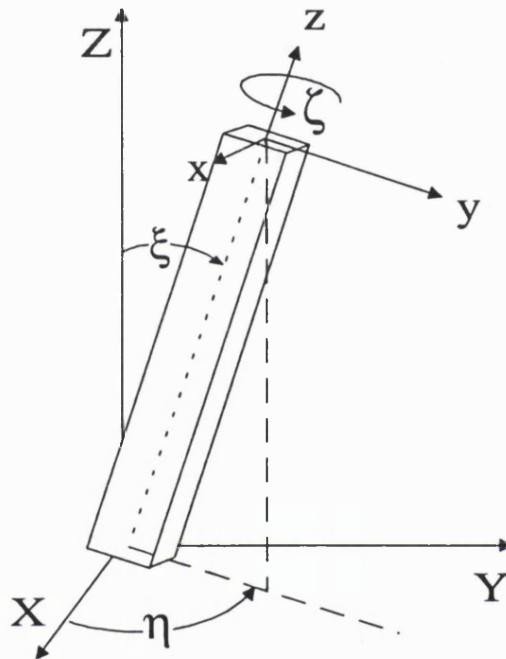


Figure 1.2. The nematic co-ordinate system.

To make an electro-optic device using nematic liquid crystal, a thin layer of nematic material is sandwiched between two sheets of glass, as shown in figure 1.3.

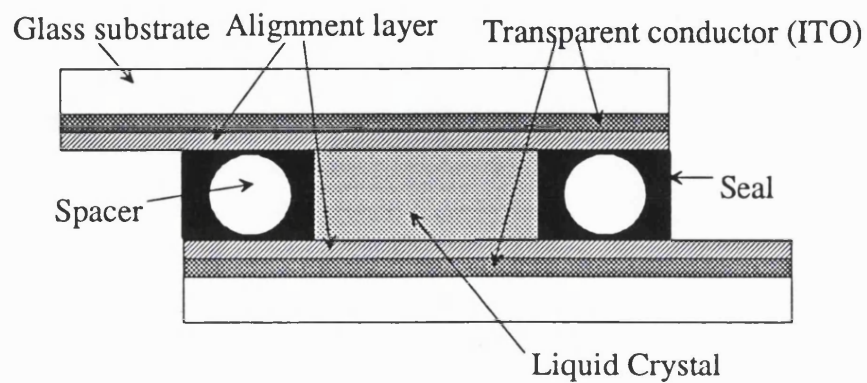


Figure 1.3 A typical liquid crystal cell structure.

A typical layer spacing of $2 \rightarrow 10 \mu\text{m}$ is achieved by using beads or fibre spacers of the required size in the adhesive seal. The alignment of the liquid crystal is obtained by treating the inner surfaces of the glass cell with a range of aligning layers. Homeotropic alignment layers such as chrome complex or lecithin induce the molecules to orient perpendicular to the cell, whereas rubbed polymers, for example polyimide, align the molecules with the director in the plane of the cell and parallel to the direction of the rub, as shown in figure 1.4.

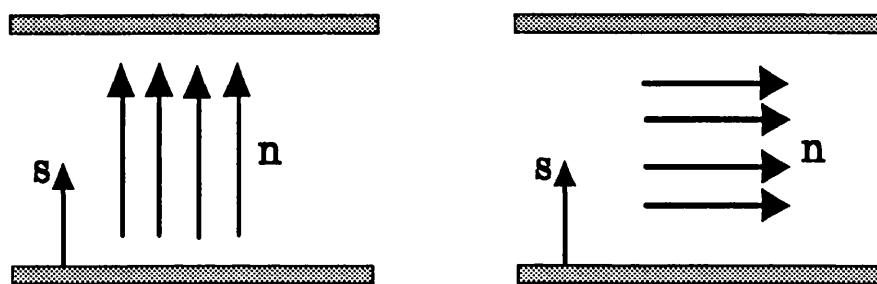


Figure 1.4 a, Homeotropic alignment

b, Planar alignment.

The most common type of liquid crystal device is the twisted nematic, used in simple displays such as watches and calculators. In this device the rubbed polyimide layers are arranged perpendicularly to induce a 90° twist in the alignment structure. This twisted structure guides light so that it emerges with its polarisation rotated by 90° to the incident light. Application of a voltage destroys the twisted structure and the guiding is lost. When used between parallel or perpendicular polarisers with one polariser aligned with the rubbing direction, this device forms an optical shutter with a response time of a few milliseconds (ms) and a drive voltage of a few volts. Its low cost, light weight and low power consumption have proved very successful for a wide range of display and optical shutter applications.

Some materials, when cooled below the nematic phase, exhibit a number of smectic phases. These form layers of molecules as well as having axial ordering. The smectic A (S_A) phase is shown in figure 1.1b with a layer spacing d_A . Of more interest to nonlinear optics is the smectic C (S_C) phase shown in figure 1.1c where the director tends to tilt away from the layer normal. The tilted smectic C phase has twofold rotation symmetry about an axis perpendicular to the plane containing the director and the layer normal (c_2 axis), and reflection symmetry in that same plane. This symmetry obeys inversion symmetry. However, the introduction of a chiral centre on the molecule removes the reflection in the mirror plane symmetry and as a consequence, permits the presence of a permanent transverse dipole moment along the c_2 axis. This is able to sum, and so produce a spontaneous polarisation across the bulk material. The c_2 axis of the molecule possesses noncentrosymmetry, and so may exhibit second order nonlinear effects. The symmetry requirements for second order nonlinear optics will be discussed in more detail in chapter 2. An example of a chiral molecule is shown in figure 1.5 and has four different groups attached to a carbon atom.

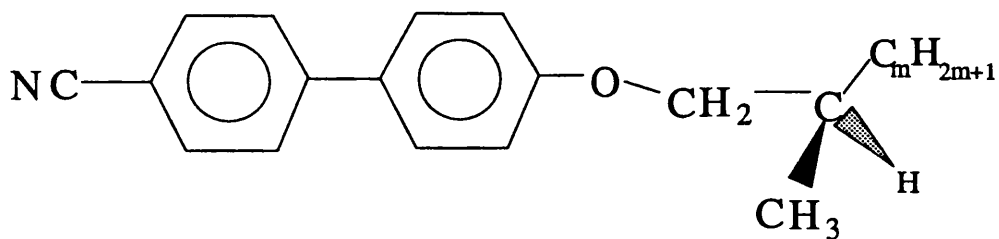


Figure 1.5 A chiral molecule.

In a bulk material the chirality of the molecules encourages the molecules to pack in a helical form, destroying the noncentrosymmetric symmetry, as shown in figure 1.6a. This can be overcome using strong surface alignments in thin films to pin the molecules at the surface and force the helix to unwind. Alternatively, an electric field can be used to align their permanent dipole moments and unwind the helix. Mixing molecules which have opposite twisting power, or introducing a second chiral centre into a molecule to counteract the twisting power, can also result in bulk materials with noncentrosymmetric symmetry.

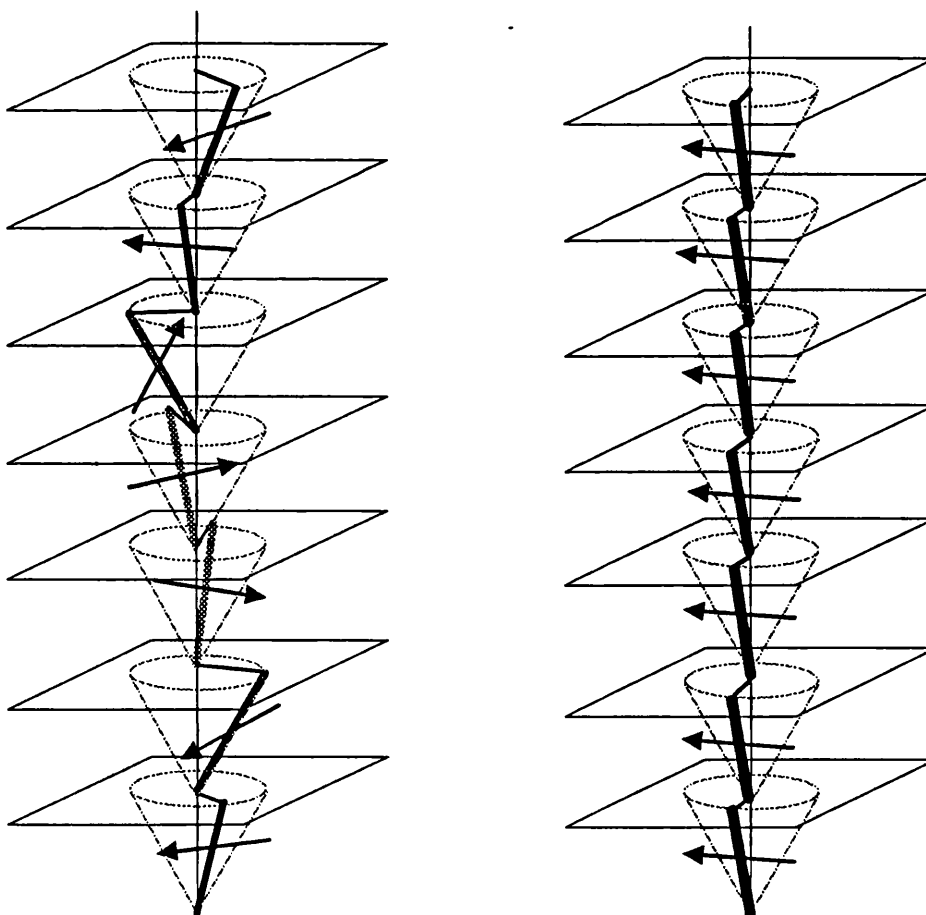


Figure 1.6a. The chiral smectic C helical structure, b. an unwound ferroelectric smectic C structure.

1.3 Polymers and Polymeric Liquid Crystals.

In the monomer form, liquid crystal materials have limited applications in devices due to the necessary requirement to contain them and maintain the molecular alignment. For nonlinear optical applications, once the material has been aligned then it will not be re-oriented, and so could be locked in place. One way of achieving this is to cool the material further into a crystalline phase, or alternatively a polymeric form of the material could be used. Polymeric materials offer similar advantages to liquid crystals in that they can be composed of asymmetric mesogenic units with control of the chemical structure by established molecular engineering techniques, and that also these mesogenic groups can spontaneously form aligned phases. They offer the additional benefits of being self supporting, easily processable, robust and low cost.

Polymeric materials are composed of long chains of identical molecular groups linked by flexible spacer chains. They can be classified by the way in which the molecular groups are organised. Main chain polymers, as shown in figure 1.7a, are of lesser interest to second order nonlinear optics because the repeat units are very difficult to align into the required noncentrosymmetric configuration. However, the processing technique of extrusion can be used to align main chain polymers into structures giving anisotropic thermal and mechanical properties.

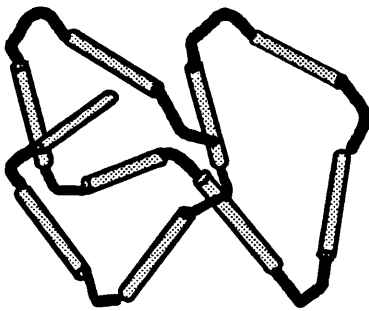
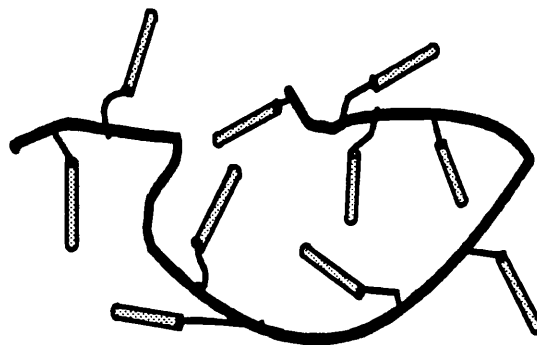


Figure 1.7 a. Main Chain Polymer



b. Side Chain Polymer

Side chain polymers have groups attached to a backbone as pendants, as shown in figure 1.7b. If these side chain groups have dielectric anisotropy and are coupled to the backbone via a flexible spacer group (commonly a CH_2 chain of 3 to 15 units), then they can be relatively easy to align using electric or magnetic fields [Finkleman, (1979)].

Liquid crystalline mesogenic groups can be linked together to form liquid crystal polymers, both as main chain and side chain structures. In a side chain liquid crystal polymer the mesogenic side groups are linked to a polymer backbone such as poly-methylmethacrylate (PMMA). If these groups are sufficiently decoupled from the backbone then the polymer material can exhibit liquid crystalline properties such as nematic and smectic phases between their glass phase and liquid phase. Other

functional side chain groups, for example nonlinear optical molecules, can be linked onto the polymer backbone to produce a copolymer.

Polymeric materials exhibit a plastic phase between the liquid and glass phase. In this phase, the polymer retains much of its mechanical integrity, but it is able to permanently deform due to a finite viscosity. When the temperature is lowered the material undergoes a second order phase transition into the glass phase, freezing in the structure of the polymer at the transition temperature T_g . Therefore below T_g the molecular ordering is no longer in thermal equilibrium with its surroundings.

Non-centrosymmetric ordering can be induced by applying a large dc. electric field to a side chain polymer containing nonlinear optical molecules, a technique called poling. The relative merits of this technique will be discussed in detail in chapters 2 and 3. The poling field is applied at or above the glass transition temperature of the polymer, using the positive dielectric anisotropy to force the side groups to reorient. The induced structure is locked in by cooling the polymer below the glass transition temperature of the polymer whilst the field is applied. At temperatures well below T_g where reorientation by thermal fluctuations is reduced to almost zero, the field can be removed. The induced order is frozen into the structure, but a slow relaxation is still present, which limits the lifetimes of devices made using this technique. Much work has been carried out to improve the lifetime of the induced ordering after the poling field has been removed. This has been achieved by raising the glass transition temperature or crosslinking, both with detrimental effects on the induced ordering.

1.4 Overview of the Dissertation.

There has been a great deal of interest in developing materials with improved nonlinear properties to meet the requirements of optical communication systems and optical information processing. It is believed that materials which naturally occur with some degree of order, and yet potentially offer the ease of fabrication of polymeric materials will have several advantages over existing inorganic and organic crystalline nonlinear optic materials. The aim of this study is to investigate the second order nonlinear optical properties of liquid crystal materials, and to find out whether the use of materials which exhibit self assembly can improve the efficiency of nonlinear optical devices.

The study has been separated into four parts. Chapter 2 reviews the origin of nonlinear optical effects in organic materials, with particular detail of poled polymeric materials. Nonlinear optical effects, and some of the more important devices which can be constructed from these materials are then summarised, with particular emphasis on identifying useful figures of merit by which different materials can be compared. A detailed comparison of different classes of nonlinear optical materials is presented with discussions of other device related parameters such as optical damage thresholds and losses, as well as ease of fabrication and potential costs.

Two alternative approaches to develop improved nonlinear optical materials may be considered and were investigated in this project. The first is described in chapter 3, and is the use of polymers, which can be designed to exhibit large nonlinear optical properties. The required ordering is induced by applying large electric fields to reorient the molecules. The presence of underlying liquid crystal phases was intended to give the benefits of high nematic order parameters without the problems of scatter usually associated with liquid crystal polymers. A study of the poling process was carried out using a simple electro-optic experiment which permitted electro-optic measurements in-situ as the poling occurred. The mechanisms of these reorientation processes have been investigated and are described together with possible methods of improving the poling process.

The second alternative is to utilise smectic liquid crystal materials, some of which are known to form phases with the required noncentrosymmetry for second order nonlinear optical effects. Chapter 4 describes this work, and the development of an experiment to measure the second harmonic generation efficiency of these materials. Although naturally possessing the required symmetry, early ferroelectric liquid crystal materials exhibited very small nonlinear coefficients due to the small transverse hyperpolarisability which contribute to the bulk coefficients. An investigation of the SHG from a commercial ferroelectric liquid crystal mixture was carried out and its measured coefficients compared to that derived from molecular modelling and bulk theory. New liquid crystal molecules with enhanced nonlinear coefficients were developed using molecular engineering techniques, and their coefficients measured. A review of the success of these materials in comparison to other nonlinear materials is discussed.

Chapter 5 describes the use of SHG as a probe into ferroelectric liquid crystal materials and devices. Several research groups have used SHG to investigate molecular alignment of liquid crystal monolayers on substrates treated with surfactants. However, this work describes a number of experiments which probe the bulk liquid crystal material to measure material parameters such as elastic constants and refractive indices, and analyse bulk alignment structures.

2. Nonlinear Optical Materials for Electro-Optic Devices.

The exploitation of nonlinear optics to produce devices to control light requires materials with highly specific properties and devices which can be easily fabricated from these materials. In this chapter a review of the general theory of non-linear optics will be described, showing how the theory can be developed to describe the electro-optic effect and second harmonic generation. The origin of nonlinear effects in molecules will be discussed, and how these effects can be translated into bulk materials. These two topics in themselves are very large and rapidly growing fields, and there are many detailed texts and so it would not be appropriate to reproduce them here.

A range of electro-optic device geometries will be discussed which will highlight the important material figures of merit for the performance of these devices. These can be used to judge the material's potential for electro-optic and frequency conversion devices. A critical review of self assembled materials in comparison with alternate technologies will be presented, with particular reference to the established lithium niobate technology, ending with a discussion of the problems and likely future of liquid crystals in both monomer and polymer form.

2.1 Theory of Nonlinear Optics.

When an electromagnetic wave propagates in a medium, the electric field vector E induces a polarisation P in the medium

$$P_i = \epsilon_o \chi_{ij} E_j \quad 2.1$$

where ϵ_o is the dielectric constant and χ_{ij} is the tensor form of the susceptibility of the material. $i, j = x, y, z$ and there is an implied sum over j . The refractive indices n of the material can then be found from

$$n^2 = \epsilon_{ij} = (1 + \chi_{ij}) \quad 2.2$$

where ϵ_{ij} is the component of the dielectric tensor. If the material is isotropic, then ϵ_{ij} can be reduced to a single term ϵ . However if the material is anisotropic in any way ϵ_{ij} has unequal components, resulting in birefringence.

When the applied field becomes sufficiently large that it can significantly perturb the atomic electric field (10^{10} - 10^{11} Vm^{-1}) [Zyss & Chelma, (1987)] then equations 2.1 and 2.2 are no longer valid. Anharmonic distortions of the induced polarisation on the electric field become important and so the induced polarisation P can be rewritten as

$$P_i = \epsilon_o (\chi_{ij} E_j + \chi_{ijk} E_j E_k + \chi_{ijkl} E_j E_k E_l + \dots) \quad 2.3$$

where χ_{ijk} etc. are the nonlinear susceptibilities. This also modifies the refractive indices

$$n = (1 + \chi_{ij} + \chi_{ijk} E_k + \dots)^{1/2} \quad 2.4$$

so that the refractive index is now dependent on the applied field.

The presence of inversion symmetry can have large implications on the induced polarisation P . Neumann's Principle states that

"The symmetry elements of any physical property of a crystal must include the symmetry elements of the point group of the crystal."

where the point group of a crystal is the group of macroscopic symmetry elements that its structure possesses. Therefore if a crystal (or any material) has inversion symmetry, then any property of that crystal must also obey inversion symmetry. Consider equation 2.3, the expansion of the induced polarisation in terms of the electric field. Applying an inversion symmetry operator I to the equation

$$I(P_i) = \epsilon_o (\chi_{ij} I(E_j) + \chi_{ijk} I(E_j) I(E_k) + \dots) .$$

Noting that $I(P_i) = -P_i$ and similarly for any vector then

$$P_i = \epsilon_o (\chi_{ij} E_j - \chi_{ijk} E_j E_k + \dots) .$$

It can be seen that the second term involving χ_{ijk} is not invariant under inversion symmetry and so must equal zero for centrosymmetric materials. In order to take advantage of this second order non-linear component it is essential that the material lack a centre of inversion.

In non-centrosymmetric materials, there can be a significant contribution to the induced dipole P_i from the second term in the expansion of equation 2.3. This term can be considered as a mixing of the two applied electric fields, E_j and E_k . If these fields with frequencies ω_1 and ω_2 respectively are incident on the material with the form

$$E_{j,k} = E_o \text{Re}[\exp i(\omega_{1,2} t - k_{1,2} x)]$$

then the induced non-linear polarisation will exhibit a frequency dependence

$$P_i^{NL}(\omega) = P^{NL} \text{Re}[\exp i(\omega_1 \pm \omega_2) t] .$$

In the situation where $\omega_1 = \omega_2$ then the non-linear polarisation would oscillate at a frequency $2\omega_1$. This induced polarisation would then re-radiate light at the new frequency, resulting in frequency doubling or second harmonic generation. However, if only one of the applied electric fields originated from a photon at frequency ω , and the other was a d.c. electric field applied to the material ($\omega=0$), then the induced non-linear polarisation would oscillate at the frequency ω , with some phase delay. This is the principle of the electro-optic effect, where an applied electric field modulates the refractive index of the material, resulting in a phase modulation of the transmitted light.

2.2 Nonlinear Optics at a Molecular Level.

In organic systems, it is the nonlinear optical response of the individual molecules which causes the macroscopically observed optical nonlinearity. The induced polarisation of a molecule p due to the presence of an electric field E is

$$p = p_o + \alpha E + \beta E^2 + \gamma E^3 \dots \quad 2.5$$

where p_o is the permanent dipole of the molecule, α is the polarisability and β , γ , ... are the second-, third-, and higher order molecular hyperpolarisability tensors. This equation can be compared directly with equation 2.3.

The polarisability of molecules is dominated by the bond-forming electrons in the molecule. The bond-forming electrons in carbon atoms lie in 2s and 2p orbitals. These electrons can form hybrid orbitals when bonding with adjacent atoms. Carbon atoms which form four sp^3 hybridised orbitals have all their bond forming electrons tied into tetrahedral σ bonds, resulting in a saturated structure. In the case of a double bond the carbon atom exhibits sp^2 hybridisation resulting in three planar σ bonds, and leaving one lone electron in a relatively distant p orbital. Because this electron is very distant from the nucleus, it is extremely polarisable. In the case of a carbon-carbon double bond two p orbitals overlap resulting in a weak π bond. The two electrons become delocalised and therefore polarisable over the length of the π bond. In molecular structures which have repeated multiple bonds such as benzene, the π electrons are delocalised over the length of the unsaturated region, and the structure is described as conjugated. The delocalised electron system makes π electrons highly polarisable, resulting also in large nonlinear polarisabilities.

Symmetry considerations require that the molecule must exhibit non-centrosymmetry to permit second order nonlinear polarisations (β). This requires the electron wave function of the molecule to be asymmetric. A suitable distortion of the π electron system can be achieved by substituting polar groups into the conjugated system. The effect can be increased by substituting electron donating and electron accepting groups at either end of the molecule, linked by a conjugated system of electrons - the 'push-pull' system. This enhances the asymmetric interaction of the electron cloud distribution with the electric field resulting in a large second order hyperpolarisability β . Examples of these molecules are shown in figure 2.1, together with their hyperpolarisability. The nitro (NO_2) group is one of the strongest acceptor groups used, and amino (NH_2) or dimethyl amino ($N(CH_3)_2$) groups are highly electron donating groups. A typical example of the push-pull arrangement is the DANS molecule where the nitrogen atom in the amino group is electron donating and the nitrogen atom in the nitro group is electron accepting.

The π electron system exhibits a low energy excitation ($\pi \rightarrow \pi^*$). Molecular hyperpolarisability β can be described as two components, β_{ct} and β_{add} , where β_{ct} is the contribution from the strong charge

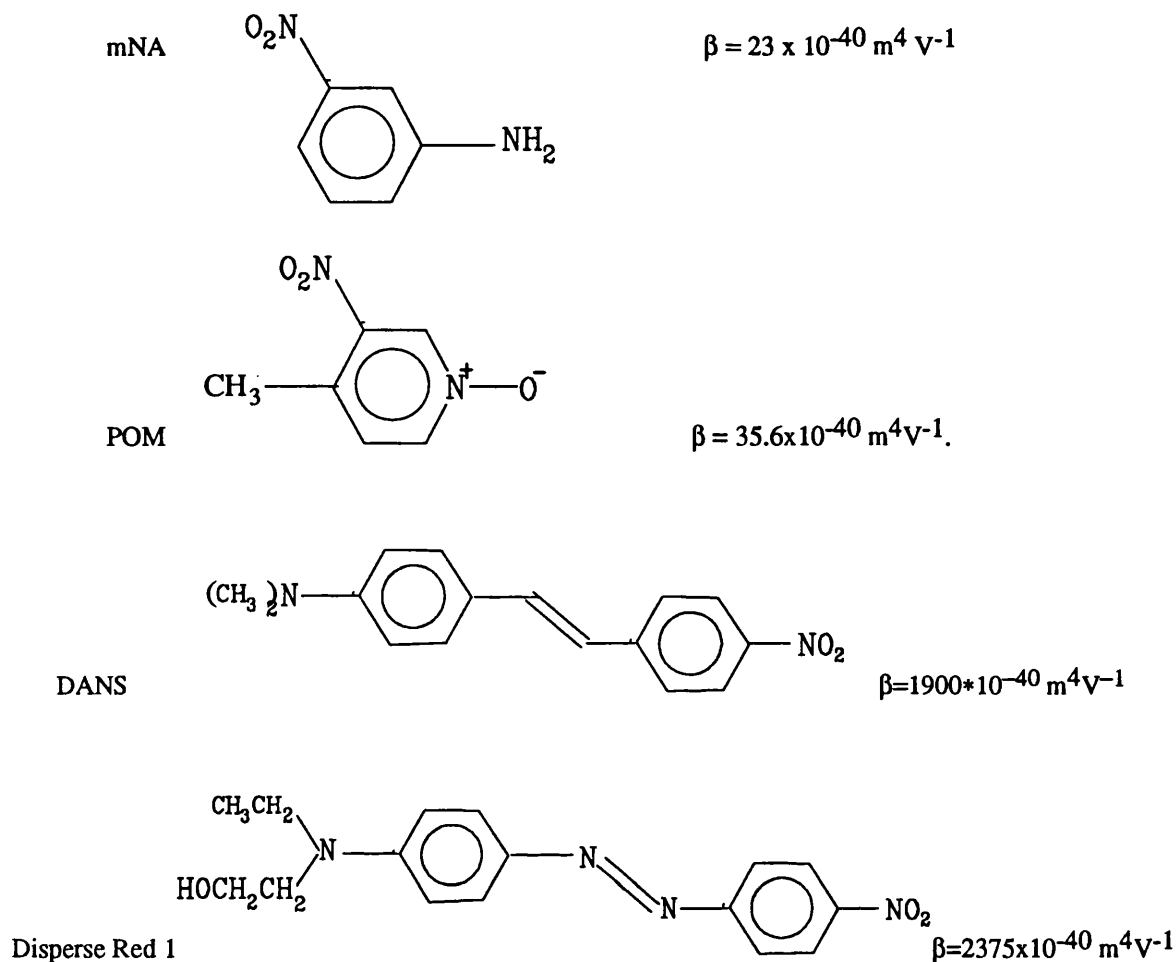


Figure 2.1 Nonlinear optical molecules.

transfer transition between the ground state π electron distribution and the first excited state π^* , and β_{add} is the contribution from all other molecular excitations.

The absorption band due to the $\pi \rightarrow \pi^*$ transition is in the near uv or blue region of the optical spectrum. Extending the conjugation length and strength of donor and acceptor groups increases β , but also reduces the energy of the transition, increasing absorption to longer wavelengths in the visible spectrum.

The molecular hyperpolarisability can be calculated from two different principles. The derivative method expands the energy or molecular dipole moment in terms of a power series, as has been described earlier, and then calculates derivatives of this expansion. Consider equation 2.5, and differentiating it with respect to the applied electric field gives

$$\frac{\partial p}{\partial E} = \alpha + 2\beta E + 3\gamma E^2 + \dots$$

and differentiating again gives

$$\frac{\partial^2 P}{\partial E^2} = 2\beta + 6\gamma E + \dots$$

Thus the second order polarisability β can be found from the second derivative of the induced polarisation (or dipole moment) when $E=0$. This calculation can be carried out using *ab initio* or semi-empirical techniques, and produces values for β in the low frequency limit $\omega \rightarrow 0$. Prasad & Williams (1991) describe a useful summary of the different modelling methods.

Computer modelling of molecules for this thesis used the semi-empirical MOPAC suite of programs using the MNDO (Modified Neglect of Diatomic Overlap) method. This calculation considers only the valence electrons of the molecule and takes into account the differential overlap of electron orbitals, with the exception of orbitals centred on different atoms. The value of β calculated by this method is in atomic units (AU) which can be converted to S.I. where $1\text{AU} = 3.206 \times 10^{-54} \text{C}^3\text{m}^3\text{J}^{-2}$. The units quoted in the literature are m^4V^{-1} , which is actually β/ϵ_0 . For reference, non-S.I. units of esu for β can be converted to SI using $1\text{cm}^5\text{esu}^{-1} \equiv 1.9 \times 10^{-9} \text{m}^4\text{V}^{-1}$.

The second method of calculating β is the sum over states method which calculates the effect of a perturbing electromagnetic field on the wave function of the electrons within the molecule. The result is expressions for the polarisability and hyperpolarisabilities in sums of dipole integrals over all excited states of the molecule. The dipolar integrals are of the form

$$er_{nn'} = \langle n | er | n' \rangle.$$

When $n=n'$ then $er_{nn'}$ corresponds to the dipole moment of state n , and when $n \neq n'$ this corresponds to the transition dipole moment between the two states. The number of states over which the summation is carried out is usually limited to a few molecular levels of the lowest energy, which artificially enhances the contribution of these states. In a simple two level quantum model, β_{cl} can be described by the equation [Zyss, (1988)]

$$\beta(-\omega_3, \omega_1, \omega_2) = \frac{3e^2\hbar^2}{2m} f\Delta\mu F(W, \omega_1, \omega_2, \omega_3) \quad 2.6$$

where the term $F(W, \omega)$ describes the dispersion as is defined by

$$F(W, \omega_1, \omega_2, \omega_3) = \frac{W[W + (\hbar^2\omega_1\omega_2 - \hbar^2\omega_3^2)/3]}{[W^2 - (\hbar\omega_1)^2][W^2 - (\hbar\omega_2)^2][W^2 - (\hbar\omega_3)^2]} \quad 2.7$$

W and $\Delta\mu$ are the difference in energy and dipole moment between the two levels, ω_i is the frequency of the electric fields, and f is the oscillator strength of the transition.

The calculated values of β can be compared with experiment using the technique of Electric Field Induced Second Harmonic generation (EFISH). This technique uses a liquid or solution form of the materials whose molecules are aligned non-centrosymmetrically by the application of large dc electric

fields to interact with the permanent dipole of the molecule. Pugh & Morley [1987] describe more experimental details about the EFISH technique.

2.3 From Molecules to Bulk Properties.

The macroscopic second order susceptibility $\chi^{(2)}$ is related to the molecular hyperpolarisability β by

$$\chi_{ijk}^{(2)}(-\omega_3; \omega_1, \omega_2) = \frac{1}{V} f_I^{\omega_3} f_J^{\omega_1} f_K^{\omega_2} \sum_q a_{Ii} a_{Jj} a_{Kk} \beta_{ijk}(-\omega_3; \omega_1, \omega_2) \quad 2.8$$

where there is a summation over all molecules q within the unit cell, V is the volume of the unit cell, f^ω are the local field factors and a_{Ii} are the direction cosines of the molecular frame of reference xyz with respect to the bulk material frame XYZ . The local field factors take into account the field experienced by a molecule is not necessarily equal to that applied to the bulk material. This may be a result of reorientation of polarisation and redistribution of space charge 'masking' the applied field. At optical frequencies the main effect is due to dipoles induced in the material by electronic polarisation. This can be described by the field factor [Zyss & Chelma (1987)]

$$f_{I\omega} = 1 + (\epsilon_\omega - 1)L_I \quad I=1,2,3$$

where $L_1 + L_2 + L_3 = 1$. The components of L describe the shape of a small volume within which the molecule can rotate. The shape of the volume is determined by the form of the constituent molecule. For an isotropic liquid or cubic crystal, $L_1 = L_2 = L_3 = 1/3$, resulting in the familiar Lorentz field factor

$$f^\omega = \left[\frac{\epsilon^i(\omega) + 2}{3} \right]. \quad 2.9$$

For a long cylindrical volume, $L_1 = L_2 = 1/2$, and $L_3 = 0$. This form is a good approximation for rod shaped liquid crystal molecules. In the low frequency limit, the applied electric fields can also reorient dipoles in the material, and so the local field factor for dc fields is described by the Onsager correction factor

$$f^0 = \epsilon_0 (\epsilon_\omega + 2)(2\epsilon_0 + \epsilon_\omega). \quad 2.10$$

In summary, the electric field applied to the material may be significantly different to the field inside the bulk material. These local field factors are well established in isotropic systems, and are adequate approximations in highly anisotropic and dynamic systems.

2.4 Classes of Bulk Nonlinear Organic Materials.

There are two independent requirements for a large bulk non-linear coefficient - a large hyperpolarisability and efficient ordering of the molecules in the bulk material. The condition of an absence of a centre of inversion must be fulfilled for each of the two criteria for second order nonlinear optical materials. The molecular asymmetry results in a large molecular dipole transition between ground and excited states, and the bulk noncentrosymmetry allows the molecular dipole (ground state and/or excited state) to combine constructively.

Organic molecules can be assembled in many different physical forms to show bulk optical nonlinearities. The only necessary requirement to exhibit second order effects is that the material does not possess inversion symmetry. Inherently non-centrosymmetric bulk materials include some crystals, ferroelectric liquid crystals and some Langmuir Blodgett films. It is also possible to induce or engineer the required symmetry in centrosymmetric materials. This has been most commonly achieved by applying large dc electric fields to liquids and polymers to force dipoles to reorient parallel to the applied field. The advantages and drawbacks of this poling technique will be discussed later in this section.

2.4.1 Organic Crystals.

Organic crystals have been grown and exhibit some of the highest bulk non-linear effects seen to date [Bierlein et al, (1990)]. Predicting the crystal group from a molecular structure is virtually impossible, and of the 32 possible crystalline classes only 21 meet the symmetry requirement. Due to the polar nature of many molecules with large β , there is a natural tendency of these molecules to align anti parallel, and hence result in centrosymmetric crystals. There have been a number of molecules specifically designed or modified to grow non-centrosymmetric crystals. One of the earliest was probably the modification of para-nitroaniline (pNA) which has a large β but grows in centrosymmetric crystals to 2-methyl-4-nitroaniline (MNA). The inclusion of the methyl group into an asymmetric position was sufficient to change the crystal group to one which lacks inversion symmetry, whilst retaining the large β . An alternative technique uses hydrogen bonding to hold adjacent molecules in the energetically unfavourable dipole alignment. There are several examples of this technique, one of the earliest is the molecule 2-(α -methylbenzylamino)-3,5-dinitropyridine (MBADNAP) [Tweig et al, (1982)], and probably one of the most successful is N-(4-nitrophenyl)-(L)-prolinol (NPP) [Zyss et al, (1984)].

It is important that the molecules lie at the correct angle within the unit cell to exploit the largest hyperpolarisabilities to produce efficient nlo materials. However, the difference in molecular organisation within the unit cell of allowable crystal point groups can have considerable effect. Midwinter and Warner [Midwinter & Warner, (1965)] published a table of calculated optimal effective phase-matched nonlinearities for second harmonic generation in all permissible crystal point groups. The highest

efficiency comes from crystal groups $1,2,m,2mm$, with the d_{eff} equal to $2/3\sqrt{3}$ ($\cong 0.38$) of the largest d_{ijk} coefficient. The engineering of molecules for optimal crystal properties has been achieved with some effect, particularly with NPP where the molecule lies close to the optimum position for phase matching in second harmonic generation.

2.4.2 Side Chain Polymers and Poling.

Nonlinear optical molecular groups can be incorporated into polymeric materials to produce extremely versatile bulk nonlinear materials. Polymeric materials exhibit a plastic phase between the liquid and glass phase. In this phase, the polymer retains some of its mechanical integrity, but it is able to deform due to a finite viscosity. When the temperature is lowered the material undergoes a second order phase transition into the glass phase, drastically reducing the mobility of groups within the polymer at the glass transition temperature T_g . Below T_g the molecular ordering is no longer in thermal equilibrium with its surroundings.

Non-centrosymmetric ordering can be induced by applying a large d.c. electric field to a polymer containing nonlinear optical molecules. When an electric field is applied to a system composed of asymmetric molecules, the molecules reorient to minimise their electrostatic energy. The energy associated with this dipole-field interaction will be at a minimum when the molecules align their net dipole in the direction of the applied electric field. In most cases nonlinear optical molecules have their net dipole parallel to the long axis of the molecule. In this case the molecules will align their long axis parallel to the applied electric field in an ∞mm symmetry, where it is assumed that the molecules are of a long cylindrical form such that there is an infinite rotational symmetry about the long axis of the molecule. Whilst a material is being poled, thermal disordering mechanisms are in competition with the alignment process. The system can be described using Boltzmann statistics, the important term being $\exp(-\mu E/kT)$, where μE is the energy associated with the molecular dipole moment μ coupling with the applied field E , and kT is the thermal energy associated with particles in a gas at temperature T . It should be noted that $kT > \mu E$ even for very large field strengths. Some disordering processes can still occur below T_g and allow the induced order to relax, as will be described in more detail in chapter 3.

The earliest and simplest approach of incorporating nonlinear optical molecular groups into poled polymeric materials was to dissolve nonlinear optical materials into a side chain polymer [Havinga, (1979)]. The rod-shaped molecules follow the alignment of the rod-like side chains using a co-operative alignment interaction. There is often a material limit to the solubility of the nonlinear molecules in the polymer, typically less than 10%. The packing efficiency of the side chain groups is also reduced slightly, increasing the relaxation of the nonlinear molecules from their induced ordering. This results in low electro-optic coefficients and poor lifetimes of any device.

A more successful method is where nonlinear molecules can be attached to the polymer backbone to form a copolymer. This increases the stability of the ordering within the polymer, permitting device lifetimes of the order of months to years. The number concentration of nonlinear molecules can also be increased up to 100%, with a direct improvement in the bulk nonlinear optical properties.

If a nematic liquid crystal copolymer is used where up to 50% of the mesogenic groups are replaced by nonlinear molecules, the polymer may retain some nematic properties. This can have a twofold advantage - the side chains have intrinsic partial ordering, and through improved packing increase the number density of side chain groups. Appendix A describes the theoretical prediction of a potential fivefold improvement in ordering due to the inclusion of nematic mesogens, and Amano [1990] described an experimentally measured enhancement of 1.6. Increasing the percentage of nonlinear groups to very large concentrations can result in the loss of the nematic phase (e.g. > 50 %).

2.4.3 Liquid Crystals.

Liquid crystal phases can exhibit bulk second order nonlinear optical effects. The lowest order phases, the nematic and smectic A phases, do not possess the correct inherent symmetry for second order effects, but can be poled in a similar manner to polymers using dc electric fields. However, there are liquid crystal phases which can exhibit inherent noncentrosymmetry - the chiral tilted smectic phases, S_C^* and S_I^* . Achiral molecules in the tilted smectic phases are forbidden from having any permanent dipole moment because of their molecular symmetry group. However, the introduction of a chiral centre on the molecule removes one of the symmetry operations (reflection in a mirror plane) and therefore permits the presence of a permanent transverse dipole moment which is able to produce a spontaneous polarisation (P_S) across the bulk material, as shown in figure 1.6 earlier.

Within a bulk material the chirality of the molecules encourages the molecules to pack in a helical form, destroying the noncentrosymmetric symmetry. This can be overcome using strong surface alignments in thin films to pin the molecules at the surface and force the helix to unwind, as exploited in the surface stabilised ferroelectric liquid crystal (ssflc) display. Alternatively, as the molecules have a permanent transverse dipole moment then an electric field can be used to align their dipole moments and unwind the helix. Mixing molecules which have opposite twisting power, or introducing a second chiral centre into a molecule to counteract the twisting power, can also result in bulk materials with noncentrosymmetric symmetry [Kobayashi et al, (1993)].

2.4.4 Langmuir Blodgett Films.

Langmuir Blodgett films are built up from individual monolayers of materials and deposited onto a substrate. The monolayer is formed by engineering molecules with a polar head group and long aliphatic tail, which float on water to form a thin layer. Compressing the layer results in the molecules standing up to form a well ordered monolayer with the polar head group at the water interface. This monolayer can then be transferred onto a substrate by carefully dipping the substrate through the monolayer. Repeated dipping results in additional bilayers being deposited. If only one material is used, the resultant structure is centrosymmetric as each molecular layer is inverted (Y-type). Alternately dipping two materials can result in structures where the inversion symmetry has been removed. The molecular order within the structure is very high, but is limited to geometries where the molecules are deposited normal (or close to the normal) to the substrate. As the number of layers is increased, the mechanical stability and order of the film decreases. The maximum number of layers deposited is approximately 3000, resulting in a layer about 1 μm thick but a film of this type would take many hours to produce [Ashwell, (1992)]. Chemical cross-linking of the layers has been used to improve their stability.

2.5 The Linear Electro-Optic Effect.

The linear electro-optic effect describes the way in which an applied d.c. (or low frequency) electric field modifies the refractive index of a material in a linear relationship. It is assumed that all terms higher than the second order in electric field are sufficiently small to be ignored.

Although the linear electro-optic effect can be described using nonlinear induced polarisations and χ_{ijk} , it is conventional to express it as a modification to the inverse dielectric constant matrix

$$\Delta(\epsilon^{-1})_{ij} = r_{ijk} E_k \quad i, j, k = x, y, z \quad 2.11$$

where r_{ijk} are coefficients of the electro-optic tensor and E_k is the applied field.

It can be shown that as a consequence of energy conservation, the dielectric tensor of a lossless and magnetically isotropic crystal must be symmetric [Born & Wolf, (1980)]. This allows the expression for the electrical energy stored in the material to be described by an ellipsoid whose normalised surface is known as the index ellipsoid and is given by

$$\epsilon_{ii}x^2 + \epsilon_{jj}y^2 + \epsilon_{kk}z^2 + 2\epsilon_{jk}yz + 2\epsilon_{ik}xz + 2\epsilon_{ij}xy = \text{const.}$$

It is possible to reduce the dielectric tensor to a diagonal form by rotational transformation of the axes, and with respect to the new axes the ellipsoid will have the form

$$\frac{x^2}{n_x^2} + \frac{y^2}{n_y^2} + \frac{z^2}{n_z^2} = 1$$

2.12

where X,Y,Z are the new axes called principal axes. This ellipsoid, shown in figure 2.2 for a uniaxial material such as lithium niobate, can then be used to determine the properties of an optical wave propagating in the material using geometrical constructions.

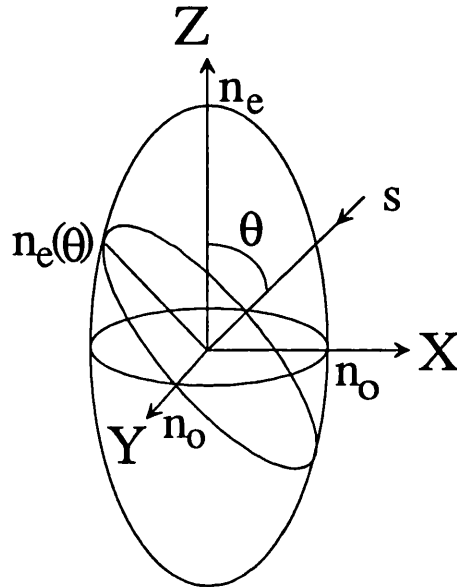


Figure 2.2 The Index Ellipsoid.

For a given direction of propagation s , then a plane normal to s which passes through the origin of the ellipsoid, intersects the ellipsoid to form an ellipse called the propagation ellipse. At the points where the propagation ellipse intersects the index ellipsoid, the normals to the surface define the directions of E for the two allowed polarisations, whilst the lengths of the ellipse axes are their respective refractive indices. From figure 2.2 we can see that for a uniaxial system, where the refractive indices along the X and Y axes are equal to n_o and along the Z axis is equal to n_e , then a general wave will experience refractive indices n_o and n_x for the ordinary and extraordinary polarisations respectively.

Symmetry arguments state that for any material the electro-optic tensor must be invariant under the direction of propagation of the light i.e. $r_{ijk} = r_{jik}$ and so a shortened notation of two parameters is usual. The suffix k takes $x=1$, $y=2$ and $z=3$, and i and j are combined to give

$$xx = 1 \quad yy = 2 \quad zz = 3 \quad yz = 4 \quad zx = 5 \quad yx = 6.$$

The effect of these off-axis elements on the index ellipsoid is to stretch and/or rotate the ellipsoid. The application of electric fields to materials with these coefficients is to modify or modulate particular refractive indices within the material. The equation

$$\Delta n_{ij} = n_{ij}^3 r_{ijk} E_k$$

2.13

describes the magnitude of the refractive index modulation Δn_{ij} where E_k is the applied electric field and n_{ij} is the refractive index experienced by the light and modulated by the applied field. From this equation it is simple to collect the material dependent terms together to describe a material figure of merit

$$n_{ij}^3 r_{ijk} \quad 2.14$$

and is commonly described in units of pmV^{-1} . This clearly indicates the importance of other material properties such as the refractive index as well as the nonlinear coefficient when assessing electro-optic materials. It is also important to note the tensorial nature of the electro-optic effect. The orientation of the material and the polarisation and direction of the light and electric fields must be chosen carefully to produce efficient devices.

2.6 Second Harmonic Generation.

The theory of second harmonic generation is described in many books e.g. Shen [1982] or Yariv [1985], and will be discussed in detail in chapter 4. The material dependent components of the equation describing SHG efficiency are d_{eff} which describes the contribution of the tensor components of the nonlinear tensor coefficient d_{ijk} when the directions and polarisations of the input and second harmonic light are considered, and n is the relevant refractive index. The ratio

$$\text{SHG Power} \propto \frac{d_{\text{eff}}^2}{n_{2\omega} n_{\omega}^2} \quad 2.15$$

describes the figure of merit of materials for second harmonic generation and has units of $(\text{pmV}^{-1})^2$. There is an additional requirement that the fundamental and second harmonic waves remain in phase to allow efficient conversion over useful optical path lengths (several mm). This requirement is called phase matching. If phase matching is not achieved, then the two waves will move in and out of phase due to dispersion in the material, and can result in destructive interference.

2.7 Requirements for Nonlinear Optical Materials.

There are a number of material criteria which are important for all nonlinear optical applications. These include:

- i. Very small absorption coefficients for the wavelengths used.
- ii. Low scattering losses within the material.
- iii. High laser damage thresholds to prevent damage to the material from the optical radiation.

- iv. Mechanical and chemical stability.
- v. Material synthesis and device fabrication.

Absorption can result in thermal damage when large laser powers are applied. Absorption is also particularly important in waveguide structures to minimise insertion losses. The optical absorption in nonlinear materials is understood sufficiently to be predicted and controlled through established modelling techniques of the electron wave functions of the atoms involved. This applies for inorganic crystalline systems as well as for organic molecules. The requirement of a large nonlinear coefficient necessitates there to be a large number of polarisable electrons in the molecule or unit cell. Unfortunately, this has a detrimental effect on the optical absorption, reducing the energy of the transition between ground and excited state and encroaching into the transmission window of the material. This will be described in more detail for the case of molecules with delocalised electrons later in this chapter. Ultimately there has to be a compromise between the losses that can be tolerated and the magnitude of the nonlinear effect.

For almost all optical effects in materials it is important to have a high optical quality within the material, for example it must be free of inclusions, stresses, and any other defects introduced when the material is formed into its solid state. This minimises the losses of the light through scatter, and also removes possible sites of laser damage in the device. Liquid crystals and liquid crystalline polymers can have particular problems with scatter from local director fluctuations and scattering from domain walls within the material unless the material is well aligned.

The stability of materials under prolonged exposure to the atmosphere, to uv radiation from sunlight, or from the high laser intensities used in many optical devices (particularly waveguides) must also be proven if commercial devices are to be developed. Some material instabilities can be accommodated by packaging the final device in some protective manner, e.g. used in hermetically sealed packages to protect from water vapour in the case of KD*P crystals. Instabilities due to high light intensities are less acceptable and must be engineered out of the material when it is designed.

It is preferable to use materials which are cheap and simple to synthesise, and to then be able to manufacture devices easily from the material. Any devices which use materials in their crystalline form are slow and complex to produce in order to achieve high optical quality. This will also impose a limit to the size of the device. It has often been claimed that polymers have advantage in that they are easy to process and are suitable for simple automated production. This is probably true to the extent that small pre-production plant has been developed and is producing useful devices. However, full scale production is still some way off.

2.8 Nonlinear Optical Devices.

The principal applications of nonlinear optical devices are the electro-optic modulation of the phase and intensity of light, and the generation of new optical frequencies by second harmonic generation

or optical parametric oscillation. The use of light as the carrier signal for information has increased the demand for efficient and high speed modulation of light, particularly in waveguide geometries for integrated optical systems. Similarly, the requirements of optical data storage have resulted in a range of techniques to produce compact and low power laser sources with wavelengths in the blue region of the spectrum. Some of these techniques involve the development of new wide bandgap semiconductor materials such as zinc selenide, and have been demonstrated briefly at room temperature [Jeon et al 1992]. Most techniques of producing blue laser light are by frequency doubling gallium arsenide semiconductor lasers using inorganic or organic crystals.

The principal material requirements of the most common types of nonlinear optical devices will now be outlined. The limitations on the performance of these devices due to materials will also be discussed.

2.8.1 Through-Plane Electro-Optic Modulators.

Through-plane devices describes a wide range of geometries used for electro-optic modulators and frequency modifying devices, including second harmonic generation and optical parametric oscillators. The devices are at present being made from inorganic crystals such as LiNbO₃ or KD*P. The crystals used are frequently in excess of (10mm)³ in size and are defect free resulting in very high costs (£100's). Large crystals are very difficult to grow, and ultimately limit the apertures to approximately 100cm². Insertion losses for these devices must be kept at a minimum, demanding very low scatter and absorption in the material. To obtain high contrast switches it is necessary to produce very flat devices, ideally with thickness tolerances less than $\lambda/10$. This is to ensure that light across the whole aperture experiences the same degree of retardation or rotation of the polarisation vector. This may prove difficult to achieve without polishing the material.

A common geometry for amplitude or phase modulators is to apply the modulating electric field parallel to the direction of light propagation and modulate the light through the r_{33} or r_{63} coefficient. This geometry is very similar to that of poled polymers. The voltage required to induce a phase delay of π radians is independent of the device thickness, and is given in equation 2.16

$$V_{\pi} = \frac{\lambda}{2n_o^3 r_{63}} \quad 2.16$$

For the material KD*P, V_{π} is calculated to be 2.6 kV. This is inconveniently high and difficult to switch on or off quickly, with voltage pulse rise times of several nanoseconds. This imposes a limit on the bandwidth of the device. The development of materials with higher nonlinear coefficients will decrease the V_{π} voltage to 100's of volts, thus making the device much easier to modulate and increase the bandwidth due to the lower drive voltages.

2.8.2 Transverse Electro-Optic Modulators.

It is possible to select the crystal symmetry group of the material to allow transverse electro-optic modulation. The symmetry group $42m$ of KDP results in an electro-optic tensor component r_{63} . In this geometry an electric field is applied along the crystal z axis to modulate the extraordinary refractive index n_e , as shown in figure 2.3.

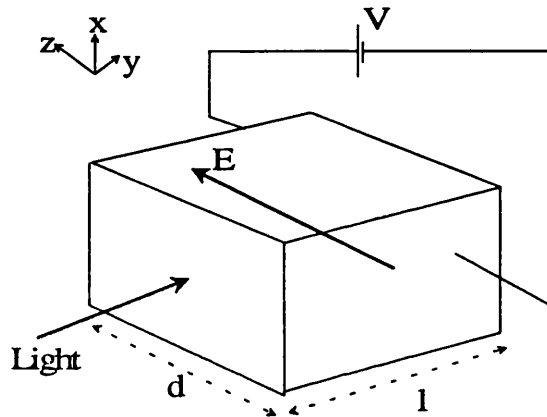


Figure 2.3 A Transverse Modulator.

The modulating field is applied perpendicular to the propagation direction of the light via transverse electrodes. When plane polarised light is introduced at an angle of 45° to the material z axis the induced phase delay $\Delta\phi$ is given by

$$\Delta\phi = \frac{\pi n_o^3 r_{33}}{\lambda} \left(\frac{Vl}{d} \right)$$

where l is the modulator length, d is the distance between the electrodes and V is the voltage applied across them.

In this geometry the optical path length and the spacing of the electrodes are independent. It is therefore possible to have long optical path lengths and high voltage gradients, reducing the voltage required to induce a π radians phase delay to less than 10V. However, this restricts the modulation bandwidth of the device. The long optical path length of these devices places particular emphasis on the transmission properties of the materials for use in such devices. Optical fibres have losses in the range of dBkm^{-1} , but waveguide devices are at best around 0.5 dBcm^{-1} . This imposes a limit to the path length that can be used at present to maintain insertion losses to acceptable levels. It is desirable to improve the insertion loss to allow devices to be cascaded for more complex signal processing.

2.8.3 Bandwidth Limits.

The simple theory of electro-optic modulation used assumes a steady state modulation is induced. However, this theory no longer holds when the pulse time of the modulation signal approaches the transit time of the light through the modulator. In this situation the modulation signal will change before light, which entered the modulator as the signal was applied, leaves the modulator. For a modulator of length l then the maximum useful modulation frequency is given by

$$v_{\max} = \frac{c}{4l.n}$$

where c/n is the speed of the light through the crystal. For a device 1cm long with a refractive index of 2.25 then this limits the modulation frequency to 3.3 GHz. It can be seen that a low refractive index is desirable together with a short device length. Organic materials can offer low refractive indices and larger nonlinear optical coefficients than equivalent inorganic materials, thereby reducing the device length and increasing the modulation frequency limit. The frequency-device length product gives a useful guide to the modulation capabilities of a material. Lithium niobate has been calculated to be $8.2 \times 10^7 \text{ ms}^{-1}$, and poled polymers offer values in the order of $3 \times 10^9 \text{ ms}^{-1}$ [Stamatoff et al, (1991)].

One way of overcoming the modulation frequency limit due to transit time is to apply the modulation signal as a travelling wave along the transverse electrodes. If it is arranged that the phase velocity of the modulation signal along the electrodes is equal to that of the light travelling through the modulator, then one portion of light will experience the same instantaneous electric field throughout the modulator. In this situation the frequency limit discussed above will not apply. Due to dielectric relaxations in materials, it is common to find the phase velocities of signals at gigahertz and optical frequencies are very different. In the situation where the phase velocities are not exactly matched, then the limit

$$v_{\max} = \frac{c}{4l.n(1 - c/nc_m)}$$

where c_m is the phase velocity of the modulation signal. At the beginning of this work it was not possible to phase match microwave and optical signals in lithium niobate devices due to the large dispersion in the material. Organic materials, with their inherent low dielectric coefficients were in a position to offer considerable benefits for the maximum bandwidth of devices, and were the only devices likely to operate at very high frequencies. Over the period of this study phase velocities in lithium niobate devices have been matched through design of the electrode, and so can now compete with organic materials with devices at frequencies of 10's of GHz [Haas, (1992)]. Thus one of the strongest arguments supporting organic devices has been lost due to developments in competing technologies.

2.8.4 Waveguide Modulators.

The demand for efficient optical waveguide modulators has risen with the growth of optical communications. The requirement is for optical waveguides which can be integrated onto the semiconductor substrate allowing direct launch of the light from a semiconductor laser into the wave guide with minimal loss. Within the waveguide, there must be the capability of modulating the light with a data signal, and routing the light between waveguides.

Techniques using lithium niobate require a separate crystalline substrate, into which waveguides are defined by diffusion or ion bombardment of titanium into the substrate. Electrodes can then be deposited using conventional photo-lithography techniques to produce transverse electro-optic modulators. The operation of modulators in waveguide structures is identical to that of bulk modulators, including the limitations of the modulation bandwidth. An important criteria is the insertion loss of a device - the total loss of intensity when an optical fibre is broken and a device inserted. Targets for cascaded systems are 3 dB. Although much work has been addressing the intrinsic losses in the material, coupling losses between the optical fibre and the waveguide are very high and will need to be reduced significantly before commercial devices are successful. Organic materials have a slight advantage, having refractive indices closer to glass than many crystals.

2.8.5 Waveguides in Poled Polymers.

Poled polymeric materials are particularly suited to waveguide operation. A solution of the polymer can be spin coated onto the semiconductor substrate with a thickness of 1-5 μm . Waveguides can be defined by a number of techniques.

- i. The semiconductor substrate is etched with the waveguide pattern before the polymer material is deposited. On deposition, the thickness is controlled so that where there is an etched waveguide, the polymer layer supports a guided mode. Elsewhere on the substrate, the polymer layer is sufficiently thin to stop any wave guiding. Poor planarisation of the substrate by the polymer layer (usually deposited by spinning) results in poor quality waveguides.
- ii. The polymer material is deposited uniformly over the substrate. Where waveguides are required, the polymer is bleached using uv radiation. This produces a sufficient variation in refractive index to define the waveguide. Problems include uncertainties in the bleaching process as it is not well understood. The dye molecules may be destroyed leaving residues in the waveguide and loss of nonlinear chromophores. The residues may increase the relaxation of any induced order or form centres for laser damage. However, the quality of waveguides is quite good, with losses less than 0.5 dBcm⁻¹ achievable, and may be reduced further towards the target of 0.1 dBcm⁻¹.

iii. Ion beam etching can be used to define waveguides in a similar manner to semiconductor structures. The etch forms a well defined waveguide structure, but has rough sides which act as scattering centres, resulting in losses of approximately 1 dBcm^{-1} . Further processing can be used to reduce this problem, and it is anticipated that this technique can also achieve losses in the region $0.1\text{-}0.2 \text{ dBcm}^{-1}$. Surface electrodes are then deposited by conventional techniques and the polymer within the modulator region is poled and the order locked in. After poling, it is extremely important that the substrate is not heated excessively as part of any further processing to preserve the induced noncentrosymmetric ordering. Scattering losses of waveguides fabricated in poled polymeric materials have been measured at 0.5 dBcm^{-1} [Stamatoff, (1990)].

2.8.6 Second Harmonic Generation Devices.

All materials exhibit dispersion, and consequently when SHG occurs, the fundamental and second harmonic waves travel through the material at different speeds. A characteristic distance, the coherence length,

$$l_c = \frac{\lambda}{2(n^{2\omega} - n^\omega)}$$

can be defined as the distance it takes for the two waves to become significantly different in phase where λ is the wavelength of the light and n^ω is the refractive index at frequency ω . Path lengths below l_c result in SHG power increasing as a function of path length squared. Path lengths greater than l_c result in interference between SHG produced at the beginning of the material, and that produced at the end. This interference can be destructive, where the second harmonic is reconverted back into the fundamental wave. To overcome this problem, it is necessary to arrange that

$$k_{2\omega} = 2k_\omega . \tag{2.17}$$

where k_ω is the wave vector of the fundamental wave.

Efficient second harmonic generation requires phase matching, and can result in efficiencies in excess of 50%. The properties of the material define which phase matching techniques are possible. Type I collinear phase matching requires a birefringence with the condition

$$n_o(2\omega) = n_e(\omega)$$

assuming normal dispersion. If this condition is not achieved, then the harmonic beam will suffer 'walk off', where the second harmonic is not collinear with the input radiation. Type II phase matching requires

$$n_e(2\omega) = n_o(\omega) .$$

2.9 Comparison of Materials for Electro-Optical and SHG Applications.

Table 1 describes a number of nonlinear optical materials together with important optical properties. The list is by no means complete, but is intended to give a flavour of the different material classes.

2.9.1 Inorganic Crystals.

Many of the inorganic crystals used in second order nonlinear optics were first identified many years ago. Quartz was the first crystal to experimentally exhibit SHG in 1961 [Franken et al 1961], it being readily available in large high quality crystals. Quartz was used in this work as a reference material against which new materials were compared.

The material lithium niobate (LiNbO_3) has been the subject of development for many years with the aim of improving the crystal quality and size by developing crystal growth techniques. Lithium niobate has been developed specifically for electro-optic applications due to its high refractive indices resulting in a large figure of merit. It is still subject to much development for the field of integrated optics, where waveguides can be produced by indiffusion of metals or protons. Waveguide losses in the region of 0.1 dBcm^{-1} have been achieved. Optical damage thresholds are limited by photorefractive damage in the material due to the absorption in the green from iron(II) impurities (approx. 0.1 GWcm^{-2}). Adding 5% magnesium oxide (MgO_2) has greatly improved its damage threshold and maintained its nonlinear coefficients. Lithium niobate has recently demonstrated spatially periodic poling along the waveguide which can achieve quasi-phase matching requirements [Khanarian et al, (1990)]. This has the effect of periodically modulating $\chi^{(2)}$ such that

$$\chi^{(2)}(x) = \chi_0^{(2)} + \chi_1^{(2)} \cos(Gx) \quad G = 2\pi/\Lambda$$

where Λ is the grating spatial periodicity. If $G=\Delta k$ then efficient phase matching occurs irrespective of birefringence. Using this technique, useful SHG conversion efficiencies have been achieved.

Potassium titanyl phosphate (KTP) has very competitive figures of merit, although there is some disagreement over the actual nonlinear coefficients. The material has favourable phase matching conditions due to the crystal being biaxial, and SHG efficiencies in excess of 80% have been demonstrated [Brown et al (1992)]. It has a low laser damage threshold ($\sim 0.65 \text{ GWcm}^{-2}$), and poor transmission in the uv, limiting its frequency doubling applications. Similar to LiNbO_3 , waveguides can be defined using ion exchange techniques achieving losses typically 0.1 dBcm^{-1} .

Gallium arsenide can be used in several different manners to produce nonlinear optical devices. The nonlinear coefficients quoted for GaAs refer to the bulk material. It is possible to enhance the nonlinear coefficients by growing asymmetric GaAs/AlGaAs multiple quantum well structures in the

Material	Symmetry Group	Refractive Index n	Electro-optic Coeff. r (pmV ⁻¹)	n ³ r	Nonlinear Coeff. d (pmV ⁻¹)	d ² /n ³	Wavelength r coeff. (nm)	Wavelength d coeff. (nm)	Reference
Inorganic Crystals.									
Quartz	32	n _o =1.5341 n _e =1.55	r ₄₁ =0.195 r ₆₃ =0.93	0.7 3.4	d _{eff} =0.32	0.028	589	1064 1064	1,2,3 1
LiNbO ₃	3m	n _e =2.2322 n _o =2.29	r ₃₃ =30.8 r ₁₃ =8.6	328 103	d _{eff} =-4.52	1.84	632.8	1064 1064	2,3 1,2
KTP	mm2	n _o =1.740 n _e =1.830	r ₆₃ =23.6	80	d _{eff} =-7.34	10.22		1064	2
GaAs	43m	n _o =3.34	r ₄₁ =1.6	59	d ₄₁ =124	412	632.8	10600	2
Organic Crystals.									
Urea		n _o =1.4	r ₄₁ =1.9	5	d ₃₆ =2.3	1.6		1064	3
MNA	m	n=2.355	r ₁₁ =60 r ₁₂ =67	784 875	d ₁₁ =250 d ₁₂ =38	4875 110	1064	1064	4
MAP	P2	n=2.0			d ₂₂ =18.4	42		1064	3
POM					d ₁₄ =9.2			1064	5
NPP	P2	n=1.8			d ₂₁ =84	1210		1064	3
Poled Polymers.									
DR1/PMA	∞mm	n=1.7	r ₃₃ =42	206			632.8		6
Xlinked	∞mm	n=1.68			d ₃₃ =13.5	38		1064	7

Table 2.1. Summary of Performance of Materials for Electro-optical and Second Harmonic Generation Applications.

Ferroelectric Liquid Crystals.

SCE9	2mm	$n_o=1.5$	$d_{\gamma\gamma}=0.027$	2×10^{-4}	1064	8
Walba	2mm	$n_o=1.5$	$d_{\gamma\gamma}=0.6$	0.1	1064	9

1. Yariv A. *Quantum Electronics* J Wiley & Sons New York (1989).
2. Landort Bornstein Numerical Data *Functional Relationships in Science and Technology* Group 3 Vol 2 New York (1971).
3. Sherwood J.N., Phil. Trans. R. Soc. Lond. A **330** (1990) 127.
4. Rao S.M., Batra A.K., Lal R.B., Evans R.A., Loo B.H., Metzger R.M., Lee W.J., J. Appl. Phys **70** (1991) 6674.
5. Nayer B.K. & Winters C.S., Optical & Quantum Electronics **22** (1990) 297.
6. Described in this work.
7. Eich M., Reck B. et al, J. Appl. Phys. **66** (1989) 3241.
8. Liu J.Y., Robinson M.J. et al, Optics Lett. **15** (1990) 267.
9. Liu J.Y., Robinson M.G., Walba, D.M. et al, J. Appl. Phys. **70** (1991) 3426.

Table 2.1 contd. Summary of Performance of Materials for Electro-optical and Second Harmonic Generation Applications.

material. By careful design of the conduction band energy levels, it is possible to achieve resonant enhancement of the order of 1900 times the bulk material nonlinear coefficients [Boucaud et al, (1990)]. Of course this will have a detrimental effect on the absorption coefficient of the material. An alternative mode of operation is the use of the Stark effect. This is the modulation of the large absorption edge of the material by the application of a voltage. This has been used to produce an efficient amplitude modulation device. This effect is often enhanced by using a resonating device structure, for example the Fabry-Perot etalon structure.

2.9.2 Organic Crystals.

The organic crystal materials MNA and MAP are well established, having been developed over 14 years ago. It can be seen that the nonlinear coefficients and figures of merit are competitive with inorganic materials. Disadvantages of organic crystals are that they are often mechanically weak and have high propagation losses. Novel approaches to overcome some of these problems have been demonstrated in MNA using, for example multilayer structures where the active layer is sandwiched in a waveguide structure between glass substrates. A DAN crystal 1.7mm thick resulted in an SHG conversion efficiency of 33.5% [Huang et al, (1991)].

The material NPP was first reported in [Baden et al, (1985)] as a suitable material for second harmonic generation. This material has very attractive nonlinear properties but suffers from difficult crystal growth. The material degrades in most organic solvents, forcing crystal growth to occur from the melt. This requires a compromise between the optical quality and the growth rate of the crystal.

The problems associated with growing organic crystals are similar to those in growing inorganic crystals. There has been a great deal of research in producing crystals which can be grown to sizes of several mm³ of the correct crystal orientation and symmetry group. It is often cited that organic materials have higher laser damage thresholds than inorganic materials due to lower dielectric constants. This is far from a universal rule, although some organic materials synthesised with great care have exhibited very high damage thresholds. MAP crystal has a damage threshold of 3 GWcm⁻² for 10ns pulses at 1064nm [Baden, (1985)]. At these incident powers the quality of the optical faces is also extremely important, as these also can suffer laser damage. In practice, laser damage thresholds are often limited by the purity of the material and the growth of defect free crystals. The mature technology of crystal growth in inorganic materials such as lithium niobate probably still retain a small advantage.

Other problems with organic crystals are that they tend to be soft, making it difficult to polish the faces of the crystals, and hygroscopic so the materials degrade in quality on exposure to air. A recent development in improving the quality of organic crystals [Rao et al, (1991)] used a mixture of two well known nonlinear materials (MNA and MAP) resulting in large transparent crystals which could be readily grown with nonlinear coefficients similar to MAP, and also exhibited improved hardness compared to

crystals from the individual materials. This may offer a way of engineering the mechanical properties of organic materials by design, and thus lead to new and robust materials.

2.9.3 Poled Polymeric Materials.

To date, poled polymer systems have achieved nonlinear optical coefficients of $d_{33} = 47 \text{ pmV}^{-1}$ [Swalen, (1992)] by applying electric field strengths close to the breakdown strength. These very large field strengths achieve a polar order parameter of about 0.2 for the side chains due to the low efficiency of the poling technique. A study into the processes which occur when poling, and attempts to improve the efficiency of the technique will be discussed in chapter 3, and so will not be discussed in detail here.

There are many poled polymeric materials with nonlinear coefficients of the same order of magnitude as those which have been quoted [Singer et al, (1988), Eich et al (1989B)]. A large range of nonlinear molecules have been co-polymerised into a number of glassy polymers, such as poly methylmethacrylate (PMMA) or polystyrene (PS). Further variations arise from the range of concentrations of nonlinear dopants used, and the magnitude of poling fields applied. The figures quoted in the table above are the long term stable values after any initial relaxation has occurred.

Much work has been carried out to improve device lifetimes to usable levels by reducing the relaxation of the induced order. At the beginning of this study devices were being reported with nonlinear coefficients of $d_{33} \approx 20 \text{ pmV}^{-1}$ and projected lifetimes of months. These have now been improved to levels of $d_{33} > 40 \text{ pmV}^{-1}$. This has been achieved by many developments in the materials. Glass transition temperatures have been raised from approximately $< 100^\circ\text{C}$ (PMMA) to over 150°C , and are increasing further. This improves the stability of the induced order significantly, and allows additional processing to occur at moderate elevated temperatures (up to 100°C) without significant loss to the induced order [Man et al, (1990)]. A technique of crosslinking the polymer to raise the glass transition and chemically bond to lock in the order has been demonstrated [Eich et al, (1989A)]. Reactive groups specifically designed into the polymer can be stimulated by either uv or thermal radiation to form a polymer matrix whilst the poling field is present, thereby locking the induced order. Some devices produced using this technique offer excellent stability, even at elevated temperatures.

Polymeric materials have the potential of being produced in large quantities at low expense. Many of the process steps require technology which is readily accessible, and can be automated. The devices fabricated from poled polymers are usually in a thin film structure with thicknesses between 1 and $200 \mu\text{m}$. The surface roughness can be less than $\lambda/10$ by using high quality substrates or compression plates, removing the requirement for polishing the optical facets. Waveguides are easily fabricated, and although waveguide losses at the present time are unacceptable, it is expected that acceptable levels ($< 0.1 \text{ dBcm}^{-1}$) are achievable.

2.9.4 Ferroelectric Liquid Crystals.

The nonlinear optical coefficients of the ferroelectric liquid crystal material are preliminary values. The material SCE9 is a commercial mixture of liquid crystals developed for display applications of which only 10% is chiral material, and has not been optimised for nonlinear properties. The development of pure materials which exhibit a chiral smectic C phase immediately improves the number density of nonlinear groups, and should be reflected in a large increase in the nonlinear coefficient. The ability to align the material by having nematic and smectic A phases above the smectic C phase can suffer in these single component materials. There is also very little control of the helical pitch of the material which can also disrupt alignment.

The largest problem in using ferroelectric liquid crystals is that the only component of the molecule which possesses the correct symmetry, and thus has a non-zero β , is a transverse component parallel to the P_S . The long conjugated electron system along the length of the molecules cannot be exploited. Transverse groups can be added to the chiral centre to increase P_S or β , but there is a limitation to the size of these groups before the smectic phase becomes disrupted. A novel approach pioneered by Walba et al [Liu et al, (1991)] was to use overhanging groups from a phenyl ring close to the chiral centre to hinder the rotation of the chiral centre with respect to the phenyl ring. This may then maintain the phenyl ring at a given angle with respect to the chiral centre and P_S , allowing the delocalised electrons of the ring to contribute towards the transverse β . Additional push-pull groups may also be added across the phenyl ring to further enhance β . Materials of this type have been developed for this thesis, and will be described in chapter 4.

2.10 Overview of Electro-Optic Materials.

Over the past three years organic materials have developed considerably. They are now beginning to fulfil their potential in the field of nonlinear optics by demonstrating a range of devices which compare well with alternative materials such as inorganic crystals. Molecular engineering techniques have been very useful in developing novel molecules with large molecular hyperpolarisabilities.

The ability of liquid crystal molecules to self assemble into partially ordered phases has yet to be fully exploited in the field of nonlinear optics. Researchers working with poled polymer materials had looked to liquid crystal polymers to improve the bulk nonlinear coefficient without the need to develop even higher nonlinear hyperpolarisabilities. Despite a theoretical gain of 5 in the nonlinear coefficient, experiments demonstrated gains less than 2. Associated with these gains were additional problems; mainly due to the inherent properties of liquid crystals - the large birefringence and high scattering losses, which reduce device performance and at the present moment, outweigh the benefits. If these problems can be

overcome by developments in the material other than for larger nonlinear coefficients, then liquid crystal polymers will be competitive.

Chiral smectic C liquid crystal materials are still a long way from challenging current nonlinear optical devices. The limitation in this case is not the polar order but the magnitude of the transverse molecular hyperpolarisability which is not forbidden by symmetry. This has been improved by several orders of magnitude, but is still lower than alternative materials. The device geometries required to align these materials are quite limiting for device applications unless additional processing such as cross linking is carried out to stabilise the alignment.

It should also be pointed out that developments have also been made in the competing material classes, particularly inorganic crystals. There are new materials continually emerging with improved nonlinear coefficients or improved physical properties, and excellent device engineering has overcome some of the earlier limitations. If organic materials are hoping to displace established materials such as lithium niobate, then further developments are necessary, particularly in device fabrication techniques and optical losses in the materials.

3. Dynamics of Poling in Side Chain Polymers.

The low efficiency of the technique of poling suggests the possibility of improvement of the bulk nonlinear coefficients without the expense of complex molecular engineering to improve the molecular hyperpolarisability. There have been many novel molecules designed and synthesised with very promising nonlinear coefficients by increasing the conjugation in the molecule. This has the disadvantage of increasing the absorption wavelengths. There has been very little work reported in the literature about the poling mechanisms and the dynamics of poling. Any developments to the poling process would probably have benefits to all materials and devices currently in use in the field of nonlinear optical polymers. In this chapter I shall describe a simple experiment to investigate the dynamics of the poling technique, in order to understand the reorientational mechanisms which occur in the material when it is poled. Knowledge of these mechanisms will assist in establishing the limitations of the poling technique, and develop possible methods of overcoming these problems.

3.1 Measurement of the Induced Non-linear Optical Coefficient.

The linear electro-optical effect, or Pockels effect was used to measure the degree of induced non-centrosymmetry in side chain polymeric materials when large electric fields were applied. The principle of the experiment was to modulate one plane of polarisation with respect to its orthogonal counterpart, and measure the induced phase delay between the two polarisations.

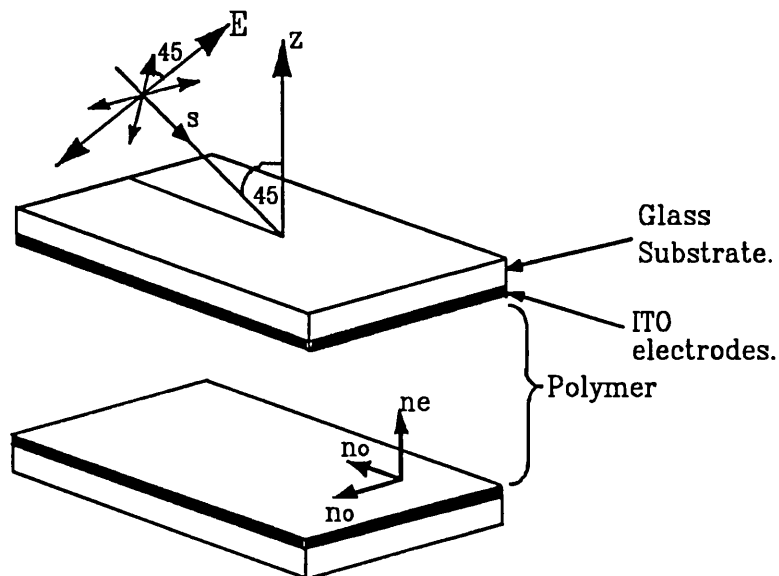


Figure 3.1 Device arrangement.

A planar cell arrangement was used, as shown in figure 3.1. The electric field could most easily be applied perpendicular to the cell (designated the z axis) using transparent indium tin oxide (ITO) electrodes. The electrodes were used not only to pole the sample and orientate the molecules but also to modulate the extraordinary refractive index, which had been induced by poling along the z axis.

The molecules in a nematic phase are approximated to be long, thin, rod-shaped objects. The point group ∞mm describes molecular systems which contain a unique axis (z axis) about which there is an infinitesimal rotational symmetry (∞) and two mirror symmetries (mm), one parallel to the long axis and one perpendicular to it. The dominant hyperpolarisability tensor component is along the long axis of the molecule, β_{zzz} . When an electric field is applied parallel to the z axis, the one dimensional molecule approximation reduces the number of non-zero electro-optic coefficients r_{33} and r_{13} , which modulate the extraordinary refractive index n_e and the ordinary refractive index n_o respectively. The difference in modulation from the two coefficients is described by r_{eff} , the effective (and usable) non-linear coefficient.

Light was passed through the cell at an angle to the cell normal which was chosen to be 45° . Incident light polarised in the plane containing the cell normal (TM) would access a combination of the ordinary and extraordinary refractive indices, n_x , as shown in figure 2.2. Light polarised in the orthogonal plane (TE) experienced only the ordinary refractive index, n_o .

The light passed through the sample was plane polarised at an angle of 45° to the plane of incidence, as shown in figure 3.1. The polarisation can be resolved into two components, one interacting with only the ordinary refractive index which had a small degree of modulation, and the other interacting with the refractive index n_x . This latter component had a larger modulation through its dependence on n_e . Because the two refractive indices seen by the two polarisations were unequal, then the light emerged from the sample with an elliptical polarisation, the phase difference between the two paths being

$$\delta = 2\pi(n_x - n_o)h / \lambda$$

where h was the thickness of the sample. It can clearly be seen that a difference in modulation between n_o and n_x would result in the phase delay δ being modulated.

There is an optimum condition for light to couple from the input polarisation to its orthogonal counterpart and hence through the analyser, when the total phase delay is increased to $\pi/2$, the condition of circular polarisation. In this position, the experiment was most sensitive to the modulation of the phase delay as illustrated in figure 3.2.

A Babinet Soleil compensator was used to adjust the total phase delay to $\pi/2$. The compensator was calibrated so a measurement of the extra phase delay introduced allowed a calculation of the birefringence of the material. The details of this measurement are given in section 3.4.2.

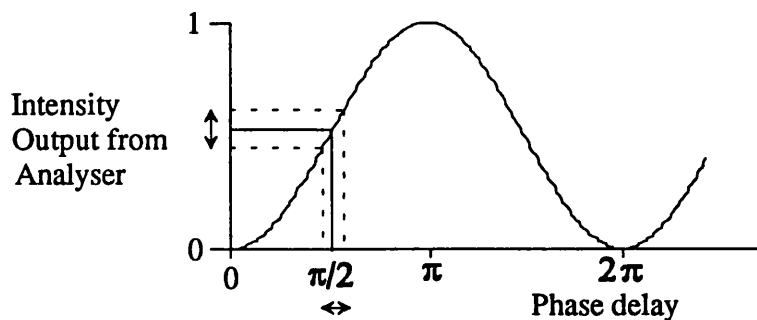


Figure 3.2. Modulation dependence on phase delay.

3.2 Preparation and Evaluation of Nonlinear Optical Copolymers.

The materials used in this study were developed and synthesised initially by GEC-Marconi Ltd for earlier work at GEC-Marconi [Griffith et al, (1991)] to obtain a suitable polymeric material which had useful nonlinear optical properties. All poled polymer experiments described in this work used the same material, which had been synthesised later in bulk by Merck Ltd.

The material selected was a copolymer of two monomeric compounds, one of which imparted liquid crystalline properties, and the other nonlinear optical properties. The nonlinear optical monomer was based on Disperse Red 1 (DR1) incorporating a polymerisable acrylate group via an ester linkage. It has the code 2/ANAS and its chemical structure is shown in figure 3.3.

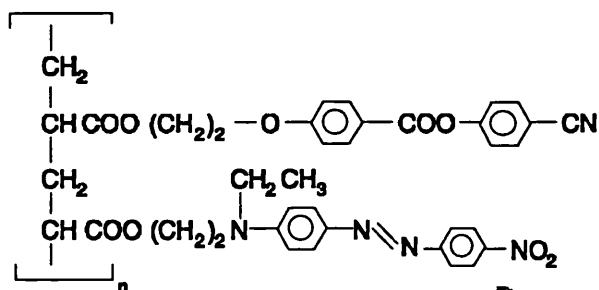


Figure 3.3 Chemical structure of copolymer used.

The liquid crystalline monomer used was A/20CPB or using its full name 4 - (2 - acryloyloxyethoxy) benzoic acid - 4' -cyanophenyl ester. The copolymer had an acrylate backbone with two methyl units separating the backbone from the mesogenic units.

The polymerisation technique used was a free radical polymerisation using AIBN as the thermal initiator. The polymer was purified by column chromatography and recrystallisation from tetra-hydro-furan

(THF) solvent. The polymer was investigated by GEC-Marconi and Merck (UK) Ltd using the following range of techniques.

1. Differential Scanning Calorimetry (DSC) and Optical Microscopy were used to measure phase transition temperatures and identify phases. A DSC trace of the polymer is shown in figure 3.4. The glass transition temperature was measured to be 79°C.
2. Gel Permeation Chromatography was used to characterise the molecular weight and polydispersity of the polymer. The polymer had a molecular weight M_w of 5000 units, and its $M_n = 3550$, giving a polydispersity ratio of 1.4. The degree of polymerisation gave a chain length of 10 units. Experiments [Hollingshurst, (1992)] have indicated that glass transition temperatures and nematic to isotropic transition temperatures do not saturate until chain lengths reach about 100 units or more. However it was shown that the material produced had a consistent chain length resulting in well defined transition temperatures.
3. The determination of the polymer composition was estimated from molar extinction coefficients using a Perkin Elmer Lambda 9 uv/vis spectrophotometer. A 29% loading of nonlinear optical mesogens was measured.

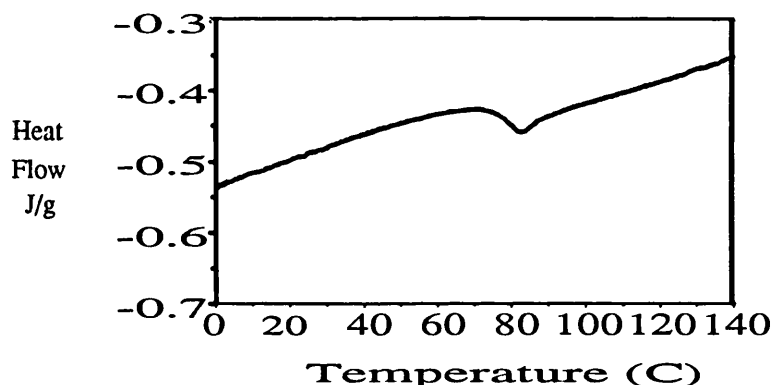


Figure 3.4 DSC of NLO polymer.

3.3 Preparation of Thin Film Samples.

A device structure was developed for the experiments in order to obtain a high optical quality film over a reasonable area (several mm^2) with a range of uniform thicknesses. The fabrication technique used was thermal compression where the polymer was sandwiched between two glass slides and compressed at elevated temperatures.

The cell fabrication was undertaken in a clean environment using ultraclean glass substrates. The polymer was heated under vacuum for several hours to remove any dissolved gases and solvent. The smallest of traces of solvent or gas appeared as voids in the material when the cells were assembled, and

also later after repeated temperature cycling. These voids prevented the application of very large electric fields due to the lowered breakdown threshold, and increased optical scatter in the cells resulting in a lower efficiency of the device.

The substrates used for the devices were 3mm thick optical quality glass which was both flat and resilient to distortion, onto which indium tin oxide (ITO) transparent electrodes had been deposited and etched. To ensure that the substrates were parallel on assembly, quartz spacers were distributed over one of the substrates. Spacers were sucked from the active area before assembly using a vacuum, as it was found that the spacers reduced the breakdown threshold of the device when poled. The polymer in solution was deposited over the active area of the other substrate, and the solvent removed by baking under vacuum overnight. The thermal compression cells were then assembled taking great care to align the active area, and the top substrate was compressed down onto the spacers by applying weights to the device and heating. However, even after heating the polymer to 50°C above its glass transition temperature, compression of the polymer to give a uniform thickness was difficult.

Solvent based techniques for producing thin films was also investigated. Dipped samples were produced by lowering a glass slide into a polymer solution and were then withdrawn carefully. A uniform film of high optical quality was produced if it was withdrawn from the solution at a constant rate. However repeated dipping to increase the film thickness resulted in a wedge film due to redissolving of the layers. This limited the thickness of the dipped films to around 1µm.

3.4 Measurement of Refractive Indices.

A high quality, uniformly flat device was essential for characterising the material. The device chosen was approximately 20 µm thick and had been poled with a voltage of 170 Vµm⁻¹ for 1 hour at 75 °C.

3.4.1 Measurement of n_0 .

The optical thickness of the film was measured using a Perkin Elmer Lambda 9 spectrophotometer by measuring interference fringes produced from reflections from the front and back faces of the cell as a function of wavelength. The interference fringes were enhanced by using partially reflecting silver layers on the substrates. These measurements give the thickness from empty areas of the cell with an accuracy of ±0.2 µm for a device typically 1-10 µm thick, and refractive indices to an accuracy of ±0.02 at best.

The material was also investigated using a spinning polarisor ellipsometer, which gave refractive index and thickness information over the wavelength range of 250-850 nm. This measurement required the removal of one of the substrates to reveal a bare polymer interface of high optical quality. The

measurement was made at an angle of incidence of 60°, close to the critical angle to increase the reflection signal. Analysis of the data indicated a slight dispersion in n_o , its value being 1.62 at 850nm, and rising to 1.69 at 630nm, as shown in figure 3.5. Accuracy was limited to ± 0.01 due to the imperfect model used to calculate the refractive index of the film. The thickness measurement gave a value of 18 μm , but was only accurate to 1 μm . An independent measurement of thickness was made using a Tencor Alpha-Step thickness measuring instrument which scanned a mechanical stylus across the sample. The thickness of the polymer film was measured with an accuracy of 0.1 μm , and scatter in the measurements taken at different positions on the film suggested a film flatness of $\pm 0.15 \mu\text{m}$.

The ordinary refractive index of the copolymer exhibits a small amount of dispersion due to an absorption band in the blue/green region of the spectrum with $\lambda_{\text{max}} = 480 \text{ nm}$. The data was fitted to a two parameter Sellmeier dispersion formula as given in equation 3.1.

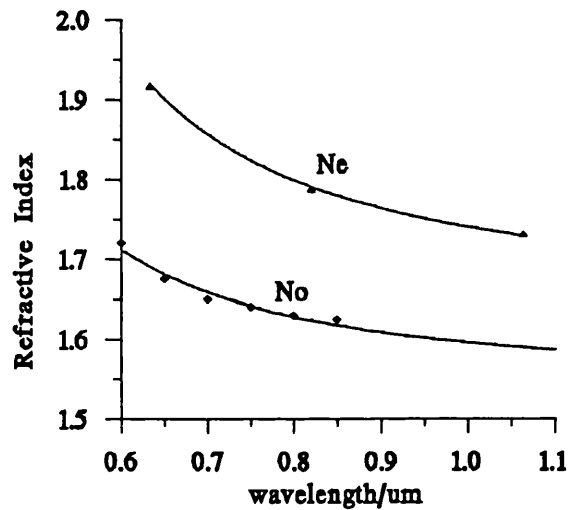


Figure 3.5 Dispersion in refractive indices of NLO polymer.

$$n^2 - 1 = \frac{A_1 \lambda^2}{\lambda^2 - B_1} \quad 3.1$$

The Sellmeier equation calculates dispersion based on a two level quantum model. The Sellmeier coefficients were calculated by a least squares fitting routine (NAG E04FDF). The coefficients were calculated to be

$$A_1 = 1.392$$

$$B_1 = 0.101$$

and the theoretical curve is also shown in figure 3.5.

3.4.2 Measurement of n_e .

The extraordinary refractive index was calculated from the phase delay between light polarised to access the ordinary refractive index, and light polarised to access the extraordinary refractive index. Light was introduced into the material at an angle i to the normal of the cell along a direction defined by the unit vector s , as shown in figure 3.1, where $n_x(\theta_x)$ is the refractive index seen by the extraordinary ray at an angle θ_x from the optic axis

$$n_x(\theta_x) = \left[\frac{\cos^2 \theta_x}{n_o^2} + \frac{\sin^2 \theta_x}{n_e^2} \right]^{-1/2}. \quad 3.2$$

Refraction must be taken into account at the boundaries of the cell structure, and so from Snell's Law

$$n_x(\theta_x) \sin \theta_x = \sin i \quad 3.3$$

$$n_o \sin \phi_o = \sin i \quad 3.4$$

θ_x is the angle of refraction for the extraordinary ray, ϕ_o is the angle of refraction for the ordinary ray, and i is the angle of incidence at the cell surface. Eliminating n_x from equations 3.2 and 3.3 gives

$$\tan \theta_x = \frac{n_e \sin i}{n_o (n_e^2 - \sin^2 i)^{1/2}}. \quad 3.5$$

From Born and Wolf [1980], the phase delay between the extraordinary ray and ordinary ray, after travelling through a uniaxial material of thickness h , when light is incident at an angle i , is

$$\delta = \frac{2\pi h}{\lambda} (n_x \cos \theta_x - n_o \cos \phi). \quad 3.6$$

If the phase delay is increased up to $\pi/2$ by including a Babinet Soleil compensator, the resultant light is circularly polarised. The phase delay δ introduced by the cell can be measured from the shift in null positions of the compensator as a fraction of the delay equal to one wavelength. Eliminating θ_x and rearranging for n_e gives

$$n_e = \frac{\sin i}{\left[1 - \frac{1}{n_o^2} \left(\frac{\delta \lambda}{2\pi h} + n_o \cos \phi_o \right)^2 \right]^{1/2}}. \quad 3.7$$

Using equation 3.4 to eliminate ϕ_o gives

$$n_e = \frac{\sin i}{\left[1 - \frac{1}{n_o^2} \left(\frac{\delta\lambda}{2\pi h} + (n_o^2 - \sin^2 i)^{1/2} \right)^2 \right]^{1/2}} \quad 3.8$$

Therefore n_e can be calculated from four known variables: i , n_o , δ , and h . The extraordinary refractive index as a function of wavelength is shown in figure 3.5, together with the fitted curve from the two parameter Sellmeier model. The parameters were calculated to be

$$A_1 = 1.745 \quad B_1 = 0.144.$$

3.5 The Experimental Arrangement to Measure r_{eff} .

The electro-optic coefficient of the polymer was measured using apparatus shown in figure 3.6. The quarter wave plate and polariser were used to produce plane polarised light at any angle defined by the polariser in the plane normal to the optic axis of the experiment. This light was then incident on the sample in the configuration discussed earlier in section 3.1. A Babinet Soleil compensator was used to measure the birefringence of the sample, and also increased the phase delay between the two polarisations to give circular polarised light, verified by the analyser.

A sample which had been previously poled was measured with a small a.c. voltage applied (squarewave, 5 kHz, 40 V_{ptp}) to induce a modulation of the birefringence of the device. The phase modulation was converted to an intensity modulation by the analyser which was then detected by a silicon PIN photodiode and lockin amplifier. The modulation signal from the lockin amplifier was divided by the average signal from the detector using an electronic divider to normalise the signal.

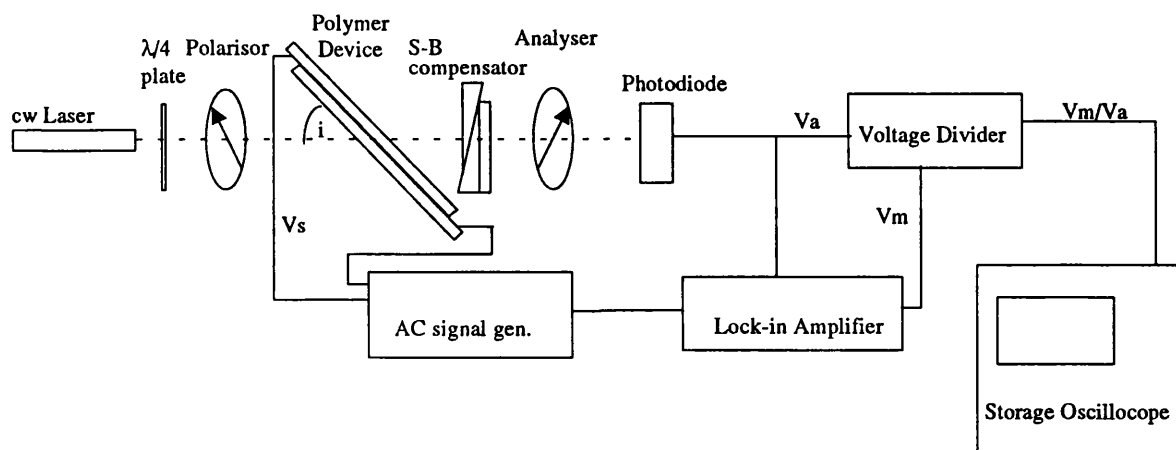


Figure 3.6 The electro-optic experiment.

Appendix B derives equation 3.9 which describes how the electro-optic coefficient r_{eff} is calculated from measured parameters.

$$r_{\text{eff}} = \frac{\lambda}{\pi n_o V_s \sin^2 i} \frac{V_m}{V_a} \left(1 - \frac{\sin^2 i}{n_e^2} \right)^{1/2} \quad 3.9$$

A 1mm thick sample of z-cut lithium niobate was measured to verify the experimental accuracy. It was assumed that z-cut lithium niobate was isotropic, and the modulating field was applied along the z axis, so making it comparable to the poled polymer materials. Assuming an average refractive index of $n=2.25$ then the r_{33} coefficient was measured to be $33 \pm 3 \text{ pmV}^{-1}$. This is in good agreement with accepted values of 31.8 pmV^{-1} within the scientific literature, taking into account the experimental accuracy of 10%.

3.6 Dispersion in the Electro-Optic Coefficient.

The electro-optic coefficient was measured in a thermal compression cell filled with the copolymer from 2/ANAS and A/20CPB which had earlier been poled at $170 \text{ V}\mu\text{m}^{-1}$ for one hour at 75°C . Table 3.1 shows the measured electro-optic coefficients at a number of wavelengths, illustrating the dispersion in the electro-optic coefficient.

Wavelength (nm)	Electro-Optic Coefficient (pmV^{-1})
632.8	43
820	11
1064	8

Table 3.1.

The dispersion in the electro-optic coefficient arises from the variation in hyperpolarisability β as a function of the wavelength of the incident light. In the simple approximation of a two level quantum model, the expression describing β is given by [Zyss, (1987)]

$$\beta(-\omega_3, \omega_1, \omega_2) = \frac{3e^2 \hbar^2}{2m} f \Delta\mu F(W, \omega_1, \omega_2, \omega_3)$$

where f contains the local field factors, $\Delta\mu$ is the difference in dipole moments between the two levels, and $F(W, \omega_i)$ is the dispersion term, defined as

$$F(W, \omega_1, \omega_2, \omega_3) = \frac{W[W + (\hbar^2 \omega_1 \omega_2 - \hbar^2 \omega_3^2) / 3]}{[W^2 - (\hbar \omega_1)^2][W^2 - (\hbar \omega_2)^2][W^2 - (\hbar \omega_3)^2]} \quad 3.10$$

where W is the energy of the excitation, and ω_{1-3} are the frequencies of the three interacting electric fields. In the electro-optic modulation case, $\omega_1 = \omega_3 = \omega$, and $\omega_2 = 0$. Figure 3.7 shows the experimental and numerical fitting to the r_{eff} data using equation 3.10. The numerical fit suggests a value for W of 2.235 eV, which corresponds to an absorption at around 550 nm, which is in reasonable agreement with the measured absorption at 480 nm, given the few data points.

As the wavelength approaches the absorption band of the molecule, both the polarisability and the hyperpolarisability undergo resonant enhancement. This resonant enhancement has been seen in many organic systems [Singer et al, (1987); Mohlmann et al, (1989)], and is a feature of highly asymmetric

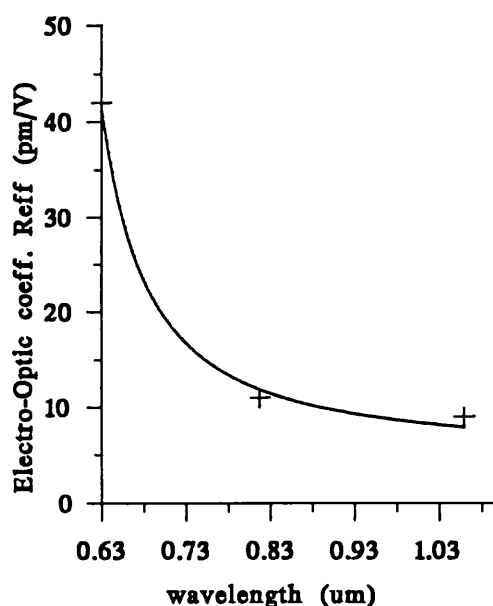


Figure 3.7 Dispersion and two level theoretical fit to r_{eff}

excited state π -electron systems which are the dominant contributor to β in these molecules [Teng & Garito, (1983)]. A discussion of these effects was held in chapter 2 and concluded that the resonant enhancement in the non-linear coefficient cannot be fully exploited because as the absorption edge is approached, the losses in the device increase and laser damage to the material can occur.

3.7 Dependence of the Non-linear Coefficient with Poling Voltage.

The poling field dependence on the induced electro-optic coefficient in the material used in this study is shown in figure 3.8. No nonlinear dependence was detected within the poling field limit achievable in this work ($75 \text{ V}\mu\text{m}^{-1}$). An earlier report [Griffith et al, (1991)] had indicated that a nominally similar polymer, although amorphous, could exhibit an unusually large order parameter when poled. The effect seen on the induced electro-optic coefficient was a non-linear step in the r_{eff} at a poling field strength above $50 \text{ V}\mu\text{m}^{-1}$.

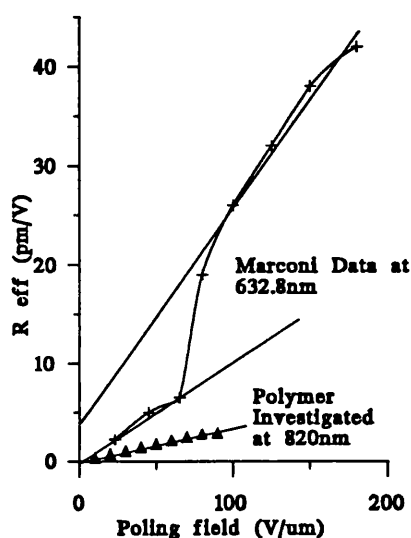


Figure 3.8 Induced electro-optic Modulation as a function of applied poling field.

Other similar copolymers with larger proportions of mesogenic groups had exhibited nematic phases above the glass transition. The unusually large degree of order in the nominally identical material was suspected to be a result of a nematic to isotropic (N-I) transition which was masked by the glass transition of this polymer. The effect of lowering the phase transitions of mesophases in copolymers until they are masked by a glass transition has also been seen elsewhere [Kiode et al, (1991)].

To confirm the theory of an underlying mesophase in the material, an attempt was made reveal the suspected N-I transition in the polymer by plasticising the glass phase of the polymer and thus depressing T_g . This can usually be achieved by mixing the polymer with a monomer of a similar structure which allows it to mix well with the polymer structure. However, the monomer could not be fully mixed with the polymer either by mixing at elevated temperatures or by using a solvent, resulting in unreproducible phase transitions in the DSC traces.

A likely explanation for the difference in poling behaviour between the two polymers is that although they had the same chemical structure, the two materials were not identical. To specify a polymer,

information such as the degree of polymerisation, the number and weight average molecular weight (M_n & M_w) and the polydispersity must be specified. This data is often not given in the literature. In this case, it was suspected that the polydispersity of the earlier material was greater than the material used here, resulting in a slightly lower glass transition (4°C lower) and increased mobility in the polymer below T_g .

If the non-linear dependence on poling field was reproducible, then it may be used to improve the efficiency of the poling technique. By applying voltages above and below the nonlinear threshold, it may be possible to pole the material whilst minimising charge injection. Charge is usually injected into the polymer as it is poled and can result in charge double layers which reduce the internal poling field experienced by the polymer. The technique to reduce this effect will be discussed in more detail in section 3.11.

3.8 Dynamic Measurements of Poling Processes.

An investigation of the poling mechanisms required a study of the dynamics of the system as poling occurred. The rate at which the noncentrosymmetric ordering was induced and then relaxed would indicate which components were re-orienting, and give information about the re-orientation mechanism. The experiment was modified, as shown in figure 3.9, so that whilst the small modulating signal was present, a large poling field could also be applied to the device. This poling voltage was mixed with the modulation signal, before being amplified to its final amplitude using a high voltage x50 amplifier.

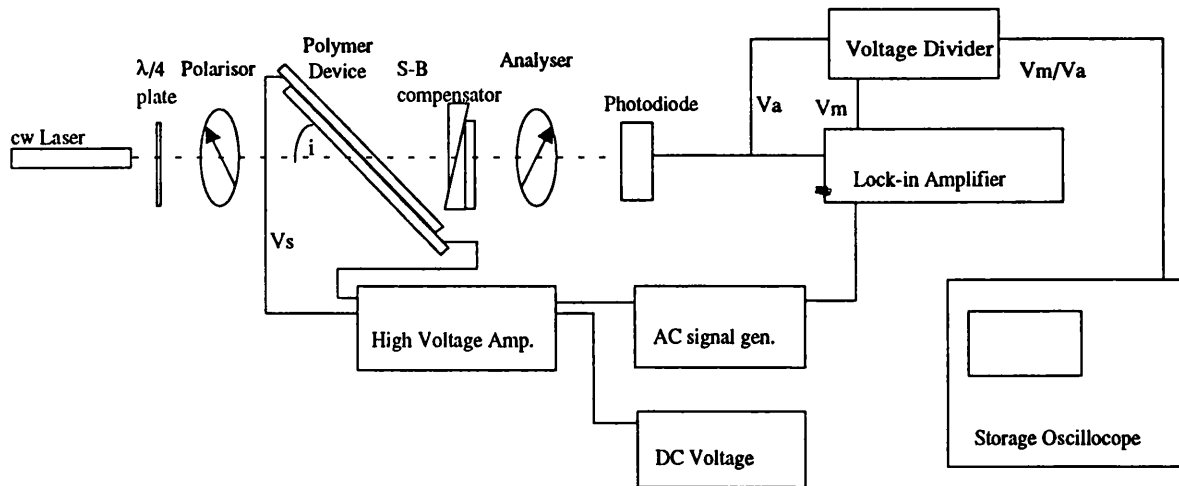


Figure 3.9 The dynamic poling experiment.

A further modification allowed the sample to be contained in a Mettler thermal management system (FP80/82) to allow temperature dependence measurements. The voltage used to pole polymer materials to achieve maximum non-centrosymmetric alignment can be up to $200 \text{ V}\mu\text{m}^{-1}$. However this is normally increased slowly from a moderate level to prevent shorting of the devices due to power surges. In this experiment the maximum voltage switched directly onto the cell was $75 \text{ V}\mu\text{m}^{-1}$ to prevent damage.

A lithium niobate sample was used to evaluate the response times of the experiment. The electro-optic effect in lithium niobate has a bandwidth limited by the RC charging time constant, where C is the capacitance of the device ($\sim 5 \times 10^{-11} \text{ F}$), and R is the resistance in the driving circuit (50Ω). The rise and decay time was less than 1 ns, which was much faster than the dynamic response of the experiment. The limiting experimental response time was found to be the lock-in amplifier with 3 ms response, which could be improved at the expense of sensitivity. A large, low noise signal such as that from lithium niobate gave the minimum experiment response time of 3ms, but smaller signals from polymeric devices required a higher sensitivity and limited the response time to 40ms. The time constant associated with charging the capacitance of the device was calculated to be less than 100ns and so assumed to be instantaneous.

A standardised technique was developed to measure the growth and decay of the nonlinear optical component r_{eff} . It was noticed that the electro-optic response was dependent on the thermal history of the device. A shortage of polymer material resulted in it being necessary to recycle samples.

Between each poling cycle the cell was heated to $20 \text{ }^\circ\text{C}$ above its glass transition for 10 minutes whilst the cell was shorted. This ensured the material was fully relaxed into its isotropic phase and did not retain any non-centrosymmetric ordering previously induced. After a large number of temperature cycles the magnitude of the electro-optic signal decreased. This was attributed to the formation of microscopic voids seen in the polymer material. These have the effect of reducing the effective area of the device and increasing scattering losses. The effect was more noticeable in thermal compression cells than for dip coated samples where one surface is free for solvent to evaporate. The formation of the voids was probably due to residual solvent leaving the polymer, or due to material breakdown. Neither of these effects would affect final devices because they would not be temperature cycled.

The electro-optic coefficient was monitored by recording the ratio of the modulation signal amplitude V_m (from the lockin amplifier) to the mean intensity V_a . This ratio was directly proportional to the electro-optic coefficient if it was assumed that the induced birefringence is small. This was reasonable because the poling voltages applied in this experiment were much smaller than those normally used in poling polymers. The ratio V_m/V_a was recorded on a digital sampling oscilloscope, permitting a maximum record length of 1000 seconds at a sampling rate of 1 sample per second. The data was stored on a personal computer for later comparison with numerical data fitting routines. Poling voltages were normally applied for a fixed period of 500 seconds.

The modulating voltage applied to the cell was a square wave signal at 5 kHz with a peak to peak amplitude of $1 \text{ V}\mu\text{m}^{-1}$. Early investigations suggested that this frequency was optimum as at lower

frequencies molecular reorientation occurs and at higher frequencies the sensitivity of the lock-in amplifier falls away.

The measurements were usually made at a wavelength of 820 nm, although other wavelengths were also used. This choice of this wavelength, and not 632.8 nm was because residual absorption in the material resulted in additional modulation effects, which will be described in more detail later in this chapter.

3.9 Results of Dynamic Measurements.

Initial studies were carried out to investigate a fast and a slow reorientation mechanism previously reported [Hampsh et al, (1990)]. The growth and decay of the electro-optic coefficient is shown in figure 3.10 for a 3 μ m cell poled at 100 V ($\sim 35 \text{ V}\mu\text{m}^{-1}$) at 75°C. Both the form and the amplitude of the alignment and relaxation processes were identical to within experimental resolution for the same temperature. This suggests that the same mechanisms are limiting the poling as allowing the induced order to relax.

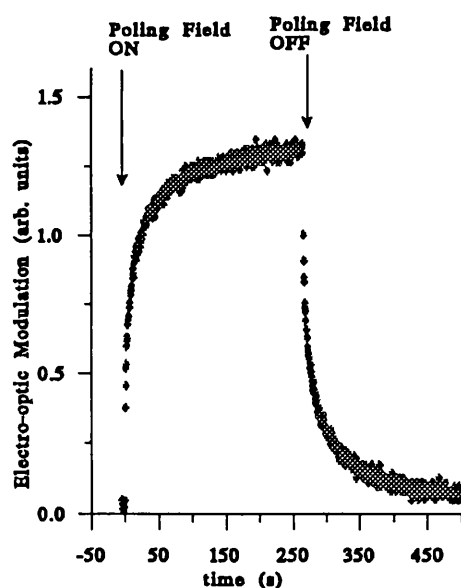


Figure 3.10. Poling and Relaxation of Side Chain Polymer at 75° C.

Wu [1991] points out that the force experienced by a dipole in an applied field is dependent on its orientation with respect to the applied field, which is not the case for the relaxation of the alignment. This would suggest that the two processes are inherently different. Within the limits of this experiment this was

not observed, noting in particular the limited size of electric field together with the very high viscosities [$\sim 10^{13}$ poise, Cohen & Grest, (1979)] of these materials would minimise these effects.

3.9.1 Above the Glass Transition.

Measurements of the electro-optic coefficient as the poling voltage was switched on followed the expected two component mechanism which can be modelled by a double exponential equation of the form

$$y = A \left(1 - \exp \left(-\frac{t}{\tau_A} \right) \right) + B \left(1 - \exp \left(-\frac{t}{\tau_B} \right) \right) \quad 3.11$$

where A , B , τ_A , τ_B are parameters to be fitted. This form of the equation describes two distinct Debye type processes which have individual amplitudes A & B , and characteristic time constants τ_A & τ_B . Sample data is shown in figure 3.11 together with a best fit solution. The amplitudes A & B exhibited a linear dependence on the applied electric field, but the time constants τ_A & τ_B did not exhibit any dependence on the poling field within the limitations of the experimental apparatus ($75 \text{ V}\mu\text{m}^{-1}$). The two processes have been attributed to (i) a fast reorientation of the side chain groups within the confines of a volume defined by the nearest neighbours, and (ii) a thermal diffusion type reorientation of the side groups in response to the applied electric field [Rusch & Beck, (1969)].

At the molecular level it is proposed that the fast initial rise in the coefficient was a result of the side chain groups partially reorienting within the free volume of the group. The free volume of a group [Laidler, (1982); Meredith et al, (1982)] describes a volume which the side chain group occupies, defined by its surrounding molecular groups. Within it a small amount of motion is possible without disturbing the nearest neighbours. The speed of this reorientation was found to be constant within the experimental resolution of the experiment. The amplitude increased with temperature as expected, in line with the increase in the thermal free volume.

The slow component of the rise in electro-optic coefficient was explained by the large angle reorientation of the side chain groups via thermal diffusion mechanisms [Valley et al, (1990)], disturbing the surrounding backbone and side groups. The torque experienced by the side groups in an external field is equal to $\mu \cdot E$, where μ is the permanent dipole on the group. This provides a potential energy gradient for the side groups, which rotate to realign along this preferred direction via a diffusion mechanism. This rotational diffusion mechanism is limited by the viscosity of the polymer. As the temperature was increased, the characteristic time constant decreased. Close to the glass transition, viscosity exhibits a strong temperature dependence. It varies from approximately $\eta \sim 10^4$ poise above T_g to $\eta \geq 10^{13}$ poise below the transition [Cohen & Grest, (1979)], diverging from Arrhenius behaviour.

3.9.2 Below the Glass Transition.

Polymers in the glass phase are not in thermal equilibrium. The free volume model of a polymer [Rusch & Beck, (1969)] describes a volume w_f which is in excess of the free volume at thermodynamic equilibrium v_f and is available for redistribution. The volume w_f represents the portion of the total free volume V_f which will relax out of the polymer given a sufficiently long period of time.

When the polymer enters the glass phase, polymer backbone mobilities are reduced by several orders of magnitude (or 'frozen out'). However, very close to the glass transition the side chain groups have a limited degree of mobility, and can be reoriented by applying large electric fields. It has been reported [Esselin et al, (1988)] that the optimal temperature for poling is at several degrees below T_g , where thermal disordering mechanisms are lower, but there is sufficient mobility to allow the side chains to align. When trying to model the dynamics of the poling process at temperatures below T_g , it was found that the experimental data deviated from the double exponential function described earlier, particularly over the longer time periods, as shown in figure 3.12. The data suggested a Kohlrausch-Williams-Watts (KWW) [Williams & Watts, (1970)] stretched exponential function of the form

$$y = A \left(1 - \exp \left(- \frac{t^B}{\tau_A} \right) \right) \quad 0 \leq B \leq 1 \quad 3.12$$

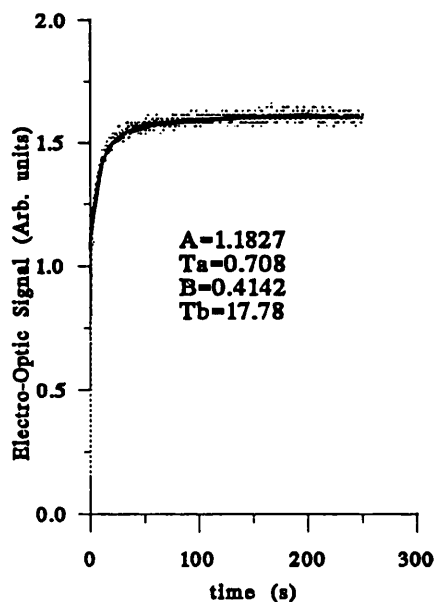


Figure 3.11 Poling at 85° C and numerical fit of the form in equation 3.11.

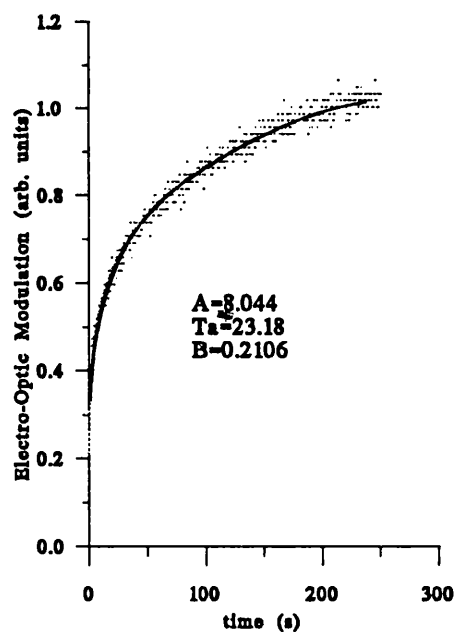


Figure 3.12 Poling at 70° C and numerical fit of the form in equation 3.12.

where A , B & τ_A are parameters to be fitted. This function has been used to describe non-Debye type relaxation processes, for example a system which has a distribution of transition energy levels. This is unlike classical Debye type processes which are based upon single transitions. The parameter B is reported to exhibit a temperature dependence [Dattagupta, (1987)], and our data exhibits this as shown in figure 3.13. This illustrates that as the temperature is reduced below the glass transition, the polymer moves farther away from thermal equilibrium.

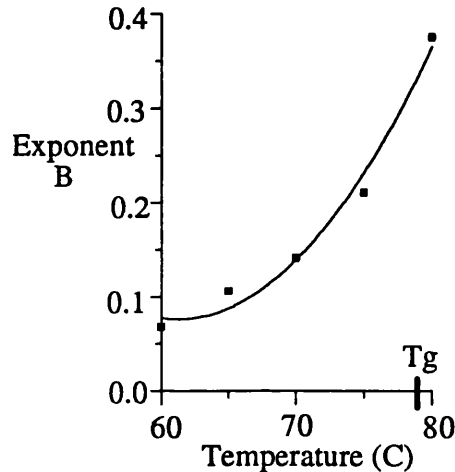


Figure 3.13 Parameter B as a function of temperature.

A model for the polymer glass which can account for the temporal data following the form of the KWW stretched exponential is outlined here. The transition into the glass phase is a second order transition, and is spread over approximately 10°C , as shown in the DSC trace in figure 3.4. It is possible that this temperature range results in molecules having slightly different thermal organisations when they enter the glass phase, at which time their ordering is quenched. Any applied field to induce order in the material would then compete against a distribution of thermal energies, and the poled polymer glass would exhibit a distribution of relaxation energies and times.

3.9.3 Poling Efficiency as a Function of Temperature.

The dependence of the degree of poling on the thermal free volume of the polymer can be measured by varying the electro-optic coefficient as a function of temperature. In this experiment, a polymer device was heated to 85°C and poled at $50 \text{ V}\mu\text{m}^{-1}$. The electro-optic coefficient was monitored and seen to saturate. Once the maximum coefficient was attained, then the temperature of the device was reduced at a steady rate of $1^{\circ}\text{C min}^{-1}$ whilst maintaining the poling field. The non-linear coefficient induced in the polymer was monitored as the polymer was cooled through its glass transition. The amplitude of the modulation was seen to decrease, as shown in figure 3.14. This is due to the reduction of the thermal free

volume in the polymer as the temperature is reduced, forcing the induced alignment into a slightly less oriented configuration.

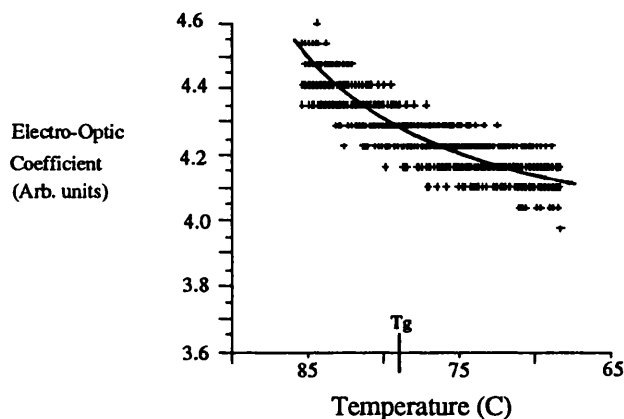


Figure 3.14 Reduction in r_{eff} as the temperature is reduced.

3.10 Fast Amplitude Modulation.

For normal electro-optic device operations it is desirable to minimise any losses of the device. One common feature of the molecular side groups which exhibit very high non-linear coefficients is an absorption towards the blue end of the spectrum. There has been much work to move this absorption to shorter wavelengths. The material used in this study was based on Disperse Red 1, which exhibited a peak absorption at 480 nm, but had an absorption tail which extended into the red part of the spectrum. At the HeNe wavelength of 632.8nm, the real part of the second order susceptibility exhibited strong dispersion, as indicated by the electro-optic coefficient rising to over 40 pmV⁻¹. At this wavelength, a fast amplitude modulation was also measured at temperatures below the glass transition. The absorption only occurred in non-centrosymmetric structures i.e. when a dc poling field was present or in previously poled samples, and exhibited a polar dependence with the poling field. The amplitude of the modulation rose very quickly (less than the response time of the detector of 1 μs) to a level which was proportional to the amplitude of the modulation voltage. The amplitude was also dependent on the degree of poling, increasing as poling occurred. The maximum modulation measured in a poled device was 1.4% of the intensity incident on the detector when a modulation voltage of 15 Vμm⁻¹ was applied to the device.

Kramers Kronig relations predict that every modification to the real component of a electromagnetic wave has a corresponding effect to its imaginary component. It is this relationship which links the dispersion of the refractive indices of a medium with its absorption. The polymer used in this study exhibited an absorption at $\lambda_{max} = 480$ nm. Dispersion in the real component of the $\chi^{(2)}$ was observed.

Correspondingly there must be an imaginary (and thus absorbing) component associated with it. Therefore it is proposed here that the modulated absorption was the imaginary component of $\chi^{(2)}$.

In proposing the origin of the absorption modulation, a range of possible alternative mechanisms for electro-optic modulation in etalon type structures were considered and discounted. Eldering and co-workers [Eldering et al, (1991)] suggests that the largest modulation effects are due to (i) modulation of the thickness of the device due to compressive forces between attractive charge layers on the electrodes, and (ii), the converse piezoelectric effect [Nye, (1964)]. The first effect exhibits a dependence on the applied electric field which is independent of its direction and any modulation would occur at a frequency of twice the drive voltage frequency. This was measured to be less than 1% of the amplitude modulation at the fundamental frequency. The second effect occurs when modulating voltages are applied to piezoelectric materials, resulting in a modulation in thickness of the device. A piezoelectric constant of approximately 1 nC/Newton would be required to account for the measured intensity modulation. This is three orders of magnitude greater than quartz, and therefore unlikely to be wholly responsible. However, it is possible that this effect contributed towards the total intensity modulation measured.

3.11 Limitations to the Poling Technique.

A process called charge double layer formation has been observed in monomeric liquid crystal devices. It occurs in devices when d.c. electric fields are applied to the device, and has the effect of creating a reverse electric field within the device, thus reducing the internal field applied. It occurs because residual ions in the liquid crystal material are attracted to the oppositely charged electrode, but are prevented from being conducted away by an insulating layer. It is common to use a thin insulating layer on top of the ITO electrodes to prevent ions moving from the ITO into the liquid crystal and lowering its resistivity. In this way, the trapped charge can create a reverse electric field which can be sufficiently large to reverse switch the device once the applied d.c. field has been removed. This problem might also be expected in poled polymer devices, where extremely large dc electric fields are applied to the device for relatively long periods of time.

Polymeric materials used for non-linear optics are of high purity to allow the maximum poling field possible to be applied to the devices. However, they are not as pure as commercial liquid crystal materials, which can have resistivities as high as $10^{14} \Omega\text{m}^{-1}$. In this study, no insulating layer was used between the electrode and the polymer to act as a barrier for ions attracted to the electrodes from within the bulk of the material. It is known that ITO injects holes into the polymer layer, and therefore this process cannot be prevented. It was hoped that the absence of a barrier layer would allow injected charge to be conducted away via the other electrode. However it is possible for ions to become trapped within the polymer material due to the presence of defects or charge traps in the material. These occur at interfaces of

materials and are due to the internal stresses originating from the material not matching the adjacent layer, or if the adjacent layer has surface topography. It is known that the ITO surface can be quite rough and was measured using the Tencor Alpha-step to have a roughness of 40 Å.

Several experiments were used to try and detect the presence of charge double layers in the polymer devices after they had been poled. The first was to measure the poling efficiency as a function of device thickness. If the defect region near the interface and thus the charge double layers are as thick as 1 μm, then it may be possible to detect a non-linear poling efficiency as a function of device thickness. A number of devices were made with thicknesses in the range of 2 to 12 μm. Due to the viscosity of the polymer, it was not possible to fabricate thermal compression cells less than 2 μm in thickness. A plot of poling efficiency as a function of thickness is shown in figure 3.15. The large variation in results was believed to be due to poor control in the flatness of the cells. This also has a direct effect on the efficiency of the device as a modulator, as discussed in the previous chapter. It was noticed that flatter cells exhibited significantly larger modulation amplitudes.

Attempts were made to monitor the charge flowing into and out of these devices whilst the poling took place. It was hoped that measurement of the current would give information about any charge double layer formation and relaxation, by detecting ion current flow after the cell had been charged and discharged respectively. The current was measured using a Keithley picoammeter connected in series with the cell. Unfortunately any ion currents were below the noise level and therefore unmeasurable. The noise was due to pickup in the leads and difficulty in isolating the sensitive picoammeter.

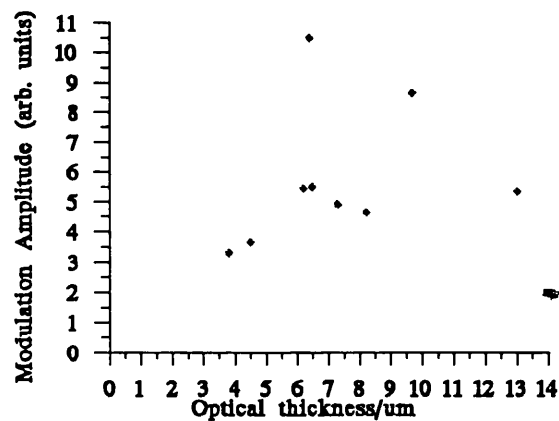


Figure 3.15 Electro-optic modulation amplitude as a function of device thickness.

A technique to overcome the problem of charge double layer formation whilst poling may have significant benefits to increase the poling efficiency. A novel poling scheme based on an asymmetric rectangular wave voltage which had no net dc component was investigated, as shown in figure 3.16.

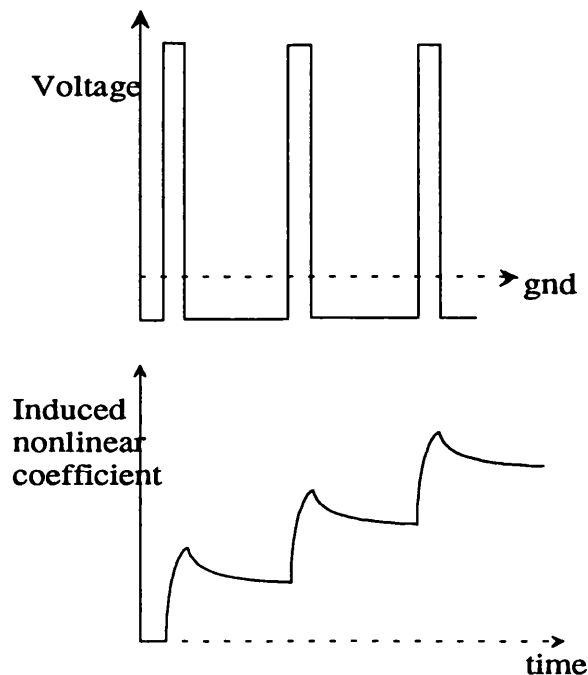


Figure 3.16. Novel Poling Scheme.

This was intended to exploit the earlier reported non-linear dependence of the induced optical nonlinear coefficient on poling field strength [Griffith et al, (1991)], and thus any difference in the voltage dependence of the reorientation and charge build up. A possible scenario would be where the large positive pulse partially orientates the molecules, together with a build up of ionic charge. The low negative pulse will then remove the charge double layers, but does not fully reorient the side chains, resulting in a net alignment. It was hoped that this simple solution would overcome the problem of charge double layer formation. Unfortunately, this could not be tested as the new polymer material synthesised for this work did not exhibit the same nonlinear dependence as reported earlier. In the 'linear' material used in all of the experiments for this study, no net ordering could be obtained using this technique.

3.12 Discussions and Further Work.

This chapter described work investigating the technique of poling side chain polymers for electro-optical applications. This study has involved the use of a wide range of measurement techniques to characterise the selected polymeric material. A novel experiment was described which probed the dynamics of poling and relaxation of polymers. The results of this work are comparable with other techniques such as SHG and dielectric relaxation. It offers the same selectivity of the non-centrosymmetric ordering as SHG, but only requires simple lasers and optics. The device configurations used are the same as

through plane Pockels cell devices, offering a technique to investigate materials and poling in-situ. The measurements can be carried out at a wide range of wavelengths.

The dynamic response to poling has been investigated and described with particular emphasis at the molecular level. The rise in induced electro-optic coefficient was discussed in terms of fast molecular reorientation within the thermal free volume of the side chain group, followed by side chain reorientation via a rotational diffusion mechanism. Below the glass transition, these two mechanisms were found to merge, resulting in a stretched exponential function, which is becoming increasingly common in the dynamics of glassy systems, in both the increasingly popular study of poling dynamics and in dielectric relaxation studies, from which the function first originated.

The work on the electro-optic measurement of poled polymers is by no means complete. The lack of retention of the induced order persists as a problem for device manufacturers where processing at elevated temperatures is required. Minimising the relaxation of the induced order when the poling field is removed is also important, and has not been eliminated even in cross-linked systems [Allan et al, (1991)]. If the model which is described here is correct, then it will be very difficult to prevent the relaxation within the thermal free volume. Annealing the samples whilst the poling field is present would be one possible route. Several groups have described annealing before or after poling has occurred to minimise the thermal free volume [McL. Smith & Coles, (1992)].

The question as to whether charge double layers are limiting the efficiency of the poling mechanism has not been fully answered. The effect is in all likelihood present, but will vary in its magnitude from material to material. It would be possible to overcome the problem using the novel poling scheme, but this requires a non-linear dependence of the induced electro-optic coefficient as a function of the poling voltage. This effect has been reported in the literature, but attempts to reproduce those results in the present work failed. Indeed the origin of the nonlinear dependence of the induced nonlinear coefficient upon poling field is still unclear. The suspected cause was probably due to the higher polydispersity in the earlier material, although this has not been investigated. Complicating issues such as the presence of unreacted monomer and other impurities may also contribute to the anomalous effect. To investigate and account fully for the effect, considerable synthetic effort would be required to isolate the cause.

Although control and characterisation of polymer synthesis is becoming increasingly important for nonlinear optical polymers, it is important to balance this particular study against the possible benefits from exploiting the nonlinear dependence which is as yet unproven. Unless the nonlinear effect can be induced in a range of polymeric materials, it may not result in devices with higher nonlinear coefficients, as optimisation of other aspects of the materials may result in a similar increase in performance of the device.

4. Second Harmonic Generation in Liquid Crystal Materials.

The requirement for compact laser sources of radiation in the blue and green regions of the spectrum has resulted in considerable interest in all classes of materials which exhibit potential for frequency doubling. The benefits to be gained from developing such light sources are considerable for the data storage and display markets. The use of shorter wavelength radiation will allow an increase in the density of information stored on optical disks, for both computing and entertainment applications. Typically, halving the wavelength would lead to a fourfold increase in information density. The development of blue and green laser sources based on semiconductor laser technology may also produce a new, highly efficient type of colour display, principally for projection applications without the requiring powerful and inefficient light sources. The potential size of the markets for such devices are very large, and the technology is sufficiently realistic to persuade many groups around the world to try and develop blue and green semiconductor laser sources.

The most common technique for producing blue and green compact lasers is to double the frequency of existing semiconductor lasers operating in the red and near infra-red region of the spectrum. The demand for compact and efficient devices places very high requirements on the nonlinear optical material to be used for frequency doubling. There are alternative techniques to produce green and blue compact lasers which also show promise. Within the last couple of years there has been a number of successes in using zinc selenide (ZnSe) as a wide band direct semiconductor material. Light emitting diodes have been demonstrated in the blue region when cooled to liquid nitrogen temperatures, and green at room temperature. Within the last year, lasing has also been demonstrated at room temperature, albeit for a short period [Jeon et al, (1992)]. The problems of device lifetimes and cooling are limited by the quality of the material, particularly associated with doping the material with donors and acceptors. There is still a long way to go before ZnSe will be a competitive technology at room temperature. However, it has clearly demonstrated that direct production of short wavelength radiation is possible in semiconductor materials, and can challenge techniques such as frequency doubling.

Chapter 2 discussed the requirements from optical materials for large nonlinear coefficients, with particular emphasis on the electro-optic effect and devices. In this chapter the nonlinear effect to be discussed is frequency doubling or second harmonic generation (SHG). The theory of SHG will be developed more fully, with particular emphasis on device requirements for frequency doubling. The relatively new class of chiral smectic liquid crystal materials for SHG shall be described, with discussions of their relative advantages and drawbacks. An experiment to measure the SHG efficiency of these materials, and theoretical analysis to account for the data will be fully described.

4.1 Theory of Second Harmonic Generation.

Second harmonic generation is the process where two identical optical electric fields are coupled by the nonlinear susceptibility of a material and light at double the incident frequency is re-radiated. Section 2.1 discussed the requirement of lack of inversion symmetry for second order nonlinear processes to occur in a material. This is also a necessary condition for second harmonic generation (SHG) and must be taken into account when the theory of second harmonic generation is derived.

A simple derivation of the electric field of the second harmonic wave is based upon Maxwell's equations and the formulation of electromagnetic waves. Including a nonlinear component to the polarisation P_j gives

$$P_i = \epsilon_o \chi_{ij} E_j + (P_{NL})_i$$

and

$$(P_{NL})_i = \epsilon_o \chi_{ijk} E_j E_k. \quad 4.1$$

To simplify the analysis and yet remain valid for experimental situations, solutions to the new wave equation are sought in the form of plane waves propagating along the z axis with frequencies $\omega_{1,2,3}$, where $\omega_1 = \omega_2$ and $\omega_3 = 2\omega_1$. The solution, described for example by Yariv [Yariv, 1989] predicts an electric field oscillating at twice the frequency of the driving force (the incident radiation) of the form

$$E_{2\omega}(z) = -i\omega 2 \sqrt{\frac{\mu_o}{\epsilon_{2\omega}}} |e_i^{2\omega} : d_{ijk} : e_j^\omega e_k^\omega| E_\omega^2(z) e^{i2\omega z} \frac{e^{i\Delta k z} - 1}{i\Delta k} \quad 4.2$$

where ω is the frequency of the fundamental electric field, Δk is the difference between the wave vectors at ω and 2ω , μ_o is the permittivity of free space, $\epsilon_{2\omega}$ is the dielectric permittivity at frequency 2ω and d_{ijk} is the nonlinear coefficient. The nonlinear coefficient is defined in tensor notation as

$$(P_i)^{NL} = 2d_{ijk} E_j E_k \quad \text{or} \quad 2d_{ijk} = \chi_{ijk} \epsilon_o \quad 4.3$$

where P^{NL} is the nonlinear component of the induced polarisation, and χ_{ijk} is the second order nonlinear susceptibility tensor. The factor isolated between the vertical lines is the effective nonlinear coefficient d_{eff} . This can be found from the product of the nonlinear tensor and the unit vectors of the three electric fields, $e_{j,k}^\omega$ and $e_i^{2\omega}$.

The approximations used in this simple derivation leading to equation 4.2 include:

- i. The incident electromagnetic wave $E_\omega(z)$ is planar. This is satisfactory, even for gaussian wave fronts, providing that the material thickness is less than the confocal parameter of the beam.
- ii. The nonlinear polarisation is small compared with the linear component. Large nonlinear effects cannot be described by a perturbation theory type derivation. However, this is satisfactory for almost all materials.

- iii. Depletion of the fundamental beam does not occur i.e. second harmonic generation is sufficiently weak not to reduce the intensity of the incident wave. Depletion can be taken into account using a more advanced theory, as can the effect of non-planar wave fronts. Yariv [Yariv, (1989)] or Shen [Shen, (1984)] develop these advanced theories in more detail than is required here.
- iv. At distance $z=0$ there is no second harmonic electric field. This defines a simple starting condition for the nonlinear wave.

The expression for the second harmonic power output $P_{2\omega}$ per unit area (or irradiance) is given by the relation

$$\frac{P_{2\omega}}{Area} = \frac{1}{2} \sqrt{\frac{\epsilon}{\mu_0}} E_{2\omega} E_{2\omega}^*$$

which can then be used to define the conversion efficiency (e_{SHG}) as

$$e_{SHG} = \frac{P_{2\omega}}{P_{\omega}} = 8 \left(\frac{\mu_0}{\epsilon_0} \right)^{\frac{1}{2}} \frac{\omega^2}{n_{\omega}^2 n_{2\omega}} d_{eff}^2 L^2 \frac{P_{\omega}}{Area} \left(\frac{\sin\left(\frac{(k_{2\omega} - 2k_{\omega})L}{2}\right)}{(k_{2\omega} - 2k_{\omega})L/2} \right)^2. \quad 4.4$$

P_{ω} is the incident power at frequency ω , L is the thickness of the material, and n is the refractive index of the material at the specified frequency. The expression for Δk can be replaced by one containing measurable parameters, the refractive indices and the wavelength.

$$\Delta k = k_{2\omega} - 2k_{\omega} = \frac{4\pi}{\lambda} (n_{2\omega} - n_{\omega}) \quad 4.5$$

From 4.4 it can be seen that efficiency e_{SHG} is dependent on the device thickness L squared. However, this is modulated by the final term - a $\text{sinc}^2 x$ function. The origin of this final term is the phase mismatch which develops between the fundamental and second harmonic waves as the two waves propagate through the material at different speeds, and can reduce the SHG output to zero in certain circumstances.

4.1.1 Phase Matching.

Equation 4.4 indicates that a requirement for efficient second harmonic generation is that $\Delta k = 0$, or

$$k_{2\omega} = 2k_{\omega}$$

which would increase the final term of equation 4.4 to unity, and so SHG efficiency would rise as a function of thickness L squared. This is a very desirable but impossible situation as SHG efficiency cannot increase indefinitely. All materials have absorption which results in dispersion in the real part of the refractive index, as described by Kramers Kronig relations. Waves of different frequencies therefore travel through the material at different speeds. It is possible for the thickness of the device to be such that second

harmonic generated at the beginning of the material is anti-phase with the second harmonic generated later in the material. In this condition the distribution of second harmonic waves generated through the material interfere with each other with the result that no net second harmonic emerges from the material.

A characteristic length called the coherence length [Yariv, (1989)] can be defined by

$$l_c = 2\pi / \Delta k. \quad 4.6$$

The coherence length is a measure of the maximum length of a material that can produce second harmonic light efficiently without phase matching, and before destructive interference reduces the output. It can be written in an alternative form shown in equation 4.7 involving the refractive indices which are easily measured. Typical values of l_c are of the order 50 μm for $\lambda = 1 \mu\text{m}$ and $\Delta n = 0.01$.

$$l_c = \frac{\lambda}{2(n_{2\omega} - n_{\omega})} \quad 4.7$$

The condition of $\Delta k=0$ is called phase matched which can be achieved in a number of ways often using the birefringence of the material. Rotating the orientation of the crystal or changing its temperature can 'tune' the material to the phase matched condition, resulting in efficient conversion from the fundamental to second harmonic frequency. In these circumstances other limits prevent infinite SHG efficiency, and for example depletion of the fundamental beam can no longer be ignored.

In a positive uniaxial material ($n_e > n_o$), co-linear phase matching can be achieved if the refractive index at n_e at angle θ_{pm} and at frequency ω is equal to that for n_o at 2ω . This is type I phase matching (o+o \rightarrow e; e+e \rightarrow o). An alternative type of phase matching can be achieved if the two fundamental beams are polarised orthogonal to one another, and the harmonic is polarised at an intermediate angle with respect to the fundamental. This is type II phase matching (o+e \rightarrow e).

A range of alternative phase matching techniques can be used in waveguide structures. Waveguides appear to be ideal for second harmonic generation due to the high light intensities and long interaction lengths. There are many variations of phase matching based on the idea that the waveguide sustains the fundamental and second harmonic in different guided modes [Hewig & Jain, (1983)]. One may be guided in the core, and the other in the cladding layer, for example. These geometries are usually troubled by the poor spatial overlap of the fundamental and harmonic radiation mode structures which reduces the efficiency of the device. A technique which overcomes this drawback involves modifying the waveguide (or nonlinear medium) in a periodic manner which is matched to the coherence length of the harmonic generation. This allows the constructive SHG over a coherence length, but suppresses SHG for the period which would normally result in destructive interference. This technique of quasi-phase matching has been demonstrated both in inorganic materials [Ishigame et al, (1991)] and poled polymeric materials [Khanarian et al, (1990)].

4.2 Materials and Device Requirements for Second Harmonic Generation.

Many of the material requirements for efficient second harmonic generation are common for all nonlinear optical materials, and were discussed in detail in section 2.11 earlier. There are, of course specific material requirements for second harmonic generation, and equation 4.4 suggested the important material parameters for efficient conversion are contained in the ratio

$$\frac{d_{ijk}^2}{n_k^{2\omega} n_i^\omega n_j^\omega} \quad 4.8$$

together with the condition for phase matching given in equation 4.5. It is important that the material be stable to the fundamental and second harmonic radiation, as very high intensities are used, and indeed desired to improve the conversion efficiency of the device. The ability to phase match the fundamental and second harmonic radiations is also of great importance for producing usable devices. The condition of phase matching must be stable and easily maintained. The alignment angle tolerance (acceptance angle) of the material may be narrow, requiring careful and stable alignment. If the refractive indices of the material exhibit a strong temperature dependence, then the control of temperature may be required to be better than 1°C, forcing the device to be used in a temperature stabilised environment. Some of these properties are now being controlled by materials engineering, resulting in a new range of nonlinear materials optimised for specific applications.

The inorganic material potassium titanyl phosphate (KTP) is becoming widespread in its use for frequency doubling, and displacing some of the earlier inorganic materials such as potassium dihydrogen phosphate (KDP) or lithium niobate (LiNbO₃). Its success is due to its wide transmission band (0.35 - 4.5 μ m), the high laser damage threshold (15 GWcm⁻² @ 1.064 μ m) and competitive nonlinear coefficients ($d_{\text{eff}} = 3.2 \text{ pmV}^{-1}$) in comparison to KDP, together with the ability for type II phase matching. It also has wide acceptance angles and thermally stable phase matching properties [Bierlein & Vanherzeele, (1989)]. It can be grown in good quality crystals up to 6x5x2 cm in size in a period of weeks.

The nonlinear coefficients of organic crystals are frequently measured by the technique of SHG, but very few materials have been developed into devices. Those devices which have been developed have been based upon well known crystals such as DAN [Huang et al, (1991)] but many of the device critical parameters are frequently not published. Organic crystals suffer from many of the same problems as inorganics, particularly the problems associated with growing large high quality crystals with high damage thresholds. This is the likely cause for the lack of device studies. The incentive for developing this class of material is that they offer amongst the highest nonlinear coefficients yet reported in nonlinear materials [Bierlein et al, (1990)]. The problems of stability of these materials on exposure to the atmosphere or high laser intensities are beginning to be addressed at the level required to make reliable devices.

The developments in polymeric materials for electro-optic devices has also improved their SHG device potential. This is particularly true in integrated optics geometries, where techniques for defining low loss waveguides and coupling to semiconductor laser sources is being developed. The materials used at present have acceptable nonlinear coefficients, and this situation is constantly being improved by developments in the materials. One of the main limitations of poled polymers is the problem of relaxation of the poled order into a centrosymmetric state which is of no use for second order nonlinear effects. This problem has been discussed in great detail in chapters 2 and 3.

Ferroelectric liquid crystals possess a transverse axis which can self assemble into a noncentrosymmetric alignment and therefore exhibit SHG [Shytkov et al, (1985)]. The following section describes how the presence of chiral molecules in the tilted smectic C phase can give rise to this axis which lacks inversion symmetry. Ferroelectric liquid crystal materials are being developed primarily for a new class of liquid crystal display, due to their exhibit fast molecular reorientation effects on application of electric fields together with their inherent bistability. Molecular engineering techniques are now being used to improve the optical nonlinearities in these materials for nonlinear optical applications.

4.3 Ferroelectric Liquid Crystals.

Liquid crystal molecules which form the tilted smectic C (Sc) phase and lack a centre of inversion have the potential for noncentrosymmetric ordering within the bulk material. This ordering is never seen in a free material, because the chirality of the molecules results in them packing in a helical form, as shown schematically in figure 1.6. External forces can be applied to unwind the helix and obtain the desired molecular ordering. These forces may be electrical or magnetic in origin, or may be due to surface alignment layers which influence the direction in which the molecules lie at the surfaces of the device. These surface forces can result in the helix unwinding in thin devices ($\sim 2 \mu\text{m}$), and so result in a surface stabilised ferroelectric liquid crystal structure (ssflc) [Clark & Lagerwall, (1980)]. However, surface effects are relatively weak and alignment of thick layers usually requires the application of electric or magnetic fields.

The symmetry of the smectic C phase is dominated by the shape of the molecules and the tilt, as shown in figure 4.1. The angles θ , ϕ , and ψ describe the tilt within the layer, rotation around the cone and rotation about the director respectively. If the molecule is symmetric, the liquid crystal phase possesses twofold rotational symmetry about the c_2 axis together with mirror symmetry in the plane containing the director n and is perpendicular to the c_2 axis, which combine to describe inversion symmetry. The only well defined molecular axes are the director n and the c_2 axis. If the molecule contains a chiral group then the reflection symmetry operation is forbidden, and the remaining c_2 rotation axis is no longer inverted under the remaining symmetry operations.

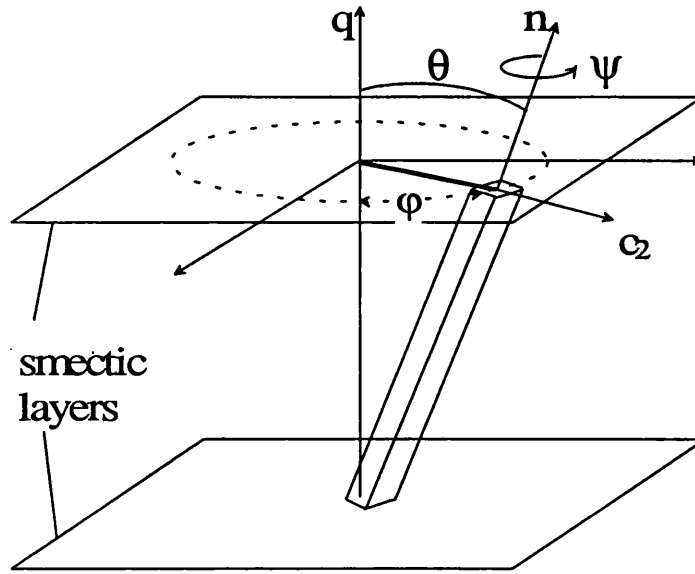


Figure 4.1 The molecular co-ordinate system for a Smectic C molecule.

A molecular dipole moment along this c_2 transverse axis cannot be inverted and cancelled, and so can combine together to form a bulk permanent dipole or spontaneous polarisation. The c_2 axis is the direction of the molecular spontaneous polarisation, P_s . The transverse component of the molecular hyperpolarisability along this axis is also no longer inverted under the symmetry operations of the bulk phase, and so can give rise to SHG from the bulk material.

When an external electric field is applied to a smectic C material, the coupling energy between the field and the permanent transverse dipole moment is minimised when the dipole is oriented parallel to the electric field. The molecules can align themselves in response to the electric field by rotating around the cone shown in figure 4.1. It is energetically unfavourable for the molecules to move outside this restricted path because the layer spacing would change. The alignment in an electric field can be enhanced because many of the molecules which form smectic C phases have negative dielectric anisotropy. This means it is more energetically favourable for molecules to align their long molecular axis perpendicular to the applied electric field than parallel to it.

The nematic liquid crystal phase was described in chapter 1 by the Euler angles ξ , ζ and η . These angles described the tilt of the molecular long axis relative to the director, n , the rotation of the molecule about the long molecular axis, and the direction of the molecular fluctuation in the plane transverse to n respectively. From these angles two order parameters can be defined where

$$S = \frac{1}{2} \langle 3 \cos^2 \xi - 1 \rangle \quad 4.8$$

describes the order parameter of the longitudinal molecular axis with respect to the director n , and

$$D = \frac{3}{2} \langle \sin^2 \xi \cos 2\zeta \rangle \quad 4.9$$

which is the order parameter for the transverse principal axis of the molecule projected onto n . In the nematic (and smectic A phase) all values of η are equally likely, and so the angle is not used in the nematic order parameters. In the smectic C phase, there is now an additional axis to which molecular fluctuations can be referenced, the c_2 axis. This results in two new order parameters, P and C. P is the order parameter of the long molecular axis with respect to the c_2 axis, and is given by

$$P = \frac{3}{2} \langle \sin^2 \xi \cos 2\eta \rangle. \quad 4.10$$

The order parameter of the short molecular axis with respect to the c_2 axis is C and is described by

$$C = \left\langle \frac{1}{2} (1 + \cos^2 \xi) \cos 2\zeta \cos 2\eta - \cos \xi \sin 2\zeta \sin \eta \right\rangle \quad 4.11$$

which represents the hindered rotation about the long molecular axis, and results in biaxiality.

The four order parameters used to describe the smectic C phase are very complex, and so a simplified geometry will be considered. The new geometry assumes perfect nematic order, i.e. $S=1$ and $D=0$. This is reasonable as the smectic C phase is quite well ordered, with less liquid-like properties. The approximation reduces C to

$$C = \langle \cos 2\zeta \rangle \quad 4.12$$

and ζ and ψ become equal as the molecular axis and the director become co-incident. The hindered rotation of the molecule about the director order parameter is

$$\Omega = \langle \cos 2\psi \rangle \quad 4.13$$

where ψ is the orientation about the director, as shown in figure 4.1. This describes the biaxiality of the phase, and may be referred to as the biaxial order parameter. Typical values of Ω are in the range $0.09 \rightarrow 0.19$ [Jones, (1991)]. If the molecules are assumed to be perfectly rigid, then a ferroelectric or polar order parameter can be defined as

$$\Pi = \langle \cos \psi \rangle \quad 4.14$$

which describes the tendency for the molecular transverse axis to be distributed about $\psi = 0$ rather than $\psi = \pm \pi$. Ω and Π are shown graphically in figure 4.2. The order parameter Ω , shown in figure 4.2a may be thought of as describing the biaxiality found in a non-chiral smectic C phase. In the chiral form of the phase at temperatures close to the C→A transition, the rotation about the director is dominated by the polar order parameter Π , as shown in figure 4.2b. If the material is cooled lower into the smectic C phase then the molecular transverse axis is described by a combination of the polar and biaxial order parameters, as shown in figure 4.2c. The polar order parameter Ω is of great importance in nonlinear optical measurements. This describes the degree of noncentrosymmetry found in the material which has a very strong influence upon the bulk nonlinear coefficient. The biaxial order parameter has very much less significance, but may affect phase matching conditions.

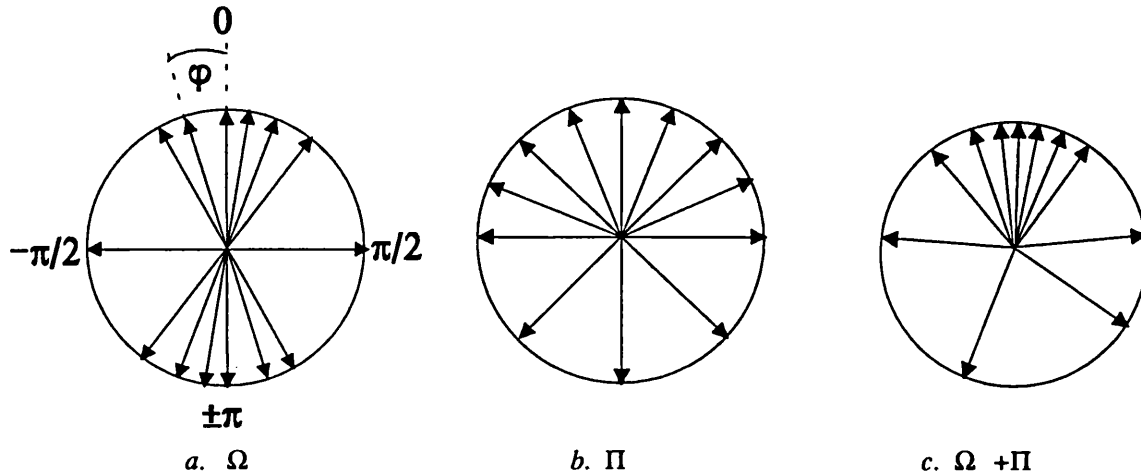


Figure 4.2 The polar and biaxial order parameters.

4.3.1 Alignment of Ferroelectric Liquid Crystals.

The unwinding of the molecular helix in the chiral smectic C phase can be achieved in one of two molecular orientations within a device. Homeotropic alignment describes where the molecules tend to align their long axis perpendicular to the device substrates, and homogeneous alignment is where the molecules lay in the plane of the device.

Surface treatments such as lecithin or chrome complex on the glass substrates (or in fact very clean glass) can induce homeotropic alignment. This arises because of a preferential bond formation between one of the ends of the molecule and the surface alignment layer. It is possible for this first layer to be highly noncentrosymmetric, for example by having different chemical end groups, only one of which forms a strong interaction with the surface alignment. However, the second layer frequently packs anti parallel with the first, resulting in no bulk asymmetry. As the smectic layers form with their planes parallel to the device substrates, there is no preferential direction for the P_S and so the helical structure as found in the bulk is formed. This helical structure destroys the bulk noncentrosymmetry. It has recently been demonstrated that circular polarised light matched to the helical pitch can give enhanced SHG compared to plane polarised light incident, although the level is still very low [Kajikawa et al, (1992)].

An electric field applied parallel to the plane of the cell using transverse electrodes within the cell can be used to unwind the helix, as shown in figure 4.3. This will induce noncentrosymmetry of the transverse hyperpolarisability in the plane of the cell which can then be accessed by light normally incident on the cell. This alignment can be easily achieved in many smectic C materials, and results in a well understood uniform structure through the cell. It is therefore one of the most favoured smectic C alignments for SHG studies.

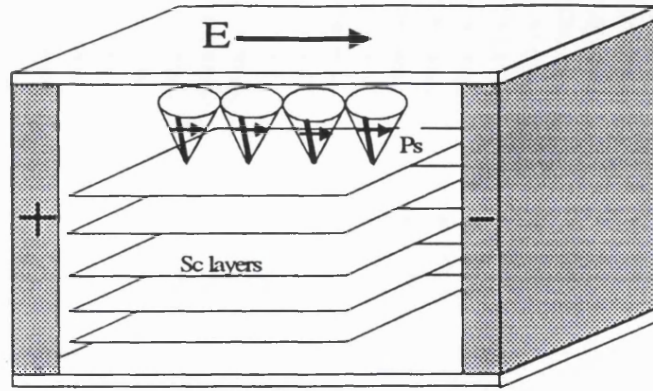


Figure 4.3 Homeotropic alignment unwound with electric field.

Homogeneous alignment layers encourage the liquid crystal molecules to lay in the plane of the interface. These polyimide or nylon layers are unidirectionally rubbed with a cloth to impart a preferential alignment direction. The action of rubbing is thought to align the polymer backbones in the alignment layer and/or form micro grooves in the alignment surface. The liquid crystal molecules adopt a preferential alignment with their long molecular axis along the rubbing direction to minimise the elastic forces in the material. The planar alignment layers can give the molecules an out of plane tilt, called the surface pretilt, ξ_s . This pretilt is usually quite small, typically 0 - 6° for rubbed polymer surfaces.

The idealised alignment of the smectic layers in this geometry is to form vertical planes between the substrates, and the molecules to lie horizontally between them. This is called the bookshelf geometry, first proposed by Clark and Lagerwall [Clark & Lagerwall, (1980)] and is shown in figure 4.4 in one of its switched states. To prevent the molecules from forming a helix in this geometry, it is necessary for the thickness of the device to be significantly less than the molecular pitch length.

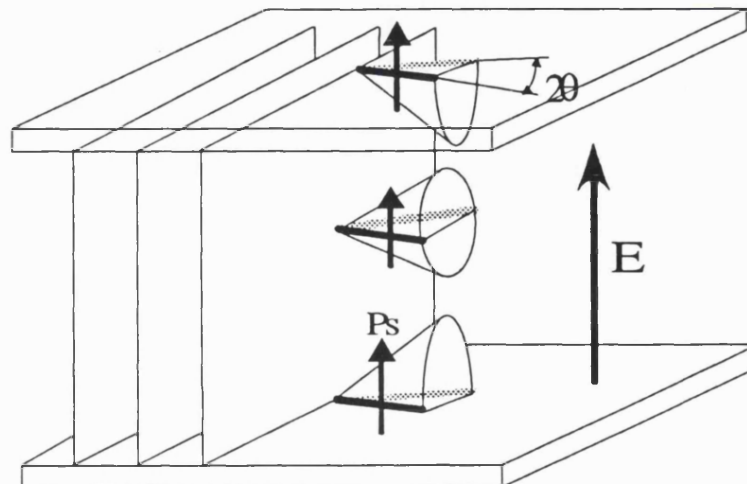


Figure 4.4 The idealised bookshelf geometry for planar alignment.

Unfortunately, without the application of large electric or magnetic fields, the bookshelf alignment is not energetically favourable. In its place, the layers spontaneously form a chevron structure [Rieker et al, (1987)] shown in figure 4.5.

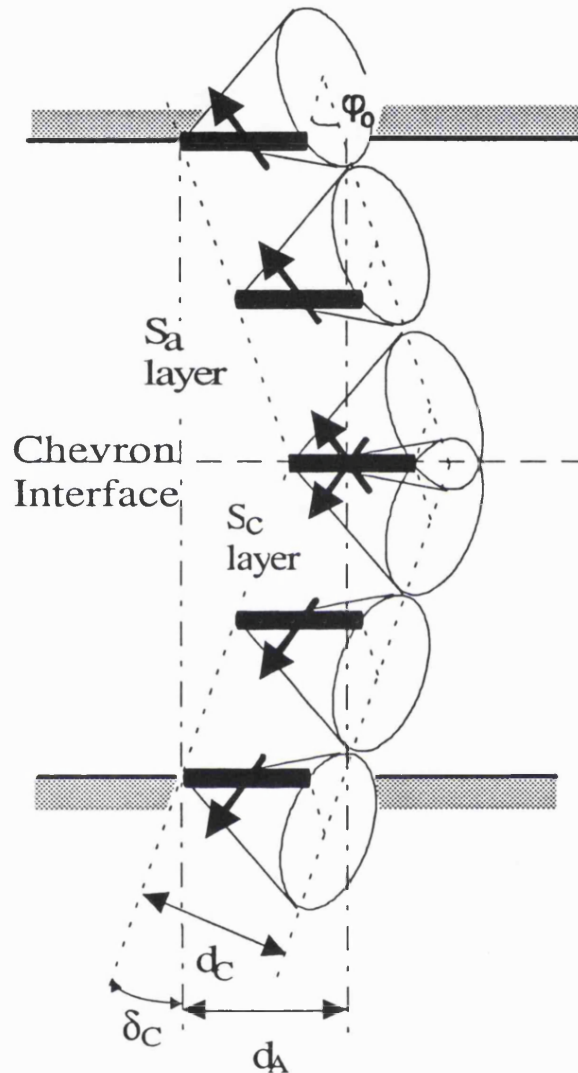


Figure 4.5 The chevron interface and alignment.

It has been found that on cooling from the smectic A to the smectic C phase, the layer spacing in the smectic C phase, d_C is smaller than in the smectic A phase, d_A , due to the tilt of the molecules within the layer. A chevron structure forms because of many factors, including the smectic layers are pinned at the surface of the device, pretilt of the rubbed polyimide alignment layer and the minimisation of splay, twist and bend energies. There is also a requirement that the director must be continuous across the cell. Preventing the layers from moving at the surfaces forces the layers to tilt by an angle given by δ_C , given by

$$\cos \delta_C = d_C / d_A. \quad 4.15$$

A typical ferroelectric display material has a cone angle of about 22.5° , and therefore δ_C is about 18° .

In one half of the chevron, the molecule sits at one side of the cone with its P_S pointing at an angle ϕ_0 towards the substrate. Across the chevron interface in the other side of the device, the molecules sit on the other side of the cone with the vertical component of P_S pointing opposite the first direction. The horizontal component of P_S remains constant through the cell. At the chevron interface, the two spontaneous polarisations almost cancel, leaving only a small component in the plane of the chevron interface. The outcome of this alignment for nonlinear applications is that P_S is partially cancelled across the device. There would be a similar effect for the bulk optical nonlinearity due to the reversal of the alignment.

If a voltage is applied across the cell, the molecules rotate around their cone to try and align their P_S with the applied field. This is limited by surface anchoring at the interfaces and continuity of the director at the chevron interface, where the molecules are unable to move. Within the two sides of the chevron the molecules rotate around the cone to approach the condition $\phi_0 = \pi/2$, which is only attainable for infinite fields. Any net alignment of the P_S of the molecules in this geometry would be normal to the cell substrates, and would not be easily accessible for nonlinear applications. To couple light with the transverse hyperpolarisability device geometries are required where light passes through the device at an angle to the normal, or is waveguided through the sample.

4.4 Experiment to Measure SHG Efficiency.

Measurement of the electronic nonlinear optical coefficients can be achieved at optical frequencies using the technique of second harmonic frequency generation [Franken et al, (1961)]. These frequencies are well above the limit of molecular reorientation, and so any nonlinear effects measured must be due only to electronic processes. This technique is therefore suitable for investigating the nonlinear optical properties of monomeric liquid crystal materials, where molecules can reorient in response to applied dc and low frequency electric fields.

It is possible to calculate the magnitude of d_{ijk} from equation 4.4 by measuring the second harmonic output $P_{2\omega}$ as a function of Δkz . Variation in Δkz can be achieved by rotating the sample away from the experimental optic axis, increasing z from L to $L/\cos\theta$, where θ is the angle of rotation between the material normal and the beam propagation direction and L is the sample thickness. This will result in Maker fringes [Maker et al, (1962)], and from these fringes it is possible to calculate the nonlinear coefficients of the material. To eliminate variations due to the laser beam, the measurement is normalised against SHG from a quartz reference crystal. This results in a parallel optical beam experiment, shown in figure 4.6, where the laser energy is divided equally between a sample arm and a reference arm. For every measurement, the ratio of SHG energies is calculated, eliminating problems such as pulse to pulse energy

variations and removing laser dependent parameters from the equation to calculate the efficiency. These parameters include the beam spot size and additional correction factors for gaussian spatial and temporal profiles of the laser pulses. The parameters which remain in the calculation are now mostly material dependent, as shown in equation 4.16.

$$\frac{P_{LC}^{2\omega}}{P_Q^{2\omega}} = \left(\frac{P_{LC}^\omega}{P_Q^\omega} \right)^2 d_{eff}^2 l^2 \frac{\sin^2 \left(\frac{2\pi l}{\lambda} (n_{LC}^{2\omega} - n_{LC}^\omega) \right)}{\left(\frac{2\pi l}{\lambda} (n_{LC}^{2\omega} - n_{LC}^\omega) \right)^2} \times A_Q \quad 4.16$$

A_Q is a constant calculated for quartz, taking into account its angle, refractive indices, thickness etc. which remain constant for each measurement. From this equation it is possible to calculate the d_{eff} for a test material in a particular alignment.

The laser source was a Nd³⁺:YAG laser producing pulsed radiation at a wavelength of 1.064 μm with a pulse duration of 10 ns, and pulse energies up to 100 mJ. The beam characteristics were TEM₀₀, with approximately single longitudinal mode temporal profile. The beam was initially horizontally polarised, but could be changed using a half wave plate to give vertical polarisation, or quarter wave plate and polariser combination to give any desired polarisation. High laser energy Glan-Taylor polarisers were used throughout the experiment to define the polarisation of the light.

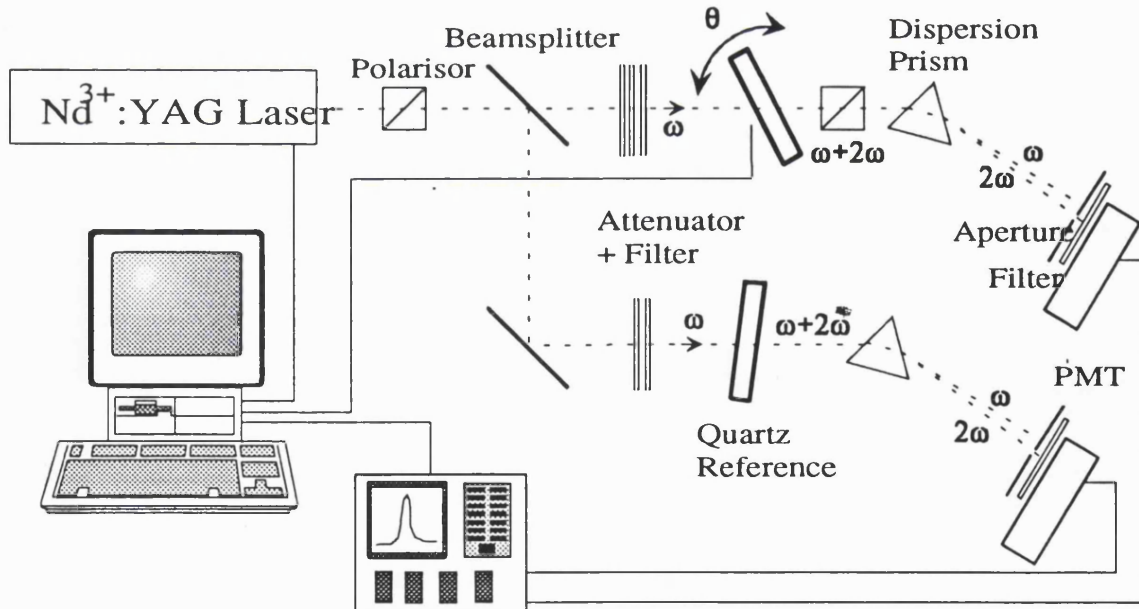


Figure 4.6. The SHG Experimental Configuration.

The requirement that liquid crystal materials be contained in a thin layer within a glass structure resulted in problems which had not been encountered in earlier SHG experiments. The source beam energy was attenuated to prevent damage to the samples and electrodes through absorption. It was found that Indium Tin Oxide (ITO), used as a transparent electrode in cells, was the most susceptible to damage and caused local heating and vaporisation of the liquid crystal material. Below damage energy levels, SHG could be detected from the ITO layer. Although very small (just above noise levels), the resonant cavity formed by the cell could increase this signal. Further attenuation of the beam energy reduced this signal to below noise levels. A visible cut-off edge filter (Schott RG830) was used to remove any radiation at the second harmonic frequency before the sample. Possible sources of this light include light from the laser flashlamps and second harmonic generation from optical components. This is particularly important for quartz wave plates which produce strong second harmonic radiation which must be removed from the beam before the sample or reference crystal.

The requirement for temperature control within the optical experiment was achieved using a temperature controlled microscope hotstage (Mettler FP82) which had been modified to transmit light with angles of incidence in the range $-50^\circ \rightarrow +50^\circ$ in a horizontal plane. To maintain temperature stability, the vertical aperture was 2mm, slightly larger than the beam diameter of the laser at that point. Whilst in the hotstage, dc or ac electric fields could be applied to the material via electrodes in the cell. The hotstage was then mounted upon a computer controlled turntable which rotated about a vertical axis, and was used to vary the angle of incidence of light through the device for Maker fringe studies. A translation stage allowed movement of the axis of rotation across the beam path to ensure the rotation axis was coincident with the laser beam.

Before detecting the second harmonic energy, it was very important to remove all of the residual light at the fundamental frequency. A combination of dispersion prisms and apertures removed any fundamental light before the remaining second harmonic light was collected by photomultiplier tubes (PMT). At the detector, the spatial separation of the fundamental and harmonic beams was greater than 10 mm, and so the two wavelengths were well resolved for spatial filtering. A final interference filter directly in front of the photomultiplier tube served to both eliminate any stray light from entering the PMT, and also offer some protection if the PMT was accidentally exposed to room lights. Both detectors were Thorn EMI side window PMTs (9781R) with 9 stage amplification. The response time of the detectors was 2 ns, and a typical laser pulse had a detected width of 14 ns. Monitoring of increases in the detected pulse width gave an indication of the detector saturating. The energy of the input beam was attenuated to prevent this. A fast digitising oscilloscope (Tektronics DSA602) measured the photomultiplier signal and displayed it with a temporal resolution of 0.5ns. Very careful earthing of the detectors and their power supplies was required to minimise electrical noise from the laser.

The experiment was controlled by a desk top computer using the IEEE488 interface. The angle of the sample could be selected by the computer using the stepper motor turntable. The oscilloscope was

armed and then the laser was triggered. Each measurement was averaged 10 times before the height was measured and stored on the computer for further evaluation. Averaging helped reduce noise levels and improve signal strength. The sample was then automatically rotated by a fixed angle and the measurement repeated. The rotation step size and the number of pulses averaged could be easily varied for particularly sensitive measurements using the computer software. This system enabled many automatic and reliable measurements of second harmonic generation to be made, allowing time to be devoted to aligning the material within the test cells for subsequent measurement.

4.4.1 Maker Fringes.

Before measuring the nonlinear optical coefficients for liquid crystal materials, the experiment was tested by measuring the Maker fringes from the quartz reference sample. Jerphagnon & Kurtz [1970] have formulated a detailed analysis of Maker fringes in quartz for two given configurations, one of which was used in this experiment. A numerical fit to the Maker fringes using this analysis produces values for the sample thickness and refractive indices, as well as the optimum angle for phase matched SHG.

The symmetry of quartz crystal is described by the point group 32, where z is a threefold rotation axis, and x is a twofold axis. From symmetry arguments, the nonlinear optical tensor can be reduced to two independent coefficients, d_{11} and d_{14} , shown in equation 4.17.

$$\underline{d}_{\text{Quartz}} = \begin{pmatrix} d_{11} & -d_{11} & 0 & d_{14} & 0 & 0 \\ 0 & 0 & 0 & 0 & -d_{14} & -d_{11} \\ 0 & 0 & 0 & 0 & 0 & 0 \end{pmatrix} \quad 4.17$$

The quartz crystal was cut in a 'y' form, where the normal to the input and output faces is parallel to the y axis of the crystal. The edges of these faces were parallel to the x and z axes, and the sample was mounted with the z axis vertical, and the crystal was rotated about this axis.

The sample was irradiated by the fundamental wave with horizontal input polarisation. Second harmonic radiation with horizontal polarisation was measured. All of these waves experience the ordinary refractive index, and can be resolved into vector components

$$\underline{E}_0 = \underline{e}_o E = \begin{pmatrix} \sin \phi \\ -\cos \phi \\ 0 \end{pmatrix} E \quad 4.18$$

where ϕ is the angle between the electric field vector and the x axis of the crystal (after refraction), and θ is the angle between the electric field vector and the z axis, which was 90° in all of these measurements. The nonlinear optical coefficient d_{eff} can be calculated to be

$$\begin{aligned} d_{\text{eff}} &= \underline{e}_o^{2\omega} \underline{d} \underline{e}_o^\omega \underline{e}_o^\omega \\ &= d_{11} [\sin^3 \phi - 3 \cos^2 \phi \sin \phi]. \end{aligned} \quad 4.19$$

The full analysis of Maker fringes must take into account the variation of the refractive indices with angle, together with the reflections and refractions which occur at the interfaces. This calculation is described in detail by Jerphagnon & Kurtz, and I shall only repeat the result. The amplitude of normalised fringes is given by equation 4.20

$$P_N = \frac{(n_{2\omega}^o \cos \theta'_\omega + n_\omega^o \cos \theta'_{2\omega}) \cos^4 \theta \cos \theta'_{2\omega} (n_\omega^o + 1)^3 (n_{2\omega}^o + 1)^3 \cos^2(3\theta'_\omega)}{(n_\omega^o \cos \theta + \cos \theta'_\omega)^3 (\cos \theta'_{2\omega} + n_{2\omega}^o \cos \theta)^3 (n_\omega^o + n_{2\omega}^o)} \sin^2 \Psi \quad 4.20$$

where n_ω^o and $n_{2\omega}^o$ are the ordinary refractive indices at each given optical frequency, θ is the angle of incidence, θ'_ω and $\theta'_{2\omega}$ are the angles of refraction at each given optical frequency, and Ψ is calculated from

$$\Psi = (\pi L / 2)(4 / \lambda)(n_\omega^o \cos \theta'_\omega - n_{2\omega}^o \cos \theta'_{2\omega}). \quad 4.21$$

This equation was fitted to the experimental data in several stages. The first step was to find values for L using the standard refractive indices by fitting to the minima, i.e. $\sin^2 \Psi = 0$, and to the amplitude at $\theta = 0$. The values of L and n^o for the best fit were:

$$\begin{aligned} L &= 2.0268 \times 10^{-3} \text{ m} & n_\omega^o &= 1.53413 \\ & & n_{2\omega}^o &= 1.54702. \end{aligned}$$

The full Maker fringes were then calculated and compared to the experimental data, as shown in figure 4.7. The correlation between the two curves is very good, and gave a high degree of confidence in the experimental configuration.

When used as a reference source of second harmonic generation, the quartz was rotated from normal incidence to its first maximum condition, at an angle of incidence $i = 10.8^\circ$. At this angle, $d_{\text{eff}} = 0.467 \text{ pmV}^{-1}$, and the effective path length $L = 2.042 \times 10^{-3} \text{ m}$. Using this data, equation 4.4 for quartz is reduced to

$$P_Q^{2\omega} = \frac{(P_Q^\omega)^2}{\text{Area}} \times 1.329 \times 10^4. \quad 4.22.$$

This equation can be substituted into equation 4.16 to calculate the efficiency and d_{eff} of the liquid crystal test materials.

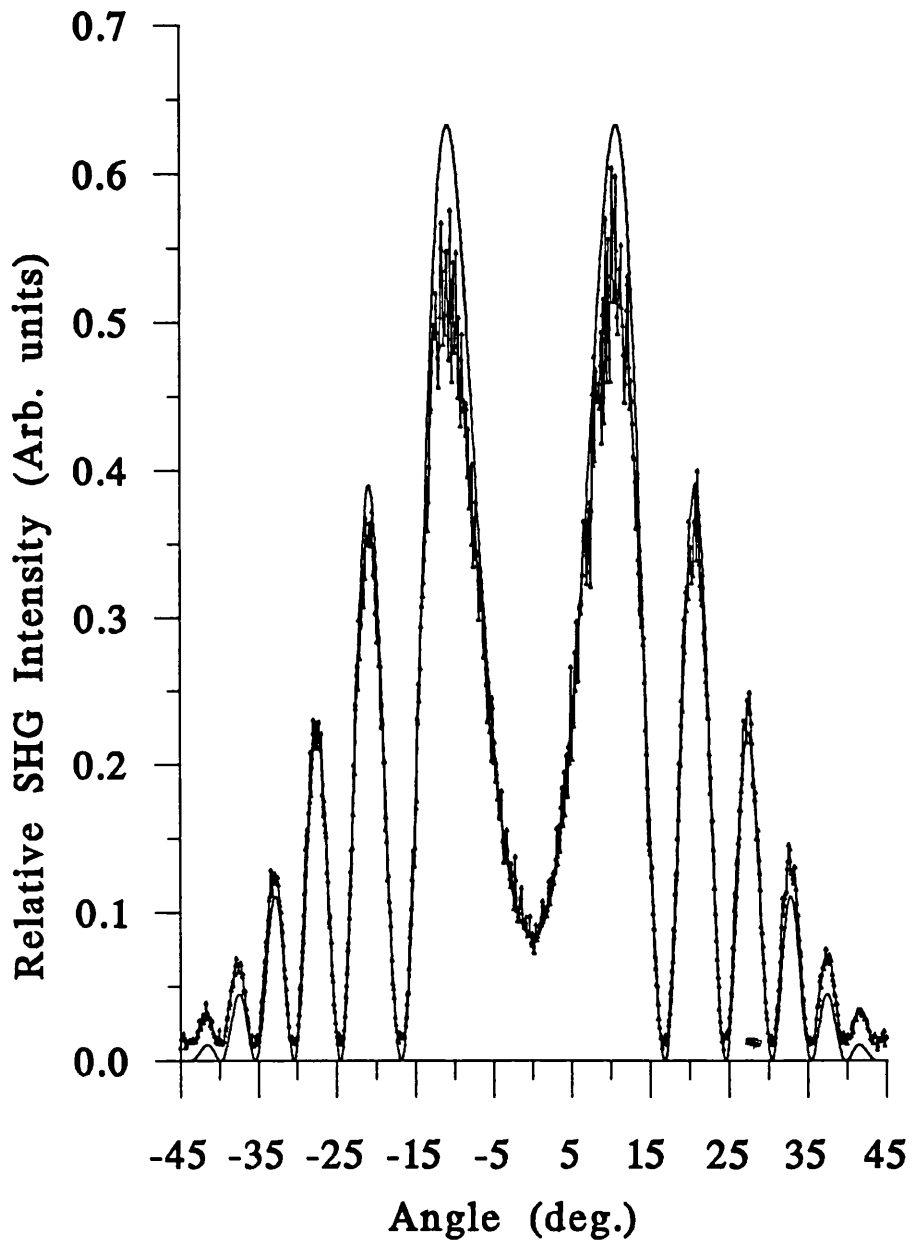


Figure 4.7 Maker fringes for Quartz with theoretical fit.

4.5 Investigation of a Standard FLC material - SCE13(*).

Most of the nonlinear optical investigations of the chiral smectic C liquid crystal phase have been carried out using the homeotropically aligned cell configuration described earlier which is fast becoming a standard in this field [Taguchi et al, (1989)]. The liquid crystal alignment is relatively simple to achieve, and produces a uniform structure through the cell with the c_2 axis in the plane of the cell. This compares well against the widely used planar cells with surface stabilised alignment used in display type applications, where a complex chevron structure is known to form in place of the simple bookshelf geometry initially expected. These cell structures are limited in thickness to a maximum of a few microns to achieve the desired surface stabilisation of the spontaneous twist in the smectic C phase. The c_2 axis in this geometry is usually pointing into the cell substrates, and is not in an accessible direction for transmissive devices.

There are a number of different surface stabilised alignments which can be achieved by varying the surface alignment layers. Some of these may result in uniform structures without the presence of a chevron interface, and have a component of the c_2 axis in the plane of the cell. These geometries would be of considerable interest as they may result in efficient configurations with phase matching abilities without the requirement for aligning voltages to stabilise the molecular structure. To investigate SHG in ferroelectric liquid crystals the commercial material SCE13(*) from Merck Ltd was chosen as a standard material. It has a useful range of overlying liquid crystal phases and has had many of its optical, dielectric and alignment properties characterised by other techniques including refractive index data, P_s and tilt angle data. SCE13 is actually composed of a mixture of materials, some of which impart smectic C behaviour, and others which introduce chirality, but are not liquid crystalline themselves. The overall result is a chiral smectic C liquid crystal which is ferroelectric with P_s dominated by the chiral dopants.

4.5.1 Analysis of SCE13(*) using Homeotropic Cells.

The homeotropic cell geometry is shown in figure 4.8 in cross-section. Surface treatments such as solutions of chrome complex, HEMAB, lecithin or silanes may be spun down or dip coated onto clean glass substrates to produce homeotropic alignment. These surface alignment agents tend to have a polar head group and a hydrophobic tail. The polar group bonds strongly to the glass substrate, leaving the hydrophobic tail standing up to interact with any similar group on the liquid crystal molecules. These molecules would then have a preference to stand up on end at the interface, influencing the direction of molecular layers above. With both internal surfaces of a cell treated, quite good alignment can be achieved in relatively thick cells, up to 100 μm in cases.

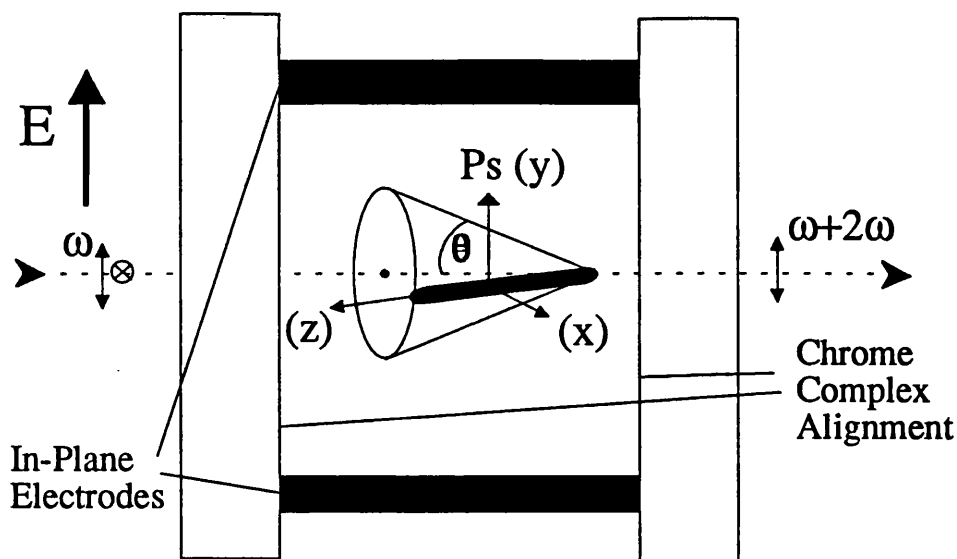


Figure 4.8 Homeotropic cell geometry in cross section.

The molecular chirality which is required to remove inversion symmetry and produce a polar c_2 axis also results in a tendency for the molecules to twist into a helical structure in the bulk material. The homeotropic surface alignment is not able to prevent the formation of a helix in the cell. The helix can be unwound by the application of external electric field which couples to the P_s of the material, or magnetic field which couples to the biaxiality in the magnetic susceptibility of the material. A uniform untwisted structure can be produced by applying transverse electric fields (along y) in the plane of the cell using in-plane electrodes. This electric field rotates all the molecules to one side of the cone. It is preferable that these electrodes extend all the way across the thickness of the device to produce a uniform electric field, and consequently uniform alignment. As the transverse electric field is increased from zero, then the SHG intensity increases until at a critical value the helix is fully unwound, and the P_s is aligned parallel to the electric field. Close investigation of this unwinding effect is described in chapter 5.

The cell used was $6 \mu\text{m}$ thick and filled with chiral SCE13, a standard ferroelectric mixture from Merck (UK) Ltd. The measurement was made at 50°C , which is 10° below the smectic C - A transition. At this temperature the pitch length of SCE13(*) was the order of $3 \mu\text{m}$. The field required to fully unwind the helix was 8 Vmm^{-1} , or 16 V across a 2 mm electrode spacing. This critical field strength depends upon elastic constants of the material and the size of the P_s , and will obviously vary from material to material.

The structure and co-ordinate system for the fully unwound material is shown in figure 4.9. The electric field was applied along the y axis, rotating the molecules to lie on one side of the cone, which has a half angle θ . The normal to the smectic layers and the cell is parallel to the Z axis, and the incident beam makes an angle of incidence α to this axis. The cell was rotated about the Y axis, allowing variation in α from -50° to $+50^\circ$. The sign of θ could be changed by reversing the polarity of the electrodes.

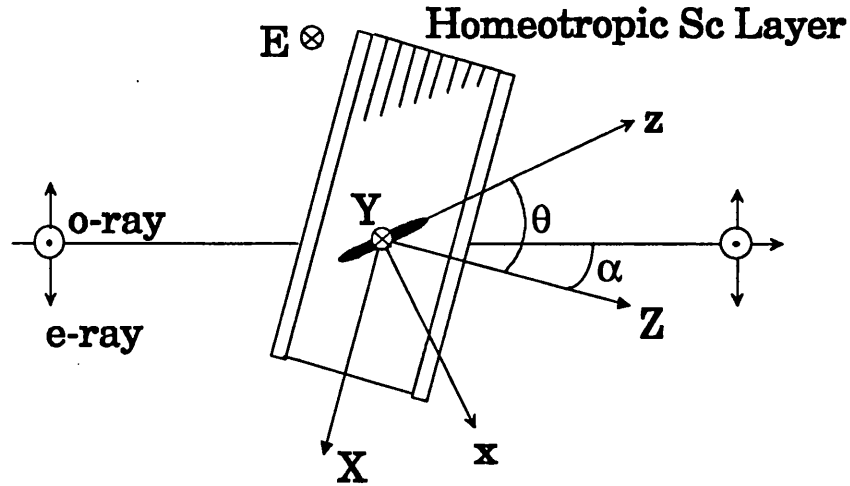


Figure 4.9 Untwisted homeotropic material geometry.

The symmetry of the ferroelectric liquid crystal material in this alignment has a 2 fold rotation axis parallel to y and two mirror planes in the xy and yz planes (class 2 symmetry or 2mm). Symmetry arguments reduce the nonlinear tensor of this alignment to

$$\underline{d} = \begin{pmatrix} 0 & 0 & 0 & d_{14} & 0 & d_{16} \\ d_{21} & d_{22} & d_{23} & 0 & d_{14} & 0 \\ 0 & 0 & 0 & d_{23} & 0 & d_{14} \end{pmatrix} \quad 4.23$$

using the assumptions of Kleinmann symmetry [Kleinmann, (1962)]. By using different combinations of input polarisation and polarisation of the second harmonic radiation, two independent combinations of nonlinear coefficients can be investigated. In the case of both input and second harmonic light being polarised parallel to the y axis

$$d_{eff} = \underline{e}_o^{2\omega} \underline{d} \underline{e}_o^\omega \underline{e}_o^\omega, \quad 4.24$$

where

$$\underline{e}_o^\omega = (\sin \phi \quad -\cos \phi \quad 0) \quad 4.18$$

relative to the molecular frame, and ϕ is the angle between the electric field vector of the light and the y axis. Thus d_{eff} can be calculated to be

$$d_{eff} = -d_{22} \cos^3 \phi. \quad 4.25$$

In this configuration ϕ is constant at a value of 0° , therefore

$$d_{eff} = -d_{22} \quad 4.26$$

for this combination of polarisations. It is expected that this component of the nonlinear tensor is one of the largest as it couples electric fields from the input and second harmonic polarised along the c_2 axis of the molecules. Unfortunately, in this geometry it is not possible to achieve the phase matching criteria of

equation 4.5, as each wave only experiences the y component of the refractive index, and $n_y^\omega \neq n_y^{2\omega}$ and so it is not suitable for efficient SHG device configurations.

The second combination of polarisations is when the input beam is polarised in the plane of incidence (an extraordinary ray) and the second harmonic is again polarised parallel to the y axis. In this geometry type I phase matching can be achieved by angle tuning the device about the y axis. For this combination of polarisations the effective nonlinear coefficient was calculated to be

$$d_{eff} = -d_{21} \cos^2(\theta - \alpha) - d_{23} \sin^2(\theta - \alpha) + d_{14} \sin 2(\theta - \alpha). \quad 4.27$$

The special case of $\theta = \alpha$ results in d_{eff} reducing to d_{21} (which is equal to d_{16} under Kleinmann symmetry conditions). However, before the Maker fringes for these configurations can be calculated using equation 4.4, the refractive indices, cell thickness and tilt angle must be measured.

The device thickness was measured when the cell was empty using interference fringes produced from a Perkin Elmer $\lambda 9$ spectro-photometer, as described in chapter 3. It was assumed that the cell thickness did not vary before and after filling. The cone angle of the material was measured as a function of temperature using a planar cell geometry and a polarising microscope. After achieving good planar alignment, the device was switched between its two fully switched states using a square wave voltage with a frequency of a few hertz. Rotation of the cell between crossed polarisers can achieve extinction of each of the two fully switched states. The angle through which the cell must be rotated to move from one extinction condition to the other is equal to twice the cone angle θ if the alignment is approximated to be bookshelf. The error in the cone angle measurement due to the chevron structure is virtually insignificant. The cone angle at 50°C was measured to be $16.4 \pm 0.4^\circ$; at 40°C was equal to 20° ; and at 25°C was equal to 23° .

The refractive indices of the material at ω and 2ω were measured using a wedge cell. This is a liquid crystal cell with the same alignment layers and electrodes as the homeotropic cell described above, but it is assembled to have a linear variation in thickness across the cell. The measurement of refractive indices by this method is described in detail in chapter 5, and in summary the values for SCE13* at 50°C were:

$$\begin{aligned} n_y^{2\omega} &= 1.489 \pm 0.002 & n_x^\omega &= 1.478 \pm 0.002 \\ n_y^\omega &= 1.479 \pm 0.002 & n_z^\omega &= 1.622 \pm 0.004 \end{aligned}$$

Maker fringes produced from the $e_o^{2\omega} e_e^\omega e_e^\omega$ polarisation configuration are shown in figure 4.10 with a numerical fit to equation 4.4 using the refractive index data above. A thick cell ($L = 46 \mu\text{m}$) was used to give a number of fringes over the measurable angle range. An electric field of $0.025 \text{ V}\mu\text{m}^{-1}$ was used to unwind the helix, and the sample measured at 50°C. The quality of the fit is surprisingly good given the non-perfect alignment when viewed under a polarising microscope.

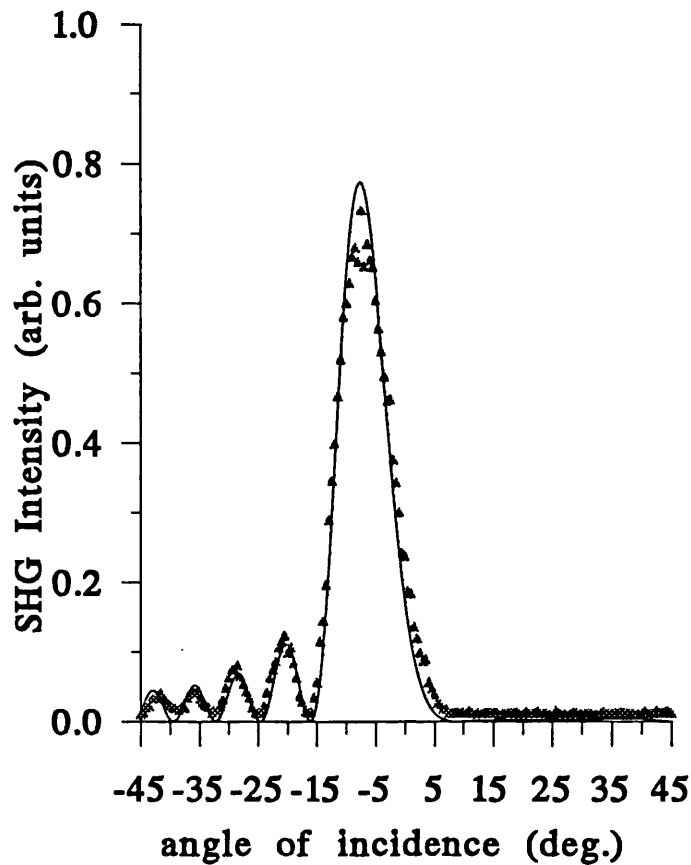


Figure 4.10 Maker fringes in homeotropically aligned SCE13.

Wedge cell measurements of SCE13* using horizontally polarised fundamental radiation at the angle of incidence 24.28° (refracted angle $\cong 16.4^\circ$) resulted in phase matched SHG from variation in device thickness across the wedge, as shown in figure 4.11. This configuration accessed only the d_{21} coefficient, and from the amplitude of the maximum, an estimate of the coefficient was made.

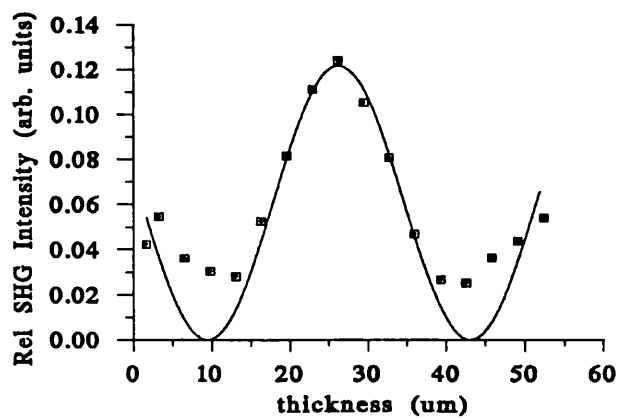


Figure 4.11 Wedge fringes for ee0 polarisations at $\alpha = 24.28^\circ$.

4.5.2 Molecular and Bulk Nonlinear Coefficients.

A measurement of the bulk nonlinear coefficient d_{eff} for SCE13 at 50°C can be made from the amplitude of the phase-matched peak in graph 4.10 using equations 4.16 and 4.22. At the angle of incidence of -6.5°, the value of d_{eff} was calculated to be 0.0008 pmV⁻¹ for eeo polarisations. The d_{21} coefficient, which had not been directly measured in ferroelectric liquid crystal materials before, was estimated from figure 4.11 to be 0.0001 pmV⁻¹. Similarly, a value of d_{22} was also calculated from the SHG data measured using ooo polarisations, and was equal to 0.0031 pmV⁻¹. Both of these values are very small in comparison to other types of materials used for second harmonic generation. However, this is not surprising, as SCE13* was not developed for nonlinear optical applications, and only about 10% of the material contained in the mixture is chiral.

In crystalline or even polymer materials for SHG, there has been a great deal of success in relating values of the molecular hyperpolarisability to the bulk nonlinear coefficient. The values for the hyperpolarisabilities have been calculated using ab-initio or semi-empirical models [Prasad & Williams, (1991)]. The molecular orientation may be calculated within the unit cell of the material, and combined with the volume of the unit cell, it is possible to produce values for the nonlinear d coefficients which correlate with the measured values. This should also be possible in liquid crystal materials.

Equation 2.8 in chapter 2 described the translation from the molecular nonlinear hyperpolarisability to the bulk coefficient for a crystalline material. This equation has also been adapted to describe poled polymers and EFISH measurements by changing the unit of material for calculation from the crystal unit cell to the number density of molecules (N) in a non-crystalline material [Zyss & Oudar, (1982)]. Equation 2.8 then becomes

$$\chi_{ijk}^{(2)}(-\omega_3; \omega_1, \omega_2) = N f_i^{\omega_3} f_j^{\omega_1} f_k^{\omega_2} \langle \beta_{ijk}(-\omega_3; \omega_1, \omega_2) \rangle_{ijk} \quad 4.28$$

and the orientational average of the hyperpolarisabilities is calculated using Euler angles from

$$\langle \beta_{ijk} \rangle_{ijk} = \int d\Omega a_{i1} a_{j2} a_{k3} G(\Omega) \beta_{ijk} \quad 4.29$$

where a_{Xx} are the direction cosines and $G(\Omega)$ is a distribution function.

It would be impossible to calculate the orientation for each molecule within the liquid crystal phase, and so to simplify the calculation I shall make a number of approximations about the molecules and the chiral smectic C phase they form. The approach shall follow the theory of Zeks et al [1988], and its application by Buka et al [1989]. The microscopic model of Zeks et al assumed that the hindered rotation of the molecules around their long molecular axis can be described by a single particle potential $U(\psi)$

$$U(\psi) = U_1 + U_2 = -a_1 \theta \cos \psi - a_2 \theta^2 \cos 2\psi. \quad 4.30$$

where $\psi = 0$ when the c_2 axis is perpendicular to the plane of the tilt (θ) and parallel to the direction of P_S . The first term describes the polar nature of the potential and the second term is due to the biaxiality of the

molecules. Generally the second term is much larger than the first, and so the combined potential has two minima and two preferred orientations exist at $\psi = 0$ and π . The minimum at $\psi = 0$ is deeper than at $\psi = \pi$, and so it is more likely that the molecules will be found at this orientation.

Buka describes how the spontaneous polarisation can be related to the polar order parameter Π for rigid molecules which have perfect nematic order ($S=1$)

$$P_s = \rho \mu_{\perp} \langle \cos \psi \rangle \quad 4.31$$

where ρ is the number density and μ_{\perp} is the transverse component of the molecular dipole moment along the c_2 axis. This expression ignores any contributions to μ_{\perp} from the longitudinal dipole moment due to molecules not having perfect order. Both the ferroelectric polarisation and the second order nonlinear coefficient have a similar requirement of noncentrosymmetry, and so have only non-zero components involving the c_2 transverse polar axis of the molecules. From equation 4.28 and 4.29, the nonlinear coefficient can be found from

$$d_{ijk} = \chi_{ijk} / 2 = N/2 f_i^{\omega} f_j^{\omega} f_k^{2\omega} \langle \beta_{ijk} \rangle_{ijk} \quad 4.32$$

In the case of input and output polarisations being parallel to the y axis, then equation 4.32 is reduced to

$$d_{yyy} = N/2 f_y^{\omega} f_y^{\omega} f_y^{2\omega} \beta_y \langle \cos^3 \psi \rangle. \quad 4.33$$

There is experimental evidence to suggest that the second order nonlinear coefficient has a similar dependence on the temperature as the P_s of the bulk material. This temperature dependence was measured in the homeotropic geometry for the coefficient d_{22} of SCE13, and is shown in figure 4.12.

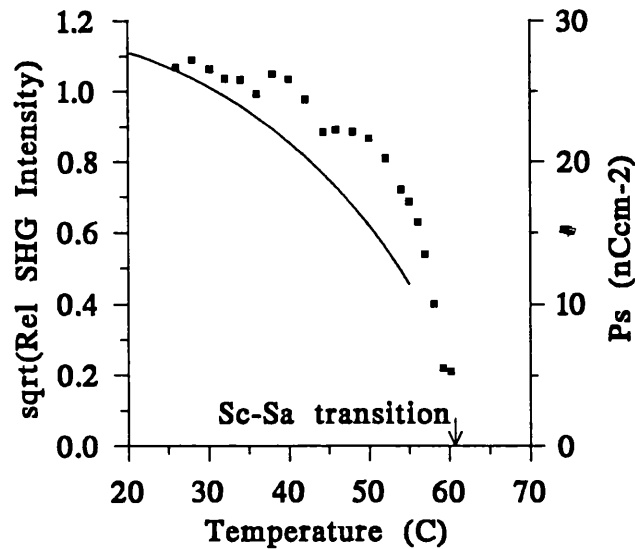


Figure 4.12 Temperature dependence of d_{22} and P_s in the smectic C phase of SCE13*.

The potential $U(\psi)$ can be used to calculate the polar order parameter from

$$\langle \cos \psi \rangle = \frac{\int_0^{2\pi} \cos \psi \exp(-U/kT) d\psi}{\int_0^{2\pi} \exp(-U/kT) d\psi}. \quad 4.34$$

Expanding $\exp(-U/kT)$ up to second order terms and integrating between the limits shown, the equation describing P_s becomes

$$P_s = \mu_{\perp} \rho \theta a_1 \frac{2kT + a_2 \theta^2}{4(kT)^2 + (a_1 \theta)^2 + (a_2 \theta^2)^2}. \quad 4.35$$

To obtain the complete temperature dependence of $\langle \cos \psi \rangle$, the temperature dependence of the cone angle θ can be found from

$$\theta = \theta_0 (T_{CA} - T)^{\alpha} \quad 4.36$$

where T_{CA} is the temperature of the smectic C to smectic A transition, and θ_0 and α were be found from fitting cone angle versus temperature data to equation 4.38 to be

$$\theta_0 = 5.0^{\circ}$$

$$\alpha = 0.4.$$

Equation 4.35 then becomes

$$P_s = A(\Delta T)^{\alpha} \frac{BT + BC(\Delta T)^{2\alpha}}{T^2 + B^2 \theta_0^2 (\Delta T)^{2\alpha} + C^2 (\Delta T)^{4\alpha}} \quad 4.37$$

where $\Delta T = (T_{CA} - T)$, $A = \rho \mu_{\perp} \theta_0$, $B = a_1/2k$ and $C = a_2 \theta_0^2/2k$. When fitting this equation to P_s vs temperature data (using NAG routine E04FDF) as shown in figure 4.13, it was noticed that there were several sets of values for A, B and C which fitted the data equally well. Therefore it was not possible to calculate a value for $\langle \cos \psi \rangle$ from this data and numerical fit alone. A value for the parameter A was calculated from the number density of the molecules together with a value for the transverse dipole moment from molecular modelling, and so the numerical fit was reduced to two variables. The values for A, B and C were

$$A = 180.1 \text{ nCradcm}^{-2}; \quad B = 105.7 \text{ K}; \quad C = 11.11 \text{ K}$$

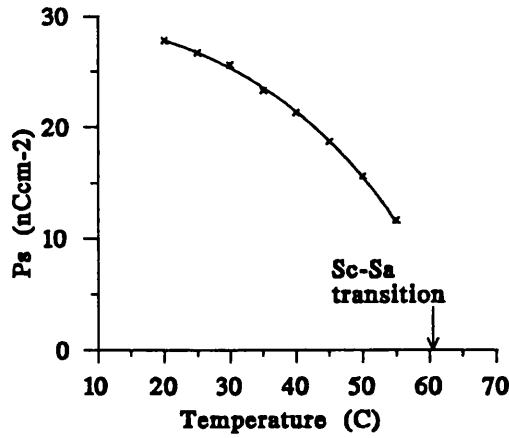


Figure 4.13 Temperature dependence of P_s and numerical fit using equation 4.36.

from which the amplitudes for the potential $U(\psi)$ were calculated to be

$$a_1\theta\cos\psi \cong 5.5 \times 10^{-23} \text{ J} \quad \text{and} \quad a_2\theta^2\cos 2\psi \cong 1.9 \times 10^{-21} \text{ J}.$$

The amplitudes of the potential wells are less than the thermal energy kT (4.5×10^{-21} J). The amplitude of the polar component is smaller than the non-polar term, close to the ratio of two hundred as reported elsewhere [Buka et al., (1989)]. There will be a small additional contribution to the polar term due to the coupling of the P_s with the electric unwinding field. Initial thoughts expected this contribution to be significant, but in fact the potential energy for a dipole of 5 Debye in a field strength of 50 Vmm^{-1} is only 1×10^{-24} J, and so has little significance.

The theoretical values for the bulk nonlinear coefficient were calculated using the value of $\langle \cos^3 \psi \rangle$, using a similar derivation to the polar order parameter

$$\langle \cos^3 \psi \rangle = \frac{\int_0^{2\pi} \cos^3 \psi \exp(-U/kT) d\psi}{\int_0^{2\pi} \exp(-U/kT) d\psi}. \quad 4.38$$

After some algebra, together with the substitution of equation 4.35 to describe the temperature dependence of the tilt angle, equation 4.38 becomes

$$\langle \cos^3 \psi \rangle = \frac{a_1\theta_o(\Delta T)^\alpha}{2} \frac{(3kT + 2a_2\theta_o^2(\Delta T)^{2\alpha})}{4(kT)^2 + (a_1\theta_o)^2(\Delta T)^{2\alpha} + (a_2\theta_o^2)^2(\Delta T)^{4\alpha}}. \quad 4.39$$

Substituting values for the various parameters found from fitting P_s data to equation 4.36, then

$$\langle \cos^3 \psi \rangle \cong 0.066.$$

This value can now be substituted into equation 4.32 to calculate a value for the bulk nonlinear coefficient, together with molecular values for the transverse hyperpolarisability calculated using molecular modelling packages. It was not the intention of this work programme to be involved significantly in the field of computer modelling of molecules. However, it is often useful to have access to such techniques to enhance a work programme. For this study, the molecular dipole moments and hyperpolarisabilities of the chiral components of the SCE13 mixture, and also other novel materials showing interesting properties were modelled by Dr David Dunmur at Sheffield University. Dr Dunmur has considerable expertise in molecular modelling of liquid crystal systems [Dunmur & Wilson, (1989); Wilson & Dunmur, (1989)].

The modelling technique initially calculated the minimum energy conformation of the molecule when isolated in free space using MM2 molecular mechanics package. Inside a liquid crystal phase the molecular potential will have a characteristic form, resulting in a slightly different shape of molecule. This effect is expected to be small for typical liquid crystals. Once the molecular conformation has been calculated, the electron distribution within the molecule can be modelled using the semi-empirical electronic structure MOPAC 5 & 6 packages [Kurtz et al, (1990)]. These programs use two techniques to calculate the polarisabilities and hyperpolarisabilities. The first calculates the energy of a molecular system within a uniform electric field, using the conventional polarisability expansion, and truncating at the (field)⁴ terms. This results in four unknowns, and so solving four field strengths ($\pm F$, $\pm 2F$) simultaneously gives equations for the dipole moment, polarisability and second order hyperpolarisability terms. The second method calculated the induced dipole moment in place of the energy, and isolated terms using different field strengths similar to the previous method. The calculations used the Modified Neglect of Diatomic Overlap (MNDO) method which was described in chapter 2. The results of both methods were very similar.

The principle axes of the molecules for these calculations are the principal inertial axes of the molecule. One of these axes (the z axis) lies approximately along the long axis of the molecule. However, it is difficult to relate the remaining two axes with the c_2 axis of the molecules. One simple approximation is to only use two dimensional molecules. This approximation is a very simple model which still accounts for polar order and biaxiality in the material. Geometrically, the molecules may be considered as flat rectangles in the plane containing the director and the c_2 axis, and the tilt is out of the plane of the rectangle. The component of the desired molecular property along the c_2 axis is approximated to be the average of the two calculated transverse components, and remaining component in the xy plane is equal to zero.

When mixtures of materials, for example SCE13, are investigated then it will be assumed that the chiral dopant dominates all polar characteristics of the material, and the liquid crystal host does not

contribute to the P_s or $\chi^{(2)}$. This is satisfactory under the conditions that the concentration of chiral dopants is small (~10%) and the transverse dipole of the chiral molecules is larger than the non-chiral host [Pikin & Osipov, (1991)]. The composition of the commercial ferroelectric mixture SCE13 has not been published, and so cannot be described here. However, the transverse dipole moment and the hyperpolarisability were calculated from modelling to be 1.12×10^{-30} Cm and 1.57×10^{-41} m⁴V⁻¹ at 1.064 μ m respectively.

From the value for μ_{\perp} , $\langle \cos\psi \rangle$ can be calculated as a function of temperature. The value of $\langle \cos\psi \rangle$ was 0.086 at 50 °C. Assuming an average molecular weight of 370 atomic units for the liquid crystal molecules, the number density of the chiral components was approximately 1.62×10^{26} m⁻³ for a 10% concentration. The d_{22} coefficient was calculated from this data to be 0.0004 pmV⁻¹, which is significantly lower than the measured value of 0.003 pmV⁻¹. The factor of 10 discrepancy must be accounted for within the model for the bulk nonlinear coefficients, as experimental values have been confirmed for similar ferroelectric mixtures [Liu et al, (1991)].

There are a number of possible sources of error in the model proposed to link microscopic and macroscopic values of nonlinear coefficients in ferroelectric liquid crystals. The largest uncertainty is associated with the calculated value of transverse hyperpolarisability for the chiral dopant molecules. The value from modelling was approximately 1.6×10^{-41} m⁴V⁻¹, which is very small in comparison to the value for nitrobenzene at 9×10^{-40} m⁴V⁻¹. It is difficult to associate an error with the calculated values of hyperpolarisabilities, particularly for a system which is relatively unknown in the nonlinear optics field (e.g. liquid crystals), and where there is no work published in modelling these systems. A similar uncertainty is associated with which value of β_{\perp} to use, as the modelling frames of reference in isolated molecules do not necessarily coincide with those used experimentally in the liquid crystal phase. The value used was the resultant of the two principal transverse components

$$\beta_{\perp} = \sqrt{\beta_{yy}^2 + \beta_{zz}^2}$$

where x is the long axis of the molecule. Including the value of a very large off-axis term (β_{yxx}) in addition to β_{yyy} and β_{zzz} terms could reduce the discrepancy between modelling and experiment to within a factor of 2.

Another possible source of error is that the molecules do have very large polarisabilities and hyperpolarisabilities along the long axis of the molecule (z). It may be possible that the unwinding field is inducing a longitudinal dipole which is then tending to align the long axis in a noncentrosymmetric manner, so that the longitudinal hyperpolarisability can contribute to the bulk nonlinear coefficient. The deviation of the system away from a perfect nematic order parameter may introduce fluctuations which contribute to this effect.

Other sources of discrepancy between the theoretical model and experimental values would be some of the simplifying approximations used in the model. The assumption that the non-mesogenic chiral

dopants have the same polar order parameter as the smectic C host molecules may be inadequate. It is well known that guest-host systems can exhibit two order parameters, where the order of the host differs slightly from the pure material by the presence of the guest, and the guest has a different order parameter to the host. There may also be a disrupting influence of anti-parallel order of the transverse dipole, however evidence of this would be expected to be seen in the value of P_S .

In many liquid crystal device structures, it is believed that the molecular orientation is not constant through the device. The chevron interface or splayed alignments are common, and it is suspected that the molecular order and alignment may change at the surfaces of the device due to the influence of the alignment layers. Any small variations in alignment was ignored in this work, and the alignment in these cases approximated to be uniform. However, large changes such as the chevron interface must be included in the model if planar cell geometries are used.

In summary, the comparison between experimental values of d_{22} and those calculated from modelling are close, but there are discrepancies. It is not unusual for modelling and experiment to have inconsistencies in the values of nonlinear coefficients, even for well defined crystalline systems [Kurtz et al, (1979)]. The assumptions used in the modelling to reduce the calculation to a manageable form will affect the accuracy of the result, e.g. the number of polarisable electrons included, and the degree of wavefunction overlap.

4.6 Novel FLC Materials with High Nonlinear Optical Coefficients.

The ferroelectric liquid crystal mixture SCE13 used in previous sections to investigate different alignment geometries is far from ideal as a nonlinear optical material. Although it has a room temperature ferroelectric phase, its nonlinear optical coefficients are very small in comparison with other classes of nonlinear optical materials. The reasons why the nonlinear coefficients are small are well understood. Firstly, the material is a mixture of chiral molecules and a non-chiral smectic C host material. The percentage of chiral molecules will be about 10%. The chiral molecules are typically cyano mesogens [Walba et al, (1991A)], and have transverse molecular hyperpolarisabilities of the order of $2 \times 10^{-41} \text{ m}^4 \text{V}^{-1}$. These values are relatively low, but it must be pointed out that these molecules were not developed for nonlinear optical applications. The second order polar order parameter was measured to be

$$\langle \cos^3 \psi \rangle \cong 0.066.$$

This suggests that very few of the molecular c_2 axes are aligned to contribute towards d_{eff} . Taking these three factors together, one would only expect very low nonlinear optical coefficients from SCE13, as the experimental measurements of $d_{\text{eff}} = 0.0008 \text{ pmV}^{-1}$ have verified.

For ferroelectric liquid crystals to be competitive as nonlinear media, the values of the bulk nonlinear coefficients must be increased from the values for SCE13 by at least two orders of magnitude,

and if possible three or more. If this were expected to be achieved solely by increasing the molecular hyperpolarisability, then this problem would probably be impossible. However, improvements in the molecular values, number density of active molecules and alignment suggest that this task is achievable.

The easiest improvement in the nonlinear coefficient was achieved by increasing the number density of chiral molecules in the material. Using a single component material where the chiral molecules alone form a smectic C phase would increase the number density from approximately 10% to 100%, giving an improvement in the bulk nonlinear coefficient of one order of magnitude. The molecular hyperpolarisability and the polar order parameter are the other two factors which may be used to increase the bulk nonlinear coefficient, but it is less obvious how to achieve this.

A new approach to the design of molecules with improved functional groups oriented along the polar (c_2) axis has been reported recently [Furukawa et al, (1988); Walba et al, (1991)B]. This work was aimed at producing molecules which possess smectic C phases and which have orientation of groups with large hyperpolarisabilities along the c_2 axis. It is well known that phenyl rings with donor and acceptor groups substituted in ortho or para positions can result in large hyperpolarisabilities (e.g. pNA, mNA, MNA), and it was the intention of this work to combine such groups into a ferroelectric liquid crystal such that the large β was oriented along the c_2 axis.

For conventional ferroelectric liquid crystals the position of the chiral centre in the chiral molecules used was of minor importance. It was usually positioned part way along an alkyl chain towards one end of the molecule. The P_S which resulted from the chiral centre was due to groups rigidly attached to the chiral atom and perpendicular to the long axis of the molecule. In most cases the P_S was quite small ($<10n\text{Ccm}^{-2}$), but could be improved by attaching a polar group to the chiral centre ($<40n\text{Ccm}^{-2}$). The approach taken by Walba et al and Furukawa et al was to move the position of the chiral centre very close to the rigid aromatic core of the molecules. Attempts to hinder the rotation of the chiral group relative to the adjacent phenyl ring allowed the ring to contribute towards the transverse dipole along the c_2 axis. This hindered rotation was achieved by attaching large groups into positions overhanging the chiral group (2 or 4 positions), which encroach into the space occupied by the previously freely rotating chiral group, as shown in figure 4.15.

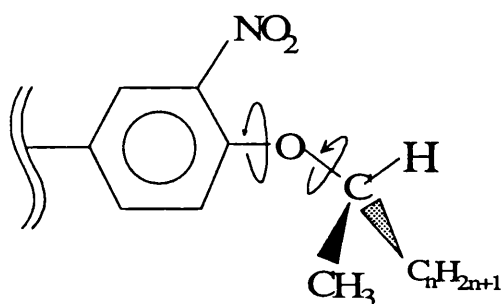


Figure 4.15 A typical molecular structure exhibiting hindered rotation of the chiral group.

The nitro group was selected as the hindering group because of its size, and because it is also a good electron acceptor which resulted in increased hyperpolarisabilities for the molecule. In fact the nitro group and the delocalised electron system of the phenyl ring result in a transverse hyperpolarisability which overwhelms the contribution from the methyl group attached to the chiral centre. This technique of increasing the transverse molecular hyperpolarisability can be developed further by including an electron donating group opposite the electron acceptor (e.g. NH_2), producing a 'push-pull' system across the molecule, with a molecular hyperpolarisability comparable to para-nitroaniline. Unfortunately, these bulky side groups have a detrimental effect on the stability of the smectic C phase of the material, and frequently destroy the C phase.

The coupling of the large functionalised phenyl ring to the chiral centre may also have an effect on the polar order parameter. This large system will probably be more difficult to rotate about its long molecular axis, and so the amplitudes a_1 and a_2 of the molecular potential $U(\psi)$ are probably larger than for simpler molecules. This effect will directly improve the bulk nonlinear coefficient from the value found in conventional ferroelectric materials.

4.7 Evaluation of New Materials for Nonlinear Optics.

A range of new molecules were designed and synthesised based on the ideas described above. Unfortunately, accurate prediction of liquid crystal phase sequences and phase temperatures from molecular structures is almost impossible, and so the materials must be synthesised to assess their suitability. The skills of liquid crystal synthetic chemists can be used to modify molecular structures to enhance the likelihood of producing materials with stable smectic C phases.

The materials synthesised for this study are shown in table 4.1 with their phase transitions and measured values of P_S and d_{22} . The materials were synthesised at Hull University by the liquid crystal synthesis group lead by Professor J.G. Goodby. The synthesis of these materials will be the subject of a thesis by S.J. Cross, and the details will not be described here.

The materials were investigated by DSC and optical microscopy to measure and identify the phase transitions. P_S measurements were made in planar cells of 6 μm thickness by the triangular wave method preferably in the pure material, and where possible at 10°C below the smectic C-A transition. Where the material did not exhibit a smectic C phase, the material was mixed with a racemic version of SCE13 host material with approximately 10% nonlinear material added. The values measured were then extrapolated to 100% concentration. This extrapolation is quite crude and the measured value of P_S dependent on the host used, but is satisfactory to obtain a guide to the values of P_S . Blank spaces in the table usually indicate that a measurement was attempted but the value was below the noise level.

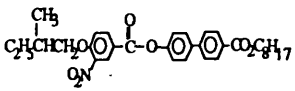
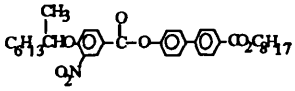
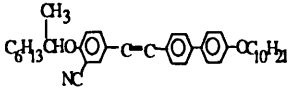
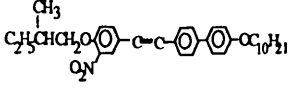
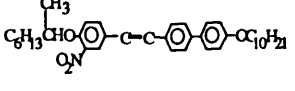
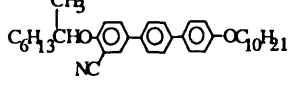
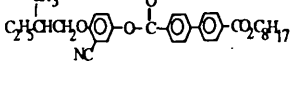
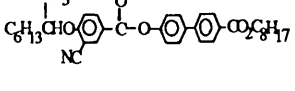
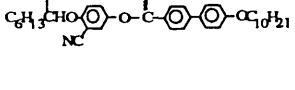
Working name	Structure	Phase transitions	Quality of alignment	P_s at -10°C (nCcm^{-2})	d_{22} (pmV^{-1})
SCE13	Commercial Mixture	$S_i < -20$ S_c 60.8 S_a 86.3 N 100.8 I	Excellent.	27.8	0.003
SJ42		K 38.1 S_c 62 S_a 134.4 I	Quite good.	14	0.003
SJ54		K 36.3 S_c 56.9 S_a 63.1 I	Moderate.	405 (max. 550)	0.04
SJ85		K 65.3 S_a 106.9 I	Poor. (9.5%)	2.4	
SJ87		K 60.5 S_c 91.1 S_a 145.9 I	Quite good.		0.0006
SJ94		K 78.7 S_a 100.5 I	Quite good. (5.2%)		
SJ97		K (59.5 S_c) 62.3 S_a 100.7 I	Good.	230 (@ 55°C)	0.015
SJ98		K 95.1 S_c 115.2 S_a 170 I	Quite good.	7	0.001
SJ101		K 57.5 S_c 62.8 S_a 65.2 I	Very poor.		0.021
SJ115		K 66.5 S_c 100.2 S_a 119.7 I	Good.	310 (max. 480)	0.046

Table 4.1 Nonlinear optical smectic C liquid crystal materials.

The measurement of the nonlinear coefficient was made using the homeotropic cell geometry using sufficient in-plane electric field to unwind the molecular helix. This configuration gave direct access to the d_{22} coefficient. Due to poor alignment, the refractive indices and dispersion for these materials could not be measured, but was approximated to be equal to SCE13 for the calculation of d_{22} . It was also assumed that the largest SHG intensity measured from these materials was in the phase matched condition. This approximation gave a minimum estimation of d_{22} - the true values for the materials may be higher than those reported in table 4.1 above.

The data in table 4.1 illustrates a number of correlations between the molecular structure and the values of P_S and d_{22} . Firstly, the presence of a CH_2 spacer in addition to the oxy- linkage between the chiral centre and the functionalised phenyl group has a large detrimental effect on the bulk values. This suggests that the spacer is sufficient to separate and decouple the chiral and phenyl groups so that no hindered rotation occurs. The P_S and d_{22} values measured in these cases originate from the chiral centre with its transverse methyl group, which has poor coefficients due to the lack of polarisable electrons.

Probably the next largest effect on the values is the ability of the material to form a stable and well aligned structure for measurement. This factor is very difficult to eliminate or account for in calculations, and so makes comparisons between two molecules (e.g. SJ54 & SJ101) difficult. It is however, a factor which must be taken into account when evaluating materials for potential device applications and so is useful to note. Strong influences on the alignment quality are the pitch length of the smectic C helix, the type of liquid crystal phases above the smectic C phase, and the width of the smectic C phase. Materials with short pitches tend to 'wind up' easily, making it difficult for the surface forces to align the molecules in a uniform structure. This may be compensated by mixing with other materials which have an opposite winding sense. It was found from P_S and SHG measurements that mixing molecules with a standard host (SCE13 Racemic) had a detrimental effect on the polar order and the value of β beyond the simple number density factor. It was believed the high concentration of host molecules disrupted the hindered rotation system, thus reducing the value of β and Π . Miscibility studies between two or more materials of the same type e.g. materials from table 4.1 may improve the smectic C phase without destroying the hindered rotation of the molecules, or the number density if both are chiral.

The presence of nematic and/or smectic A phases above the smectic C phase can assist alignment by reducing the enthalpy change at the phase transition into smaller amounts, and giving the molecules an opportunity to align in each phase so that only small molecular reorientations are required on changing phase. All of the materials in this study had an overlying smectic A phase which was useful when aligning the material. It was found that several narrow smectic C phases were not stable, but slowly crystallised. Measurements may be made in the smectic C phase for these materials (e.g. SJ97), but the alignment deteriorated as a function of time (< 1 hour) as the material crystallised.

Detailed comparison of P_S and d_{22} with molecular structure was limited due to the strong dependence upon the quality of the alignment. Most of the modifications to the molecules were targeted at

improving the smectic C phase alignment by varying the alkyl tail lengths, inclusion of ester groups or tolane linkages etc. using techniques developed over many years of synthesis of ferroelectric liquid crystals. Relatively small modifications to the molecules could have a dramatic affect on the phases and alignment quality (compare SJ101 & SJ115). Modifications which were expected to affect the transverse hyperpolarisability were the use of nitro and cyano groups on the phenyl rings, and the effect of different groups (e.g. ester, tolane, biphenyl) attached to the other side of the functionalised phenyl ring. The range of useful materials (ones with S_C phases) limited an attempt of such a comparison due to the varied structures and alignment qualities.

Future molecular designs which may improve the nonlinear coefficients of this class of material are restricted because of the requirement to retain the smectic C phase. This limits the size of donor and acceptor groups which can be attached transversely to the chiral centre or coupled groups. Early reports of combining a para-nitroaniline functionalised group into the molecule have resulted in the destruction of almost all mesogenic properties [Walba et al, (1991)]. It will be a difficult challenge to synthetic chemists to recover the smectic C phase in these molecules.

The hindered rotation system has been demonstrated to work, and results in a degree of coupling between the chiral centre and the functionalised phenyl ring. Figure 4.15 shows some of the possible bond rotations which are hindered. The degree of hindrance is far from perfect - the functionalised phenyl ring is still free to rotate through large angles relative to the chiral centre, reducing the polar order parameter for the phenyl ring. If this coupling could be made more rigid, then the polar order parameter would be increased, with a corresponding increase in the bulk nonlinear coefficient. This may be achieved using a single bond between the chiral group and the functionalised phenyl ring, or using hydrogen bonding between the transverse group on the chiral centre and the phenyl ring. Materials to test this theory are being synthesised at present, and so the results will be reported elsewhere.

Another technique to improve the bulk nonlinear coefficient still further is to increase the number density of the chiral groups by incorporating more than one into each molecule. This technique has been attempted with chiral molecules [Kobayashi, (1993)], but is fraught with difficulties. The synthesis of such materials is possible, but the largest problem is ensuring that the polar axes align parallel and so combine additively. It is more energetically favourable that the polar axes align antiparallel within each molecule, and so reduce the bulk coefficients in comparison with single chiral materials. Another problem associated with these materials is that each chiral centre produces a twisted structure, with double chirals often the structure is even more tightly twisted, causing difficulties in aligning the material. Loss of overlying nematic and smectic A phases can also reduce alignment quality.

As the understanding of these structures develops, more complex and elegant molecules will be designed and synthesised, producing further improvements in the bulk nonlinear coefficients. These values are already beginning to challenge conventional inorganic materials, and will probably surpass them in the next few years. It is doubtful that the coefficients will challenge those found in some of the organic crystals

due to the limitation that smectic C properties must be retained for these materials to offer advantage over crystals for processing. The final step in the development of these materials will probably be their incorporation into polymeric structures. This is most likely to be achieved by photo cross-linking the material whilst it is in an aligned state. This compares well with poled polymeric materials as discussed in chapters 2 and 3, but whilst the molecular hyperpolarisabilities will be smaller in ferroelectric materials, the degree of order will be higher, and without any tendency to relax due to the material being in thermal equilibrium. It is not clear at this moment which technique will be the most successful.

5 Using SHG as a Measurement Probe in Liquid Crystals.

The experimental measurement of second harmonic generation has principally found application in characterising and developing new materials with improved nonlinear optical coefficients. This technique has been used successfully with probably all phases of matter: solid, liquid and gas, and liquid crystals. Some of the benefits of this technique are that many non-crystalline or multi-domain forms of materials can be probed, enabling quick and early evaluation of new materials, and that SHG is very specific to the absence of inversion symmetry in the material.

The specific symmetry requirements of second order nonlinear optical effects can make SHG a very selective optical probe to investigate optical materials, and particularly liquid crystals. In the absence of applied electric fields, then very few situations can give rise to SHG in organic materials: bulk noncentrosymmetry, and interfaces which induce polar molecular alignment. One common application of SHG as a probe in organic systems is to investigate dynamics of the poling process in amorphous and nematic side chain polymers [Singer & King, (1991)], as discussed in chapter 3.

The measurement of SHG at interfaces or from monolayers deposited on a substrate, has been used as a probe of the molecular orientation at the interface. The use of surfactants and rubbed alignment layers to preferentially align liquid crystal molecules is extremely important for liquid crystal technology. The orientation of liquid crystal molecules on these alignments has been investigated using SHG by Shen [Shen et al, (1991)], giving excellent information about how the molecules align on these treated substrates. Several other groups have also recently begun to use SHG to investigate liquid crystal alignment layers [Kurata et al, (1992)]. The main drawback of much of this work is that the surface alignment of a ferroelectric liquid crystal material cannot be studied whilst the bulk is present, as the SHG from the bulk material is significantly larger than that from the first monolayer. This has been partially overcome by depositing only a monolayer of material, but it is expected that the presence of bulk material will have a significant effect on the way molecules align on these layers due to the effects of elastic forces and the short range order due to the liquid crystal potential.

It is the intention of this final chapter to describe how the technique of SHG may be used to obtain information about the liquid crystal materials and structures in the bulk material. The material characterised in the previous chapter (SCE13*) was used, so that other parameters such as the alignment structure and order parameters may be evaluated. A technique to measure the refractive indices, and particularly the optical biaxiality of smectic C materials as a function of temperature will be described. This is of importance for calculating the numerical fit to Maker fringes as described in the previous chapter, but is also important for materials assessment for ferroelectric display applications and calculating device performance. A similar experimental geometry was also used to measure the twist elastic constant of the smectic C material. This is very important in supporting the theoretical understanding of smectic C materials. A smectic C continuum theory [Carlsson et al, (1991)] has predicted the existence of 21 elastic constants needed to fully describe the smectic C phase.

Application of the continuum theory is greatly helped by the measurement of some of these elastic constants.

A novel alignment structure of smectic C materials which is potentially phase matchable will also be assessed. This geometry is surface stabilised and so does not require the presence of a electric field as used in homeotropic alignments. It will form a uniform alignment with a component of the c_2 axis in the plane of the device, unlike the chevron structure. This device geometry would be of interest for large area transmission second harmonic generation devices, and for liquid crystal device studies.

5.1 Measurement of Smectic C Refractive Indices and Optical Biaxiality.

The evaluation of SCE13* in section 4.5.1 required the measurement of the refractive indices with sufficient accuracy to fit the Maker fringe data shown in figure 4.10. This measurement is also of interest to liquid crystal scientists as a technique of measuring the refractive indices of the material in the S_C^* phase as a function of temperature. This experiment has the potential for measuring the optical biaxiality of the material and the order parameters of the three principal molecular axes.

The optical arrangement to measure the refractive indices is shown in figure 5.1. This used a liquid crystal cell with the same alignment layers and electrodes as the homeotropic cell described in chapter 4, but it was assembled to have a linear variation in thickness across the cell. The wedge angle δ was measured to be $0.27 \pm 0.03^\circ$ by reflection, which was small and so did not significantly disrupt the homeotropic alignment of the smectic C material.

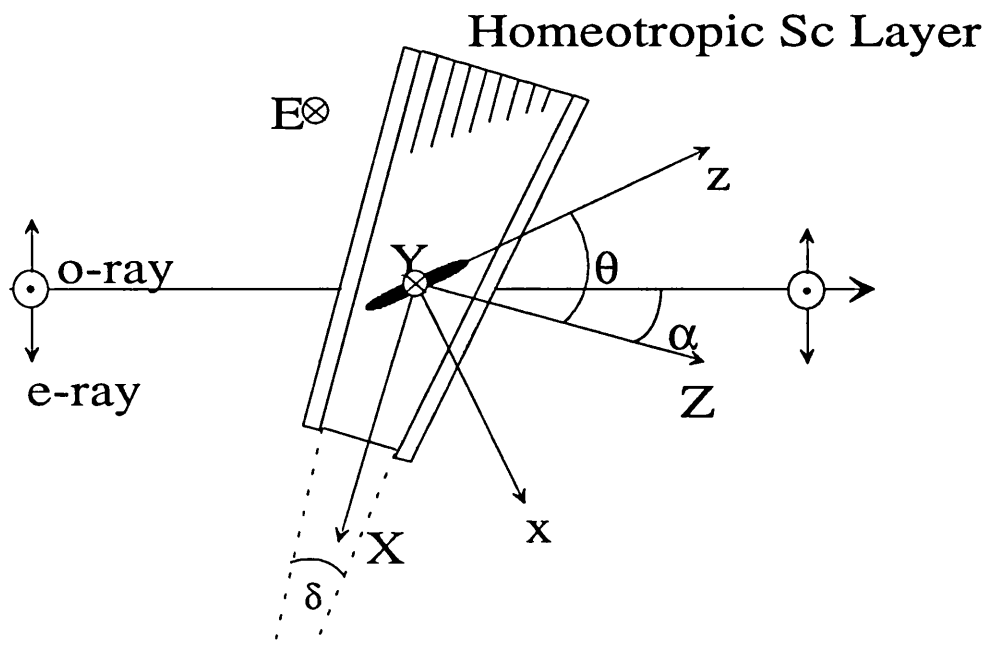


Figure 5.1 Wedge cell measurement configuration.

The smectic C helix was fully unwound by applying sufficient dc electric field in the Y direction. The cell could be rotated to the desired angle of incidence, and then translated along the X axis across the optical beam. This permitted variation of the cell thickness whilst keeping all other parameters constant, and so the interference fringes detected originated from the modulation from the $\sin^2\Psi$ function in the equation 4.4 describing SHG intensity where

$$\sin^2 \Psi = \sin^2 \left(\frac{\pi L}{l_c} \right), \quad 5.1$$

and

$$l_c = \frac{\lambda}{2(n^{2\omega} - n^\omega)}. \quad 5.2$$

Measurement of the y component of the refractive index was achieved using vertically polarised (ordinary ray) input radiation and detecting only vertically polarised second harmonic signal. This was measured at normal incidence ($\alpha = 0$) so that the relative thickness is simply

$$L' = X / \sin \delta$$

where X is the position along the X axis. As only the difference in thickness was of interest, it was assumed that the thinnest accessible part of the cell was zero for convenience.

Interference fringes from the wedge cells containing SCE13* at 50°C using $e_o^{2\omega} e_o^\omega e_o^\omega$ polarisations are shown in figure 5.2a. A numerical fit using NAG routines calculated the best values for constants A, B and C using the equation

$$\text{SHG Intensity} = A \sin^2 \left(\frac{\pi L}{B} + C \right) \quad 5.3$$

where A is the amplitude, B is equal to the coherence length l_c as defined in equation 5.2 earlier, and C is a zero offset necessary for fitting the data. The best fit is shown by the solid line in each figure. From equation 5.2 and the value of B it was possible to calculate the dispersion in the y refractive index

$$n_y^{2\omega} - n_y^\omega = 0.0103.$$

The x component of the refractive index was measured using $e_o^{2\omega} e_e^\omega e_e^\omega$ polarisations and directing the light along the z axis of the material, i.e. along the director. Refraction at the air-glass-liquid crystal interface was taken into account assuming the material was approximately uniaxial and thus n_x was approximately equal to n_y . The results were relatively insensitive to the refracted angle, but if more accuracy was required, the angle of incidence could be varied and the maximum value of l_c used. For an angle of refraction equal to the tilt angle of 16.4° (refer to section 4.5.1 for the measurement and discussion), the angle of incidence at the glass-air interface must be 24.6°. The fringes from this angle are shown in figure 5.2b, and from the numerical fit

$$n_y^{2\omega} - n_x^\omega = 0.0109.$$

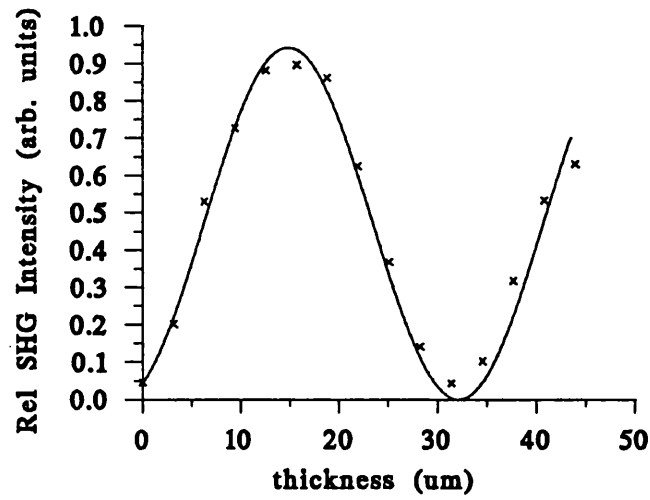


Figure 5.2a Wedge fringes for ooo polarisations giving $l_c = 51.75 \mu m$.

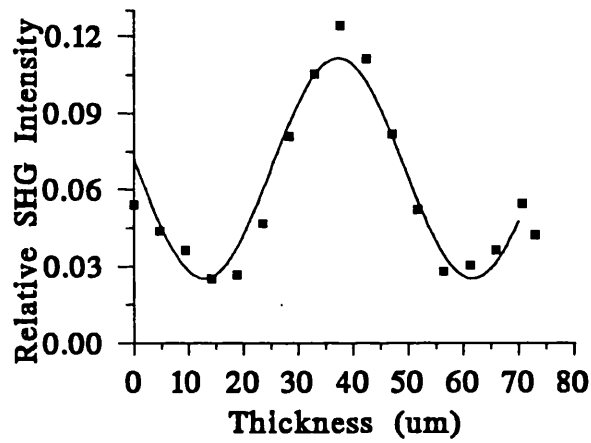


Figure 5.2b Wedge fringes for eeo polarisations at $\alpha = 24.58^\circ$ giving $l_c = 48.79 \mu m$.

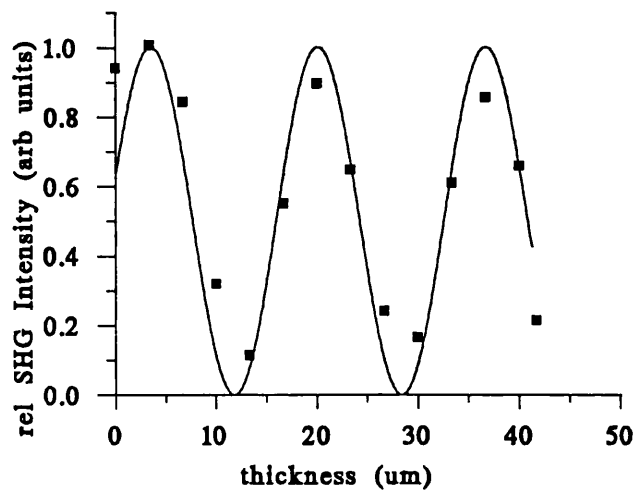


Figure 5.2c Wedge fringes for eeo polarisations at $\alpha = -30.50^\circ$ giving $l_c = 16.62 \mu m$.

The z component of the refractive index was calculated from a combination of x and z refractive indices at a different angles of incidence using $e_o^{2\omega} e_e^\omega e_e^\omega$ polarisations. The angles at which measurements were made were -30.5° and -24.6° , corresponding to refracted angles in the material of -19.7° and -16.5° respectively. The fringes at -30.5° are shown in figure 5.2c together with a numerical fit, giving

$$n_y^{2\omega} - n^\omega(\theta - \alpha) = 0.0320.$$

where $\theta - \alpha$ is the angle between the refracted beam and the director. The value of n_z^ω may be calculated from

$$\frac{1}{[n(\theta - \alpha)]^2} = \frac{\cos^2(\theta - \alpha)}{n_x^2} + \frac{\sin^2(\theta - \alpha)}{n_z^2}. \quad 5.4$$

From this interference data alone it is impossible to calculate the absolute values of the refractive indices. An independent value for one of the four refractive indices is required and was found from approximating the value of $n_y^{2\omega}$ (532 nm) to equal the value of n_y at 589 nm which has been measured using the Abbé refractometer. The error associated with the dispersion of $n_y^{2\omega}$ was not significant. The refractive indices of SCE13 are given in table 5.1 for several temperatures.

The errors in the refractive indices were dominated by the errors associated with the measurement of $n_y^{2\omega}$. The source of this error was most likely the quality of the liquid crystal alignment that can be obtained between the Abbé prisms. The wedge cell measurement is an interference method and is capable of high accuracy, but again was limited by the quality of the material alignment. The absolute measurements indicated there to be a very small biaxiality ($\delta_n = n_y - n_x$) which was difficult to resolve within the experimental error, was equal to

$$\delta_n = 0.0006 \pm 0.0005$$

at 50°C . The error is an indication of the low signal in graph 5.2b and consequent poor fit. The maximum shown in this graph is only 3 times the noise level of 0.03 arbitrary units. This SHG arose directly from the small d_{21} coefficient, measured in chapter 4.

The optical biaxiality of SCE13* was measured at a number of temperatures. It was expected that as the material was cooled further into the smectic C phase, the optical biaxiality would increase from zero at the transition from the smectic A phase. It has been predicted that the biaxiality will be small [Takezoe et al, (1984)], and less than 0.01.

The wedge fringes from $e_o^{2\omega} e_e^\omega e_e^\omega$ configurations at 40°C and 27.5°C are shown in figure 5.3. The refractive indices calculated from these fringes are also given in table 5.1 together with the values of $n_y^{2\omega}$ measured using an Abbé refractometer at the different temperatures. The data used to calculate n_x is shown in figure 5.4 for the same temperatures.

Clearly the measured biaxiality of SCE13 given in table 5.1 is small. The values at temperatures near the c-a transition are very close to zero within the accuracy of the measurement. The change from positive to negative is probably due to scatter in the data. Only at the lower temperature

	50°C	40°C	27.5°C
Cone Angle (deg.)	16.4	20	23
$n^{2\omega}_y (\pm 0.002)$	1.489	1.492	1.496
$n^\omega_y (\pm 0.002)$	1.479	1.481	1.484
$n^\omega_x (\pm 0.002)$	1.478	1.481	1.486
Biaxiality (± 0.0005)	0.0006	-0.0004	-0.0019

Table 5.1 Refractive indices of SCE13*.

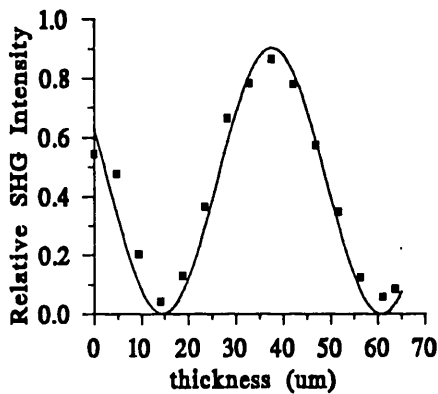
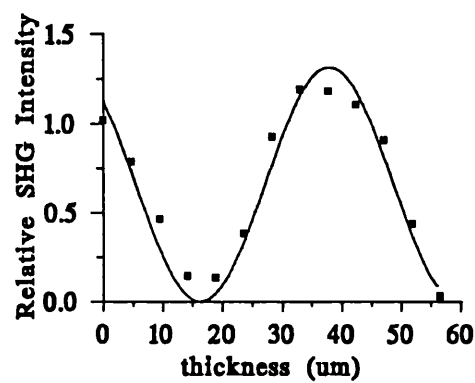


Figure 5.3a Wedge fringes at 40° C giving $l_c = 46.25 \mu m$.



5.3b Wedge fringes at 27.5° C giving $l_c = 43.34 \mu m$.

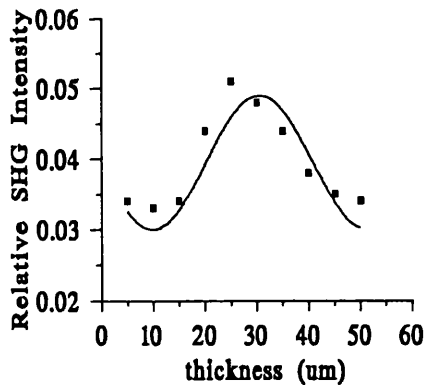
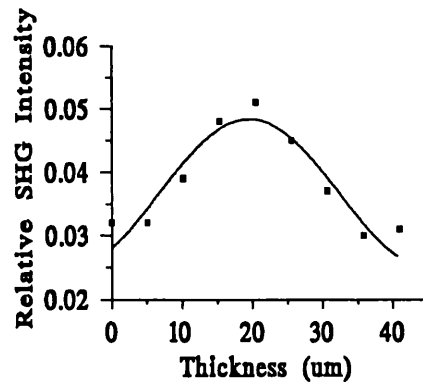


Figure 5.4a Wedge fringes at 40° C giving $l_c = 48.14 \mu m$.



5.4b Wedge fringes at 27.5° C $l_c = 51.03 \mu m$.

does the value become significant, where the phase is known to become biaxial dielectrically [Jones et al, (1990)]. The accuracy of the measurement was disappointing, but would have been difficult to foresee due to the previously unmeasured small d_{21} coefficient. Many more measurements at different temperatures would be required to fully characterise a material and obtain its temperature dependence. Initial comparisons to other techniques of measuring optical biaxiality e.g. Abbé refractometer, suggest it to be a slight improvement. It is unlikely that optical refractive indices can be measured with

significantly greater accuracy due to the limitation in quality of the liquid crystal alignment, which will change the molecular orientations locally. One exception to this is the guided wave and surface plasmon techniques. These techniques measure the intensity of reflected light from a high index glass - liquid crystal interface at angles close to the critical angle. Waveguiding manifests itself by a fall in the reflected signal as a function of angle of incidence. Surface plasmon-polaritons can also be excited when a thin silver layer is deposited at the interface. Modelling of the waveguiding conditions can give accurate information about the refractive indices of the liquid crystal layer. Elston [1991] has measured the biaxiality in a similar material (SCE3) using surface plasmons to be less than 0.0015.

5.2 The Critical Unwinding Field and the B_3 elastic constant.

Chiral liquid crystal molecules have a natural tendency to form a helical bulk structure, as described in chapter 1 in both the cholesteric and smectic C phases. This helical structure must be unwound for the material to possess bulk noncentrosymmetry. This has been achieved using surface stabilisation [Clark & Lagerwall, (1980)] or coupling of the permanent transverse dipole moment (P_d) with an applied electric field. The size of electric field required to unwind the structure has been predicted to have a threshold [Meyer, (1977)], with a critical unwinding field value E_c . From the measurement of these critical field strengths it is possible to calculate values for some of the many elastic constants in these materials. The smectic C continuum theory describes the chiral smectic C phase in terms of 21 elastic constants. The ferroelectric c_2 axis has three principal elastic deformations: in-layer splay of c_2 ; in-layer bend of the c_2 axis, and twist of c_2 through the planes. The smectic C continuum theory in Carlsson notation [Carlsson et al, (1991)] describes these deformations as B_2 , B_1 , and B_3 respectively. The continuum theory is of importance to describe and predict the structure of the molecular alignment in ferroelectric liquid crystal devices. It is only through understanding of the molecular alignment that improvements in liquid crystal displays and optical information processing technology will be achieved.

All of the SHG studies described earlier have used the assumption that the helix had been fully unwound by the application of a transverse electric field, and so the material formed a monodomain with a well defined molecular alignment. The field required to achieve this is quite small, 50 V applied across the 2 mm electrode gap was sufficient. The amount of SHG from the cell is very dependent on the alignment quality, and particular the requirement of bulk noncentrosymmetry, and so should prove a selective probe to determine the threshold when the structure starts to re-form a helix, and thus degrade its symmetry.

5.2.1 Derivation of the Critical Unwinding Field.

The bulk free energy of the chiral smectic C phase can be described by the free energy density

$$g(z) = g_O + g_E \quad 5.5$$

where g_O can be found from the Landau expansion of the two smectic C order parameters and their derivatives in a direction perpendicular to the layers (z), and g_E is the energy associated with the dipole interaction between the transverse spontaneous polarisation P_S and an electric field E applied perpendicular to the helical axis. A more complete description of the derivation that follows can be found in Zeks et al [1991].

The classical model used by Meyer assumed that the critical unwinding field is proportional to the tilt angle for all temperatures in the smectic C phase. This is not in agreement with experiments [Zeks, (1991)], and so for this calculation a generalised Landau model for the free energy density was used. This included additional terms giving a quadratic coupling the molecular tilt ξ and the polarisation P_S . The tilt angle and spontaneous polarisation are described by an amplitude and azimuthal twist angle φ dependence

$$\begin{aligned} \xi_1 &= \theta \cos \varphi & \xi_2 &= \theta \sin \varphi \\ P_x &= -P \sin \varphi & P_y &= P \cos \varphi \end{aligned} \quad 5.6$$

It is assumed that the amplitudes of the tilt and polarisation are constant through the device (θ and P), and that only the twist angle $\varphi(z)$ can vary as a function of z (the helical axis). It can be shown that the twist angle dependent part of the free energy density can be expressed as

$$g(\varphi) = -\left(\Lambda + d\theta^2 + \mu \frac{P}{\theta}\right)\theta^2 \left(\frac{\partial \varphi}{\partial z}\right) + \frac{1}{2} B_3 \theta^2 \left(\frac{\partial \varphi}{\partial z}\right)^2 + P \sin \varphi E, \quad 5.7$$

where B_3 is the twist elastic constant of the c_2 axis, and Λ is a coefficient in the Landau expansion responsible for the helicoidal structure. In the absence of an applied electric field, the energy density is minimised when the value of the gradient of the twist

$$\frac{d\varphi}{dz} = \frac{\Lambda}{B_3} = q_0, \quad 5.8$$

which represents the undisturbed helix with helical pitch vector $q_0 (=2\pi/p)$.

The application of a transverse electric field prefers the azimuthal angles

$$\varphi = -\frac{\pi}{2} + 2\pi n$$

where n is an integer, which deforms the helix. This may be thought of as unwinding the helix, as shown in figure 5.5. Minimising the energy density in equation 5.7 gives a second order differential equation in terms of the twist angle, from which there are periodic solutions. As the applied electric field E is increased, the period of the solution for the twist increases and goes to infinity at the critical field E_c . At infinite period of helical pitch, the critical field can be calculated to be

$$E_c = \frac{\pi^2}{16B_3} \left(\Lambda + d\theta^2 + \mu \frac{P}{\theta}\right)^2 \frac{\theta^2}{P}. \quad 5.9$$

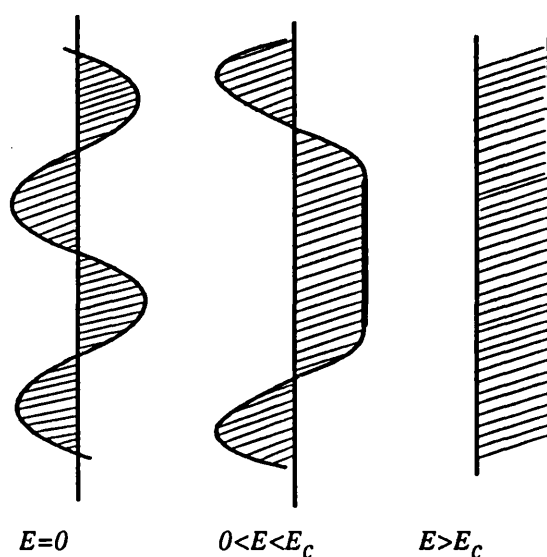


Figure 5.5 Schematic diagram to illustrate the response of the helix to an electric field. The lines correspond to the c_2 axis of the molecules (reproduced from Meyer, 1977).

Taking the amplitudes of θ and P to be equal to the zero field values, and using the expression for the zero field helical wave vector q_0 and the pitch of the helix $p = 2\pi/q$, then equation 5.9 reduces to

$$E_c = \frac{\pi^4}{4} B_3 \frac{\theta^2}{p^2 P}. \quad 5.10$$

Given values of the helical pitch p , the tilt angle θ and spontaneous polarisation P for zero field, then a measurement of the critical unwinding field can be used to measure the B_3 elastic constant.

In experiments, it was much easier to start with a uniform untwisted alignment, achieved by cooling into the smectic C phase whilst applying sufficient electric field to ensure the helix is fully unwound. The field was then reduced, and at a critical field strength the uniform unwound alignment began to distort and twist. The threshold occurs because of a degeneracy in the direction in which a molecule will start to twist. Although a molecule will prefer to twist in a particular direction relative to one of its neighbours corresponding to the handedness of the chiral centre, it will be in the unfavourable direction relative to the opposite neighbouring molecule. Therefore in uniform alignments there cannot be any preference as to which layer the twist will grow from, and thus the threshold occurs. Of course in cells where defects exist in the alignment, then this threshold may not be seen.

5.2.2 Measurement of the Critical Unwinding Field.

It is very important to have uniform alignment and to apply the electric field perpendicular to the helical axis. This is usually achieved in the planar cell geometry with the helical axis in the plane of the cell, and the electric field applied perpendicular to the cell. To minimise any surface effects, the

cell would preferably be very thick (typically 200 μm), but this is counter-productive as the alignment is difficult to achieve in such cells.

The experiment described here used the homeotropic cell geometry and in-plane electrodes to arrange the helical axis perpendicular to the cell. This geometry has the potential benefit that there is no azimuthal surface anchoring energy which would otherwise distort the helix and affect the threshold. To eliminate any memory effects at the surface, the material was fully unwound in the smectic A phase before being cooled into the smectic C phase in the presence of an electric field greater than the critical field along the y axis. When at the appropriate temperature, the field was slowly reduced and the SHG from the sample measured. Both input and second harmonic polarisations were parallel to the Y axis, thus accessing the d_{22} nonlinear coefficient.

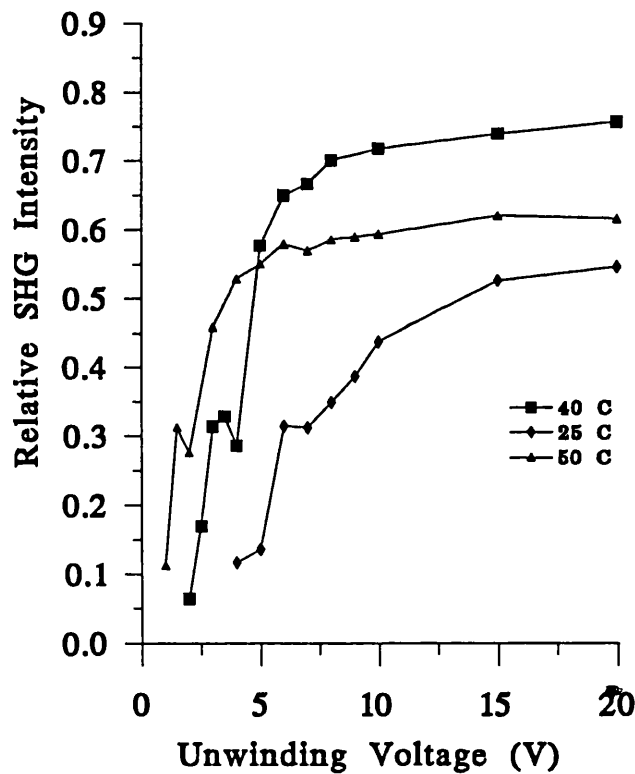


Figure 5.6 Response of SCE13* to an electric unwinding voltage across 2mm as it is removed.

Figure 5.6 shows the measured second harmonic signal as the material reforms the helix as a function of temperature as the unwinding field was reduced. The cells were about 50 μm thick, and the in-plane electrode spacing was 2 mm. The electrodes were about 6 μm thick, and so were not all the way through the cell, resulting in a small non-uniformity in the electric field across the thickness of the cell. Approximating the electrodes to parallel thin wires [Rosenblatt, (1978)], the electric unwinding field strength in the central region is

$$E \approx \frac{2V}{\pi l}$$

5.11

for this geometry. Moving 50 μm away from the centre line of the electrode pattern does not have a significant effect on the electric field strength at that point.

On analysing the data in figure 5.6, the first point to note is that there was no plateau region where the alignment was undistorted, or an identifiable sharp threshold field. This may have been because the alignment was not perfect, and so the degeneracy between the two twisted states was removed. However, the non-uniform electric field may also contribute to this effect, although the distortion was small. The variation in maximum signal was due to the change in alignment quality between heating and re-cooling into the smectic C phase. The alignment used was chrome complex which started to degrade through repeated temperature cycling and laser damage.

The small step seen in each of the traces about half way down the steepest part of the curve was attributed to the formation of the first twist reforming the helix. This stabilised the structure and lead to constant or even increased SHG intensity for a limited range of unwinding field. The SHG intensity at this region was about one half of the maximum measured, suggesting the presence of one 'twist' in the helix. The voltage at which this twist occurred exhibited a temperature dependence, with the lower temperatures twisting up earlier at higher electric field strengths as expected. The identification of further 'twists' were prevented by the low signal and the low twisting power of the material. The material was probably not the most favourable to demonstrate this measurement, but illustrates the sensitivity of the experiment.

The experiment raised a question about the identification of the critical field strength. Theory describes it as the beginning of a first distortion from the uniform alignment, but how is this measurable? The value measured and quoted in this work is related to the formation of the first 2π twist in the structure. In the ideal alignment case, then these two values may be the same, but in a typical cell then the first distortion may not result in a measurable effect (or even exist). As both criteria must be well defined in theory, and the formation of the first twist is easily measurable, then the work here defines the strength of the electric field at which the formation of the first twist occurs as the critical field E_c .

Figure 5.7 illustrates the unwinding of the helix in the S_c phase at 50°C after the material had been cooled to that temperature with no field applied. There was a considerable difference between both the form of the curve and the voltage required to produce an untwisted alignment. The difference was accounted for by assuming that although there was no variation in the azimuthal surface energy, the molecules could be weakly anchored in azimuthal position when the material was cooled into the smectic C phase. This surface anchoring is due to a finite coupling at the surface, possibly due to the intertwining of hydrocarbon tails from the liquid crystal molecules and the surfactant molecules. When the liquid crystal material was cooled into the S_c phase with excess unwinding field present, then the molecules at both surfaces were pinned in a position where the c_2 axis was parallel to the electric field. These molecules remained pinned as the field was reduced and the helix began to reform.

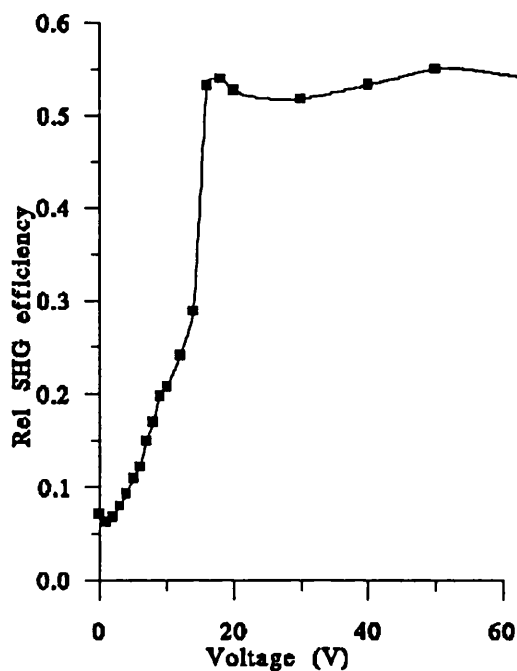


Figure 5.7 Response of SCE13* to an electric unwinding field as it is applied at 50° C.

When the liquid crystal was cooled into the smectic C phase without any unwinding field, then the molecules at the surface could be pinned at any azimuthal position, which may not be identical at either surface. When the unwinding field was then applied, then helix would begin to unwind, but could not do so fully until the molecules at the surface were rotated to align their c_2 axis parallel with the applied field. Switching the surface pinned molecules required much larger electric field strengths than to simply untwist the helix in the bulk. The difference in field strengths observed may give an indication of the strength of the surface pinning or memory effect in homeotropic alignment agents.

The twist elastic constant B_3 was measured for SCE13* at the temperatures 50, 40 and 25°C, which were 10, 20 and 35 °C below the smectic C- A phase transition. The layer tilt θ was measured at these temperatures, and the pitch length of approximately 3 μm has been measured from laser beam diffraction. Substitution into equation 5.1D yields values for the elastic constant, as given in table 5.2 below.

Reduced temperature (°C)	B_3 (Nm^{-1})
-10	2.0×10^{-12}
-20	2.9×10^{-12}
-35	5.3×10^{-12}

Table 5.2 Temperature dependence of B_3 of SCE13*.

These values of B_3 are similar in size to other elastic constants measured in smectic C liquid crystals. However, there are no known measured or theoretical values with which this data can be

compared. The errors associated with these values are probably limited by the accuracy of the measurement of the helical pitch, which had an accuracy of $\pm 1 \mu\text{m}$ [Jones, (1993)]. The pitch of $3 \mu\text{m}$ was inconveniently long for most measurement techniques, but had been designed to simplify alignment of the material in thin planar cells. Using a material with a pitch length of the order of the wavelength of light would probably improve accuracy if the required alignment could be achieved.

In summary, the twist elastic constant B_3 was measured as a function of temperature in SCE13*. It has been shown that the homeotropic cell geometry with in-plane electrodes is suitable for this measurement as the surface effects are relatively small. It is proposed that the difference in critical field strengths between unwinding the helix and allowing it to wind up was a result of weak surface pinning which needed the application of higher electric fields to re-orient the molecules at the surface. This may yield information about the azimuthal anchoring energy of these alignments.

5.3 Uniform Planar FLC Alignment Geometry.

The work in the previous sections was based on the experimental geometry of homeotropic alignment with 'in plane' electrodes for measurement of the d_{22} coefficient. This configuration has been reported in the literature as a SHG measurement configuration as it allows direct access to the d_{22} coefficient using input and harmonic polarisations along the c_2 axis, and also type I phase matching can be achieved using input light polarised perpendicular to the c_2 axis. The alignment which can be achieved using the transverse unwinding field is very uniform, and readily attainable for most liquid crystal materials. However, the geometry suffers from the limitation that there must be a dc electric field applied to the material to unwind the helix. This is not desirable for device applications, where passive devices are available and preferred. The dc field also has detrimental effects on the liquid crystal materials. It is well known that liquid crystal materials can suffer electrolysis effects in dc electric fields (liquid crystal displays always use fully ac balanced drive voltages). It may be possible to synchronise the drive voltage to pulsed laser sources, but this is inconvenient and unsuitable for some applications eg. frequency doubling of continuous wave lasers.

An additional disadvantage of the in-plane electrode cells is their fabrication. In order to use the geometry to characterise materials the cells must have very accurately aligned parallel electrodes to produce a uniform electric field through the active area. To achieve the parallelism required, cells for this work had electrodes defined by a lithographic technique and then electroplated through a photoresist mask onto a substrate. However, it was difficult to produce thick electrodes ($>10\mu\text{m}$) whilst maintaining a rectangular cross section, as thicker electrodes developed a tapered cross section due to the etching process. It was believed that this deviation in cross section was acceptable in preference to using individual thin metal sheets for the electrodes, where the required parallelism is very difficult to achieve.

The conventional planar alignment in liquid crystal devices, achieved using rubbed polymer alignment layers, results in a chevron structure described earlier, and not the uniform bookshelf alignment initially expected. This is a complex, non-uniform liquid crystal structure where the direction of the c_2 axis changes significantly between the two halves of the device. Such a structure is of little interest for nonlinear optical device applications or as a geometry to evaluate new materials. The ideal would be to achieve surface stabilised uniform alignment of both the c_2 and director axes using simple cell configurations, preferably without the presence of 'holding' electric fields.

It should be possible to achieve uniform alignments within planar cell structures using alignment layers which give very high surface pretilts. This would combine the simple and efficient uniform alignment of homeotropic cells without the need for in-plane electrodes, with the c_2 axis rotated away from the cell normal. There has been no previous reports of exploiting this alignment for nonlinear optical applications.

Anti-parallel aligned substrates produce layers which are tilted in the smectic A phase. The angle of tilt of the layers, δ_A , is equal to the surface pretilt ξ_S . On cooling into the smectic C phase, the S_C layer tilt can be found from

$$\cos \delta_C = \frac{d_C \cos \delta_A}{d_A} \quad 5.12$$

Silicon monoxide (SiO) evaporated at 85° to the substrate normal can produce surface pretilts of about 25° . Equation 5.12 predicted that δ_C was 31° for an anti-parallel 85° SiO cell. The layer tilt in this situation was greater than the cone angle of the material, and the chevron interface does not form, as the condition of director continuity cannot be met. A uniformly tilted structure may form as illustrated in figure 5.8, which will result in the c_2 axis at an angle to the cell normal without any reversals as seen across the chevron interface.

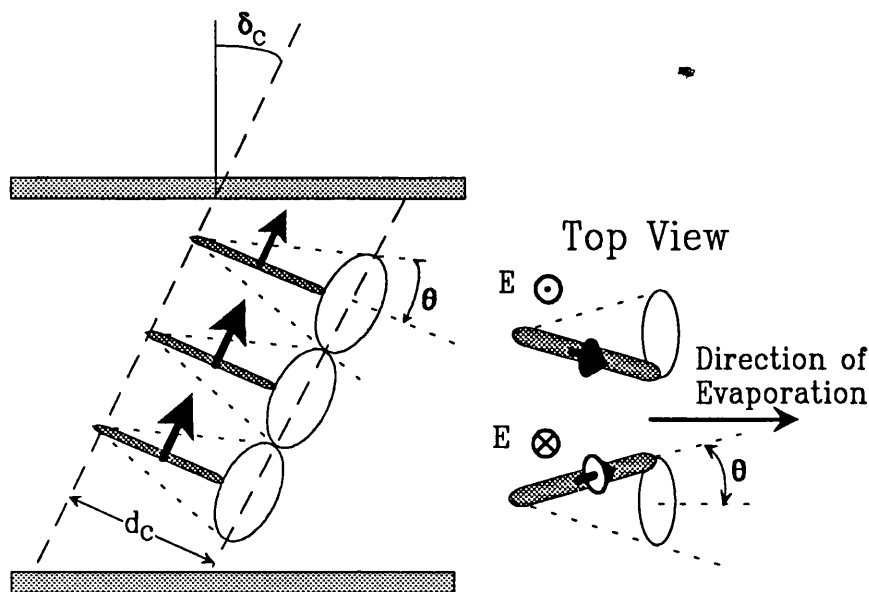


Figure 5.8 Tilted planar S_C alignment.

The alignment in the smectic C phase was found to be fairly poor for cells of 6 μm thickness filled with SCE13. From polarised microscope studies, the alignment comprised of many small domains with what were believed to be a twisted structure. These domains were smaller than the spot size of the laser beam, and so could not be probed individually. Reducing the cell thickness to between 2 and 3 μm improved the alignment quality, with uniform domains forming which were separated by the twisted structure. The uniform domains produced black states between crossed polarisers, and appeared to be in one of two orientations, separated approximately by 30° - an angle close to double the cone angle as expected. The domains were still too small to be individually probed by the SHG experiment. The alignment became quite good when the cell thickness was reduced to between 1.5 and 2.0 μm . The smectic C phase produced alignment which was again dominated by two uniform domains separated by an angle of 30° , however no evidence of the twisted domains was seen. Application of an electric field ($2 \text{ V}\mu\text{m}^{-1}$) readily switched the liquid crystal molecules between the two states. The alignment was bistable as the molecules could be switched into one of the two states and when the voltage was removed, the alignment would remain switched for periods of minutes.

For the experimental investigation of this structure, the molecules were switched into one of the uniform states by the application of a small dc voltage. This voltage was applied throughout the experiment as a precaution to ensure none of the material relaxed into the alternative alignment. The cell was rotated about its normal by an angle equal to the cone angle of the material to align the z axis of the molecules in the horizontal plane. The incident radiation was horizontally polarised, as was the detected harmonic radiation. The cell was then rotated about the molecular x axis (vertical) and the SHG intensity measured as a function of angle of incidence.

In this geometry, both the input and output polarisations access a combination of the ordinary (y axis) and extraordinary (z axis) refractive indices, and so are called extraordinary rays. The effective nonlinear coefficient may be calculated for this geometry from

$$d_{eff} = e_e^{2\omega} : \underline{d} : e_e^\omega e_e^\omega$$

and was calculated to be

$$d_{eff} = -d_{22} \cos^3 \theta - d_{23} \cos \theta \sin^2 \theta \quad 5.13$$

where θ is the angle between the incident radiation (after refraction) and the z axis of the molecular alignment. It was assumed that $\phi = 90^\circ$ for this geometry. Modelling suggested that this geometry was phase matchable, but for SCE13* the phase matching condition required a device thickness greater than 100 μm , as shown in figure 5.9.

Initial measurements of empty cells with the 85° SiO alignment layers found that the one phase matchable configuration of eee polarisations also gave rise to measurable SHG from the SiO. Other polarisation configurations did not detect any SHG above the background noise level. The SHG signal as a function of angle of incidence had the form of interference fringes as illustrated in figure 5.10. It was not unexpected that the SiO was SHG active - the alignment layer was deposited by thermally evaporating SiO under vacuum 1. As the crystalline layer formed, some of it probably formed SiO_2 or quartz, which is well known as a nonlinear optical crystal. The very thin coatings gave

rise to significant SHG because of the resonant etalon type cell structure. Angle tuning of this etalon resulted in the observed fringes, as verified by modelling the transmission of the etalon which is shown as the solid line in figure 5.10.

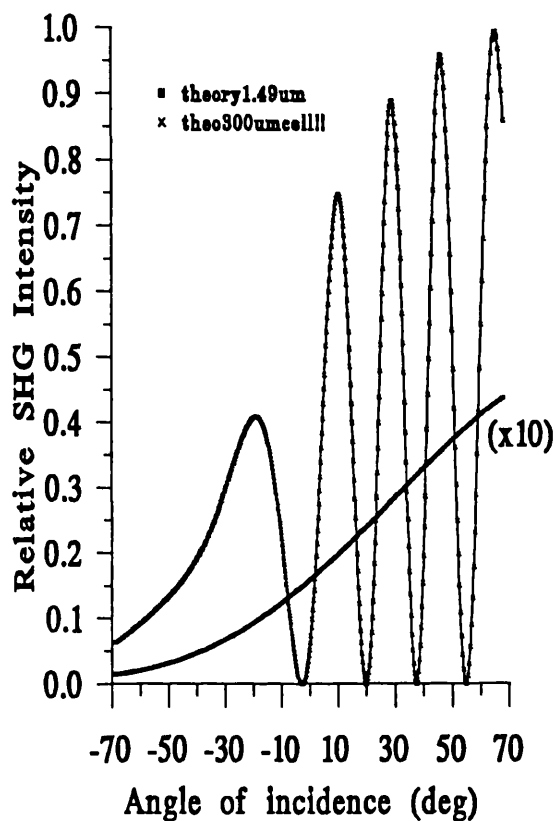


Figure 5.9 Theoretical phase matched SHG in tilted planar alignment.

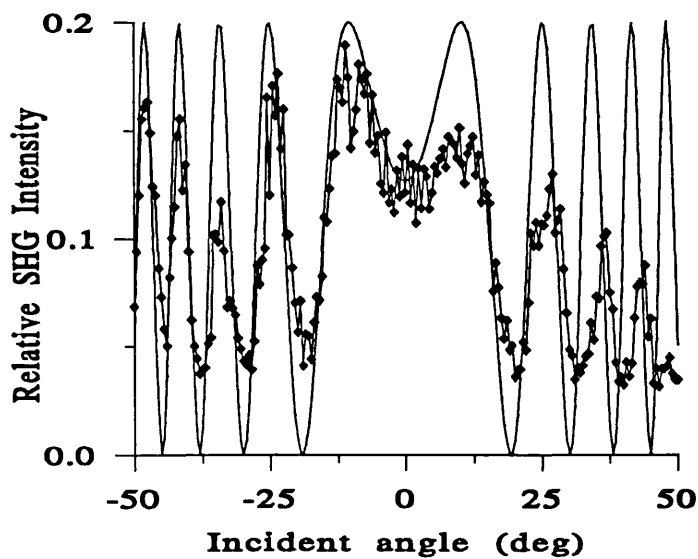


Figure 5.10 SHG from empty high tilt SiO cell and modelled etalon transmission.

When SCE13* was included in the cell, the measured SHG intensity changed, as shown in figure 5.11. The increased SHG signal and its asymmetric form may be interpreted as the combination of both the interference fringes from the SiO₂, and the phase matching curve predicted for SCE13*. Because it was not possible to obtain uniform alignment in this geometry for cell thicknesses greater than 2 μm , then the measured cell could not achieve full phase matching conditions.

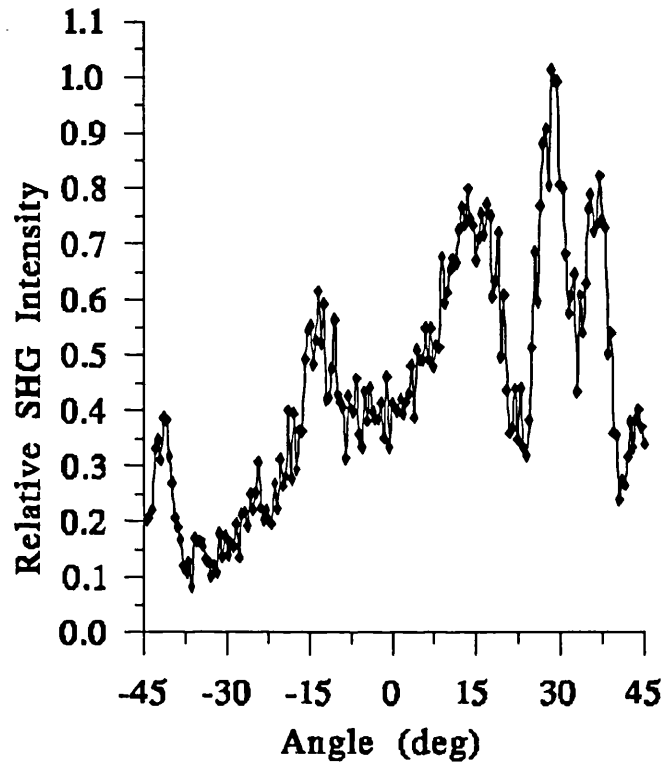


Figure 5.11 SHG from SCE13* in high tilt SiO cell 1.43 μm thick.

For this alignment configuration to be successful in nonlinear optics, then alternative high surface pretilt alignments are required, and the ability to align thicker cells is necessary. At present the SHG signal is unfortunately dominated by that from the SiO₂ alignment layer. There are a range of rubbed polymer planar alignment treatments with large values of pretilt, which may be suitable alignment agents for this geometry. The pretilt depends upon the length of time and temperature that the polymer was baked, as well as whether the polymer was rubbed before or after baking. Pretilts as high as 15° have been obtained with some materials [Jones, (1993)], although even higher pretilts may need to obtain this particular alignment. The use of rubbed polymer surface treatment would suppress the etalon transmission interference pattern found at present in the SiO₂ cells, and allow the SHG from the ferroelectric liquid crystal test material to be detected and analysed.

5.4 Other SHG Probe Measurements.

SHG has potential for probing liquid crystal devices in more detail than has been described above. However, before more sophisticated measurements are made, then many of the problems identified in these simple experiments must be overcome. Much of this centres on the key role of alignment quality, whose importance cannot be underestimated. The ability to produce high quality, uniform and reproducible alignment layers which are themselves not SHG active, but are resilient against laser damage is fundamental for this study. Alignment layers are beginning to be adequately understood and controlled, partly due to the work pioneered by Shen using SHG to probe the interaction between the alignment layer and liquid crystal molecules, and partly by a range of other optical and dielectric probes. As the quality and control of alignment layers is improved, more refined measurements will become possible, which will further enhance the understanding of liquid crystal devices.

The high tilt planar geometry described in the previous section is also of interest to investigate the structure of the liquid crystal alignment in display devices. The predicted molecular alignment is similar to one half of the chevron in a display-type low tilt planar cell [see figure 4.5]. Once the difficulties with SiO alignment have been overcome, this geometry may help in modelling the chevron structure by measuring SHG from two cells in series, where the layer tilts are arranged to simulate a chevron type structure, as shown in figure 5.12. The chevron structure has been measured using optical and X ray probes, both of which are sensitive to the orientation of the long axis of the molecule. The SHG probe is sensitive to the c_2 axis of the molecules, and so will provide information about the direction of the P_s of the molecules through the structure. This would greatly assist development of theories and models of the chevron structure.

The very short pulse length of the Nd³⁺:YAG laser (10 ns) may prove useful in time resolved measurements as a ferroelectric device is switched electrically. This may yield useful information about the reorientation of the c_2 axis in response to the applied field. Due to energy considerations, it is believed that the molecules reorient by rotating around the smectic C cone, rather than across it. Measuring the SHG as the device is switched may be the first experiment to confirm this theory. Using a material which switches in the 10 μ s regime, then the 10 ns laser pulses offer up to 1000 time slots within the material switching regime. A very advanced timing and triggering system would be needed to obtain such resolution as the measurement would have to be carried out stroboscopically i.e. only one 10 ns slot may be measured each time the device was switched, and signal averaging over the same time slot would also be needed to improve the signal to noise ratio of the data. This measurement is of interest to ferroelectric liquid crystal device engineers to support modelling of the device as it is switched, and to understand the effects of different drive schemes on the switching behaviour. This may then lead to improved drive schemes and consequently faster and more complex displays.

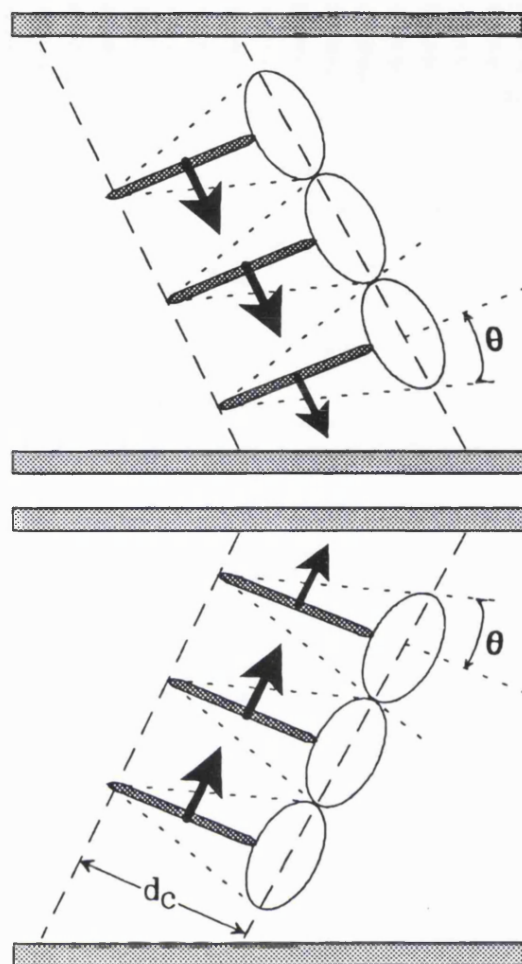


Figure 5.12 Two high tilt cells arranged to simulate a chevron structure.

5.5 Summary of Chapter.

The contents of this chapter have covered a wide range of experiments designed to support the ferroelectric liquid crystal science community and advance the understanding of this exciting class of liquid crystals and devices. Some of the measurements described are not unique to SHG probes, for example the measurement of the refractive indices or the B_3 elastic constant. These measurements have been made by other techniques, for example using the Abbe refractometer to measure refractive indices, or light scattering to measure the critical field needed to unwind the molecular helix. However, each of the previous measurements have many difficulties, and so the search for simpler and improved measurement techniques has continued. In both of the examples mentioned, the measurements using SHG have proved useful, and often raised more questions than answers. This is the nature of science and is the process of how an understanding of a system develops.

As the technique of SHG is developed and refined, then more information will be extracted about the liquid crystal structure, and in particular the alignment of the c_2 axis of the molecules. This

will be of great use to complement the other liquid crystal measurement techniques, including optical probes e.g. guided waves and surface plasmons, Abbe refractometer, transmission as a function of wavelength; and other probes such as X-rays and dielectric data. Almost all measurement techniques until now have been sensitive primarily to the long axis of the molecule, due to the anisotropic shape of the molecules. SHG offers a highly selective probe of the c_2 axis of the molecular alignment. The combination of information about the director configuration and the c_2 axis configuration are needed to describe fully the smectic C* phase, which is of great importance to provide experimental data to support the development of the smectic C* continuum theory and ferroelectric liquid crystal device modelling to further exploit this unique class of material.

6. Conclusions.

The successful implementation of nonlinear optical devices into optical information systems and optical data storage has been limited by the lack of suitable materials. A successful material needs many attributes including: nonlinear optical coefficients, low optical losses, ease of processing, low cost, photochemical and temporal stability and high laser damage thresholds, before being widely adopted. For some applications lithium niobate has been used, however its limitations make it far from ideal due to its cost and requirement to grow large, high quality crystals, its moderate nonlinear optical coefficients, high refractive index and low laser damage threshold. Several other classes of materials have addressed specific requirements of applications, but none have yet achieved all of the requirements requested in table 1.1 simultaneously.

The aim of this study was twofold: firstly to investigate the potential advantages of self assembled organic materials to enhance the nonlinear coefficients and stability of poled polymeric materials and to investigate ways of improving the poling technique efficiency; and secondly to develop new ferroelectric liquid crystalline materials which exhibit spontaneous noncentrosymmetry and therefore remove the requirement of poling and its inherent problems for second order nonlinear optical applications. This work involved developing two optical experiments to measure the nonlinear optical coefficients of these materials, an electro-optical measurement and the measurement of second harmonic generation (SHG).

The result of this work was an increased understanding of the poling mechanisms of side chain polymeric materials through measurement of the temporal dependence of poling and relaxation. Different mechanisms were identified above and below the glass transition. This information is essential when optimising the poling technique for specific materials, and can lead to improved nonlinear coefficients and increased lifetimes. This work developed a new and simple experiment to measure the poling efficiency as a function of time without the requirement for expensive second harmonic generation experiments. The second part of this study developed and measured second harmonic generation in ferroelectric liquid crystals. A commercial material (SCE13*) was assessed and its coefficients compared well with results from molecular modelling and structural information. This is the first time a comparison has been reported for ferroelectric liquid crystal materials. New uniform planar cell geometries were modelled and evaluated for nonlinear optical applications. The measurement of SHG in ferroelectric liquid crystal materials also demonstrated the application of SHG as a highly selective optical probe to measure refractive indices, optical order parameters, and elastic constants of ferroelectric materials and device structures to support ferroelectric liquid crystal display technology.

The search for efficient nonlinear optical organic materials can be broken down into two requirements: the development of molecules with large nonlinear polarisabilities (β coefficients), and the organisation of these molecules into a highly ordered, noncentrosymmetrically aligned bulk material. Side chain polymeric materials have used molecular groups with large molecular coefficients, but required

poling to achieve noncentrosymmetric alignment. The status of poled polymeric devices at the beginning of this work was promising, offering ease of processing with moderate nonlinear coefficients, but low poling efficiency and lack of poled stability prevented adoption of this technology. Over the period of this study, development of new materials coupled with the investigation of the relaxation processes in these materials has resulted in nonlinear coefficients which now surpass lithium niobate, which are stable and have achieved low optical losses ($< 0.5 \text{ dBcm}^{-1}$). These successes have led to automated production facilities for integrated electro-optic devices based on this technology to be developed.

A study of the temporal behaviour of poled materials was carried out to investigate the poling technique and its limitations. The induced nonlinear coefficient r_{eff} ($r_{33}-r_{13}$) was measured using a new simple technique as poling occurred, followed by its relaxation. The importance of optimising the poling parameters of temperature relative to the polymer glass transition temperature, voltage and time period, was emphasised by the different side chain reorientation mechanisms which were identified above and below the polymer glass transition. The poling process was optimised by poling at temperatures about 10°C below the glass transition temperature of the material. Understanding the temporal dependence of the poling processes is essential to determine the length of time for which the poling field must be applied, to achieve maximum poling efficiency. It is important that the poling period gives sufficient time for the nonlinear groups to reorient, but must be limited to minimise the formation of charge double layers due to charge trapping of ionic impurities close to the device electrodes. In place of the arbitrary periods previously used, an optimum period can now be identified using this technique, which is a function of individual materials, the temperature and poling field strength, and the material purity.

The theoretical enhancement of the nonlinear optical coefficient by a factor of 5 by using perfectly ordered liquid crystalline polymers in place of amorphous materials has not been achieved in practice. There has been reported a small improvement in the nonlinear coefficient and stability of the noncentrosymmetric alignment after the field was removed. However, device considerations offset these benefits. The more complex chemical synthesis often results in liquid crystal polymers with lower dielectric breakdown strengths due to the presence of impurities, thus reducing the maximum poling field, and hence the maximum nonlinear coefficient that can be obtained. The very high birefringence of liquid crystal polymers can result in tighter device flatness tolerances in electro-optical switching applications. Increased optical losses due to scatter is also a problem with high birefringence liquid crystalline materials. It has been reported that chemical cross-linking whilst poling has resulted in significantly improved device lifetimes without inhibiting other aspects of device performance. In summary, the benefits of using liquid crystal side chain polymers for nonlinear optical materials have not been significant, and are now being surpassed by the application of new processing techniques. These improvements have allowed poled polymeric materials to become established as a competitive technology to lithium niobate, and many of the device related issues are being overcome as materials and processing techniques become established and understood.

Ferroelectric liquid crystal materials exhibit spontaneous noncentrosymmetry without the requirement of poling. These materials at the beginning of this work had not been exploited for nonlinear optical applications. Measurements made on materials developed for ferroelectric liquid crystal displays showed they had molecular and bulk nonlinear coefficients several orders of magnitude lower than that required for useful application. This class of materials does offer considerable potential due to the ease in which noncentrosymmetric alignment could be achieved, the stability of this alignment, and the high degree of control of the molecular properties possible through established molecular engineering techniques. This study developed a new class of ferroelectric liquid crystal material specifically for nonlinear optical applications, which showed improvements of over a factor of 10 increase nonlinear coefficient than the previous best materials. Further improvements in the molecular coefficients are required before these materials can compete with lithium niobate and poled polymer technology, however given the short history of these materials in comparison with the other technologies, there is still a high potential that ferroelectric liquid crystal nonlinear optical materials can become a competitive technology. There are two essential steps before this becomes possible. Firstly, more sophisticated molecular designs exploiting hydrogen bonding and other intramolecular effects must be developed, and secondly, these materials must be polymerised to form stable, self supporting materials. This work is already in progress, but it must be born in mind that some of the limitations of competing technologies are at the same time being overcome, making the demands for any new technology even greater.

The development and characterisation of chiral smectic C liquid crystal materials for nonlinear optical applications also illustrated the sensitivity of second harmonic generation as a useful and selective optical probe in ferroelectric liquid crystals. The selectivity of SHG to the c_2 axis of the molecules is almost unique, and has enabled measurement of the optical biaxiality of these materials with improved accuracy and measurement of the B_3 twist elastic constant of the c_2 axis with sufficient accuracy to question the definition of critical unwinding field strengths and the effects of surfaces.

Assessment of the interaction between the liquid crystal molecules and the aligning layers has previously been reported in nematic liquid crystals and monolayers of smectic C materials using SHG. From the insight of this study, an experiment has been proposed which may allow the selective probing of the surface layer of a bulk chiral smectic C material whilst the bulk is present but is not SHG active. This is an important measurement for evaluating ferroelectric materials and surface interactions in a conventional display geometry. Structural information about the organisation of the molecules through the cells may also be obtained from bulk measurements within different cell geometries. A number of different alignment geometries were assessed, with particular emphasis on a new cell geometry suitable for nonlinear optical devices which did not require in-plane electric fields to unwind the natural helix of chiral smectic C materials, but can be phase matched. This new and valuable role of second harmonic generation as an optical probe in chiral smectic C liquid crystal materials will provide new insight into this exceptional class of material and support a highly promising new display technology.

References.

- Allen S., Bone D.J., Carter N., Ryan T.G., Sampson R.B., (1991), in *Organic Materials for Non-linear Optics II*, R.A. Hann and D.Bloor, eds., R. Soc. Chem., London.
- Amano M., Haino T., Yamanoto F., Takeuchi Y., (1990), *Mol. Cryst. Liq. Cryst.*, **182A**, p81.
- Ashwell G., et al. (1992) *Poster at OMNO III*, Oxford, England.
- Baden J., Hiere R., Perigaud A., Zyss J., (1985), in *Nonlinear Optical Properties of Organic and Polymeris Materials* ed. D.J. Williams ACS Symp. Ser. vol 233 Washington D.C..
- Bierlein J.D., Cheng L.K., Wang Y., & Tam W., (1990), *Appl. Phys. Lett.*, **56**, p423.
- Bierlein J.D. & Vanherzeele H., (1989), *J. Opt. Soc. Am. B.*, **6**, p622.
- Born M. & Wolf E., (1980), *Principles of Optics* Pergamon Press, Oxford, 6th edition.
- Bouchaud P. et al, (1990), *Appl. Phys. Lett.*, **57**, p215.
- Brown A.J.W., Bowers M.S., Kangas K.W., Fisher C.H., (1992), *Optics Letters*, **17**, p109.
- Buka A., Siemensmeyer K., & Stegemeyer H., (1989), *Liquid Crystals*, **6**, p701.
- Carlsson T., Stewart I.W., & Leslie F.M., (1991), *Liquid Crystals*, **9**, p661.
- Clark N.A. & Lagerwall S.T., (1980), *Appl. Phys. Lett.*, **36**, p899.
- Cohen M.H. & Grest G.S., (1979), *Phys. Rev. B*, **20**, p1077.
- Dattagupta S., (1987), *Relaxation Phenomena in Condensed Matter Physics*. Academic Press.
- Donaldson A., (1991), *J. Phys. D: Appl. Phys.*, **24**, p785.
- Dorn R., Baums D., Kersten P. & Regener R., (1992), *Advanced Materials*, **4**, No 7/8, p464.
- Dunmur D.A. & Wilson D.R., (1989), *Mol. Sim.*, **4**, p37.
- Eich M., Reck B. et al, (1989), *J. Appl. Phys.*, **66**, p3241.
- Eich M., Sen A., Looser H., Bjorklund G.C., Swalen J.D., Twweig R., & Yoon D.Y., (1989), *J. Appl. Phys.*, **66**, p2559.
- Eldering C.A., Knoeson A., & Kowel S.T., (1991), *J. Appl. Phys.*, **69**, p3676.
- Elston S.J., (1991), *Liquid Crystals*, **9**, p769.
- Esselin S. et al., (1988), *SPIE Nonlinear Optical Properties of Organic Materials*, **971**, p120.
- Franken P.A., Hill A.E., Peters C.W. & Weinreich G., (1961), *Phys. Rev. Lett.*, **7**, p118.
- Furukawa K. et al, (1988), *Ferroelectrics*, **85**, p451.
- Griffith M.S., Worboys M.R., Davies N.A. & McDonnell D.G., (1991), in *Organic Materials for Non-linear Optics II*, Hann R.A. & Bloor D., eds, R. Soc. Chem., London.
- Haas D., (1992), *Oral presentation, Rand Prize Funds "Polymeric Materials for Electro-Optic Applications"*, Broadway, England.
- Hampsch H.L., Torkelson J.M., Bethke S.J., & Grubb S.G., (1990), *J. Appl. Phys.*, **67**, p1037.
- Havinga E.E., Vanpelt P., (1979), *Ber Bundsenges Phys. Chem.*, **83**, p816.
- Hewig G.H. & Jain K., (1983), *Optics Comms.*, **47**, p347.

- Hollinghurst J., Toyne K.J. & Goodby J.W., (1992), *Oral presentation, Rand Prize Funds "Polymeric Materials for Electro-Optic Applications", Broadway, England.*
- Huang G.F., Hwang M.Y., Chong S.W. & Lin J.T., (1991), *Optics Comms.*, **82**, p539.
- Ishigame Y., Suhara T. & Nishihara H., (1991), *Optics Letts.*, **16**, p375.
- Jeon H. et al., (1992), *Appl. Phys. Lett.*, **60**, p2045.
- Jerphagnon J. & Kurtz S.K., (1970), *J. Appl. Phys.*, **41**, p1667.
- Jones J.C., (1991), "*Optical and Dielectric Studies of Smectic C Liquid Crystals.*", PhD Thesis, University of Hull.
- Jones J.C., Personal communication, 1993.
- Jones J.C., Raynes E.P., Towler M., Sambles J.R., (1990), *Mol. Cryst. Liq. Cryst. Lett.*, **7**, p91.
- Jungbauer D., Rech B., Tweig R., Yoon D.J., Willson C.G. Swallen J.D., (1990), *Appl. Phys. Lett.*, **56**, p2610.
- Kajikawa K., Isozaki T., Takezoe H., Fukuda A., (1992), *Jpn. J. Appl. Phys.*, **31**, p679.
- Kaneko E., (1987), *Liquid Crystal TV Displays*, KTK Scientific Publishers, Tokyo.
- Khanarian G., Norwood R.A., Haas D., Feuer B. & Karim D., (1990), *Appl. Phys. Lett.*, **57**, p977.
- Kiode N., Ogura S., Aoyama Y., Amano M. & Kiano T., (1991), *Mol. Cryst. Liq. Cryst.*, **198**, p323.
- Kleinmann D.A., (1962), *Phys. Rev.*, **126**, p1977.
- Kobayashi S., Ishibashi S., Takahashi K., Tsuru S., Yamamoto F., (1993), *Adv. Materials*, **5**, p167.
- Kurata T., Fuchigami H., Koezuka H., Yamamoto T., Fukuda T., (1992), *Jpn. J. Appl. Phys.*, **31**, p3869.
- Kurtz S.K., Jerphagnon J., & Choy, (1979), in *Numerical Data and Functional Relationships in Science and Technology*, Landort & Bornstein, New York, p671.
- Kurtz H.A., Stewart, J.J.P., Dieter K.M., (1990), *J. Computational Chem.*, **11**, p82.
- Laidler K.J., & Meiser J.H., (1982), *Physical Chemistry*, Addison Wesley, California.
- Liu J.Y., Robinson M.G., Johnson K.M. & Doroski D. (1990), *Optics Letters*, **15**, p267.
- Liu J.Y., Robinson M.G., Walba, D.M. et al, (1991), *J. Appl. Phys.*, **70**, p3426.
- Maker P.D., Terhune R.W., Nisenoff M., Savage C.M., (1962), *Phys. Rev. Lett.*, **8**, p21.
- Man H.T., Chiang K., Haas D., Teng C.C., Yoon H.N., (1990), *SPIE vol. 1213 "Photopolymer Device Physics, Chemistry and Applications."*, p7.
- McL.Smith D.A. & Coles H.J., presented at ILCC, Pisa 1992, to be published in *Mol. Cryst. Liq. Cryst.*
- Meredith G.R., Van Dusen J.G. & Williams D.J., (1982), *Macromol*, **15**, p1385.
- Meredith G.R., Vandusen J. G., Williams D. J., (1985), in *Nonlinear Optical Properties of Organic and Polymeric Materials* ed by Williams D. J. ACS series Washington D.C..
- Meyer R.B., (1977), *Mol. Cryst. Liq. Cryst.*, **40**, p33.
- Midwinter J.E. & Warner J., (1965), *J. Appl. Phys.*, **16**, p1135.
- Milomi P.W. & Eberly J.H., (1988), *Lasers*, John Wiley & Sons, New York.

- Mohlmann G.R., van der Vorst C. P. J. M., (1989), in *Side Chain Liquid Crystal Polymers* ed by McArdle, C. B. Blackie, Glasgow.
- Nye J. F., (1964), *Physical Properties of Crystals* Oxford University Press, London.
- Ou Z.Y., Pereira S.F., Polzik E.S., Kimble H.J., (1992), *Optics Letters*, **17**, p640.
- Pikin S.A. & Osipov M.A., (1991), in *Ferroelectric Liquid Crystals*, Goodby J.W. et al, Gordon & Breach, Philadelphia.
- Prasad P.N. & Williams D.J., (1991), *Introduction to Nonlinear Optical Effects in Molecules and Polymers.*, John Wiley & Sons, New York.
- Pugh D., & Morley J.O., (1987), in *Nonlinear Optical Properties of Organic Molecules and Crystals Vol. 1.* eds. Chelma & Zyss, Academic Press, Orlando.
- Rao S.M., Batra A.K., Lal R.B., Evans R.A., Loo B.H., Metzger R.M., Lee W.J., (1991), *J. Appl. Phys.*, **70**, p6674.
- Rieker T.P., Clark N.A., Smith G.S., Parmar D.S., Sirota E.B. & Safinya C.R., (1987), *Phys. Rev. Lett.*, **59**, p2658.
- Rosenblatt C.S., (1978), "*A Light Scattering Study of Ferroelectric Thin Films.*", PhD thesis, Harvard University, p82.
- Rusch K.C. & Beck R.H., (1969), *J. Macromol. Sci.-Phys.*, **B3**, p365.
- Shen Y.R., (1984), *Introduction to Nonlinear Optics*, John Wiley & Sons, New York.
- Shen Y.R., Chen W., Feller M.B., Huang J.Y., Superfine R., (1991), *Mol. Cryst. Liq. Cryst.*, **207**, p77.
- Shytkov N.M., Barnik M.I., Blinov L.M. & Beresnev L.A., (1985), *Mol. Cryst. Liq. Cryst.*, **124**, p379.
- Singer K.D. & King L.A., (1991), *J. Appl. Phys.* **70**, p3251.
- Singer K.D., Kuzyk M.G., Holland W.R., Sohn J.E. & Lalama S.J., (1988), *Appl. Phys. Lett.*, **53**, p1800.
- Singer K.D., Kuzyk M.G. & Sohn J.E., (1987), *J. Opt. Soc. Am. B*, **46**, p968.
- Stamatoff J.B., Buckley A., East A.J., Goldberg H.A., Khanarian G., Norwood R.A., Sounik J.R., Teng C.C., (1991), in *Organic materials for Nonlinear Optics II*, ed. Bloor & Hann, RSoc. Chem., Cambridge.
- Sugihara O., Toda T., Ogura T., Kinoshita T. & Sasaki K., (1991), *Optics Letters*, **16**, p702.
- Swalen J.D., (1992), *Oral Presentation, Rank Prize Funds "Polymeric Materials for Electro-Optic Applications"*, Broadway, England.
- Taguchi A., Ouchi Y., Takezoe H. & Fukuda A., (1989), *Jpn. J. Appl. Phys.*, **28**, p997.
- Takezoe H., Kondo K., Miyasato K., Abe S., Tsuchiya T., Fukuda A. & Kuze E., (1984), *Ferroelectrics*, **58**, p55.
- Teng C.C. & Garito A.F., (1983), *Phys. Rev. B*, **28**, p6766.
- Twig R.J., Jain, K., Cheng, Y.Y., Crowley, J.I., & Azema, (1982), *A. Polym. prepr., Am. Chem. Soc. Div. Polym. Chem.*, **23**, p214.
- Valley J.F., Wu J.W. & Valencia C.L., (1990), *Appl. Phys. Lett.*, **57**, p1084.

- Walba D.M. et al., (1991A), *Ferroelectrics*, **121**, p247.
- Walba D.M., Ros M.B., Clark N.A., Shao R., Johnson K.M., Robinson M.G., Liu J.Y., Dorski D., (1991B), *Mol. Cryst. Liq. Cryst.*, **198**, p51.
- Williams G. & Watts D.C., (1970), *Trans. Faraday Soc.*, **66**, p80.
- Wilson D.R. & Dunmur D.A., (1989), *Liquid Crystals*, **5**, p486.
- Wu J.W., (1991), *J. Opt. Soc. Am. B*, **8**, p142.
- Yariv A., (1989), *Quantum Electronics*, J. Wiley & Sons, New York.
- Yariv A. (1985), *Optical Electronics*, CBS College Publishing, New York.
- Zeks B. & Blinc R., (1991), in *Ferroelectric Liquid Crystals*, Goodby J.W. et al, Gordon & Breach Science Publishers, Philadelphia.
- Zeks B., Carlsson T., Filipic C. & Urbanc B., (1988), *Ferroelectrics*, **84**, p3.
- Zyss et al, (1984), *J. Chem. Phys.*, **81**, p4160.
- Zyss J., (1988), in *Nonlinear Optical and Electroactive Polymers*, eds. Prasad & Ulrich, Plenum Press, New York.
- Zyss & Chelma, (1987), in *Nonlinear Optical Properties of Organic Molecules and Crystals*, Vol 1 eds. Chelma & Zyss, Academic Press Inc., Orlando.
- Zyss J. & Oudar J.L., (1982), *Phys. Rev. A*, **26**, p2028.

Appendix A.

A1 The Relationship between the Microscopic Hyperpolarisability and the Bulk Susceptibility.

The macroscopic second order susceptibility $\chi^{(2)}$ is related to the molecular hyperpolarisability β by

$$\chi_{ijk}^{(2)}(-\omega_3; \omega_1, \omega_2) = \frac{1}{V} f_i^{\omega_3} f_j^{\omega_1} f_k^{\omega_2} \sum_q a_{ji} a_{jk} a_{ki} \beta_{ijk}(-\omega_3; \omega_1, \omega_2) \quad 2.8$$

where there is a summation over all molecules q within the unit cell, V is the volume of the unit cell, f^ω are the local field factors and a_{ji} are the direction cosines of the molecular frame of reference xyz with respect to the bulk material frame XYZ. To simplify the form of $\chi^{(2)}$ a suitable symmetry group is applied which describes the symmetry of the bulk material.

The noncentrosymmetric point group ∞mm is applicable to systems which lack any positional ordering, but which contain a unique axis, about which there is infinitesimal rotation. This point group describes the poled nematic and smectic A liquid crystal systems, to which we will restrict the following arguments. The effect of applying the ∞mm point group on the tensor $\chi^{(2)}$ is to limit the number of non-zero components [Nye, (1964)] to four: χ_{333} , $\chi_{113} = \chi_{223}$, $\chi_{131} = \chi_{232}$, $\chi_{311} = \chi_{322}$. The superscript (2) is omitted for clarity.

There are a number of theoretical models for the electric field poling of hyperpolarisable molecules. These are the isotropic model, the Ising model [Meredith et al, (1985)], the Singer Kuzyk and Sohn model (SKS) [Singer et al, (1987)] and the Maier-Saupe model extended by van der Vorst and Pinken (MSVP) [Mohlmann & van der Vorst, (1989)]. The isotropic model assumes no preferential packing of molecules in a material, whereas the Ising model assumes molecules are cylindrical and pack perfectly to give an order parameter S equal to unity. The real life situation lies somewhere between the two models and can be described by either the SKS or MSVP models.

The SKS model utilises the axial order parameters $\langle P_2 \rangle$ and $\langle P_4 \rangle$ of the liquid crystalline host to describe the ordering and it is assumed they are insensitive to the applied field. The MSVP model is a self consistent calculation of the ordering of a system using three energy terms for the constituent molecules. These are the potential energy of a single molecule in a self ordering system described by $\langle P_2 \rangle$, the energy of the permanent dipole inside a field, and the energy of the induced dipole inside a field. The SKS and MSVP models give almost identical results for poled nematic systems, the only difference being the starting conditions. The SKS model requiring independent measurements of $\langle P_2 \rangle$ and $\langle P_4 \rangle$, and the MSVP model requiring the magnitude of the three energy terms. I shall concentrate on the SKS model.

A2 Calculation of the Orientational Ordering.

The bulk susceptibility of the material will be calculated for an orientated material at the elevated temperature at which the material was poled. When the material was cooled to lock in the induced alignment, the thermal disorder associated with the elevated temperature was also stored. It must be remembered that the energy associated with ordering is a combination of the short range intermolecular interaction as seen in nematic phases, and the externally applied field, which is comparable to the thermal energy kT . It is assumed that the molecular nonlinear optical properties were not significantly perturbed by the neighbouring molecules. The bulk susceptibility can then be described as the statistical average of the molecular hyperpolarisability

$$\chi_{IJK}(-\omega_3; \omega_1, \omega_2) = N \langle \beta_{ijk}^*(-\omega_3; \omega_1, \omega_2) \rangle_{IJK} \quad A2$$

where N is the number density of the nonlinear optical molecules and β_{ijk}^* is the hyperpolarisability including local field effects. The molecular and bulk coordinate systems are related by the Euler angles φ , θ , and ψ , which can be transformed using the matrix \mathbf{a}

$$\mathbf{a} = \begin{pmatrix} \cos \theta \cos \varphi \cos \psi - \sin \varphi \sin \psi & \cos \theta \sin \varphi \cos \psi - \cos \varphi \sin \psi & -\sin \theta \cos \psi \\ -\cos \theta \cos \varphi \sin \psi - \sin \varphi \cos \psi & -\cos \theta \sin \varphi \sin \psi - \cos \varphi \cos \psi & \sin \theta \sin \psi \\ \sin \theta \cos \varphi & \sin \theta \sin \varphi & \sin \theta \end{pmatrix}.$$

The orientational average of the hyperpolarisabilities in the presence of a poling field E_p is of the form

$$\langle \beta_{ijk}^* \rangle_{IJK} = \int d\Omega a_{ii} a_{jj} a_{kk} G(\Omega, E_p) \beta_{ijk}^* \quad A3$$

where the volume element is given by

$$\int d\Omega = \int_0^{2\pi} d\varphi \int_0^{2\pi} d\psi \int_{-1}^{+1} d(\cos \theta) \quad A4$$

and $G(\Omega, E_p)$ is a distribution function. If the poling field couples with the molecular dipole moment m^* which has been corrected for local field factors, and U describes the short range interaction potential between molecules which is significant in liquid crystal phases, then $G(\Omega, E_p)$ is described by

$$G(\Omega, E_p) = \frac{\exp\left[\frac{-1}{kT}(U - m^* \cdot E_p)\right]}{\int d\Omega \exp\left[\frac{-1}{kT}(U - m^* \cdot E_p)\right]} \quad A5$$

It is assumed the molecular interactions described by the potential U are only dependent on θ for materials with uniaxial symmetry, and it is noted that U does not distinguish between alignment parallel or

antiparallel with respect to the director n . In the case where the interaction between the applied field and the molecular dipole is smaller than the thermal energy, then the exponential can be expanded to

$$\exp\left[-(U - m^* \cdot E_p / kT)\right] \approx \left[1 + (m^* \cdot E_p) / kT\right] \exp[-U/kT]$$

The function $G(\Omega, E_p)$ can be expanded in terms of Legendre polynomials

$$G(\theta, E_p) = \sum_{i=0}^{\infty} \frac{2i+1}{2} A_i P_i(\cos \theta) \quad \text{A6}$$

with

$$A_i = \int_{-1}^{+1} d(\cos \theta) G(\theta, E_p) P_i(\cos \theta).$$

The A_i are the orientational average of P_i , denoted $\langle P_i \rangle$, and are defined as the microscopic order parameters. It is assumed that $\langle P_i \rangle$ can be independently measured. The product of the transformation components and the distribution function shown in equation A3 can also be expanded in Legendre polynomials. Integrating this over φ and ψ , within the limits from A4, then the macroscopic second order susceptibility becomes

$$\chi_{ijk} = \frac{NE_p}{kT} \left[u_{ijk}^{(0)} + u_{ijk}^{(2)} \langle P_2 \rangle + u_{ijk}^{(4)} \langle P_4 \rangle \right] \quad \text{A7}$$

where the order parameter coefficients are expressed in terms of the molecular hyperpolarisability b_{ijk}^* and the molecular dipole moments μ_{ijk}^* . Singer et al [1987] describe the full expansion of $u^{(l)}$ for all components allowed within the ∞mm symmetry.

Physical insight can be gained by considering the simplified situation of a one dimensional molecule, where only β_{zzz}^* and μ_z^* are nonzero. This approximation is not unreasonable for the rod shaped molecular systems likely to be encountered. Equation A6 can be written

$$\chi_{333} = \frac{NE_p}{kT} \beta_{zzz}^* m_z^* \left[\frac{1}{5} + \frac{4}{7} \langle P_2 \rangle + \frac{8}{35} \langle P_4 \rangle \right] \quad \text{A8}$$

and

$$\chi_{113} = \chi_{131} = \chi_{311} = \frac{NE_p}{kT} \beta_{zzz}^* m_z^* \left[\frac{1}{15} + \frac{1}{21} \langle P_2 \rangle - \frac{4}{35} \langle P_4 \rangle \right]. \quad \text{A9}$$

The local field factor can be isolated in this approximation as

$$\beta_{zzz}^* (-\omega_3; \omega_1, \omega_2) \cdot m_z^* = f^{\omega_3} f^{\omega_1} f^{\omega_2} f^0 \beta_{zzz} (-\omega_3; \omega_1, \omega_2) \mu_z \quad \text{A10}$$

where μ_z is the molecular dipole moment. The local field factors have been discussed in section 2.3 for the particular case of liquid crystal materials using the long thin cylinder approximation for molecules. In

the isotropic phase the local fields at optical frequencies can be described by the Lorenz- Lorentz expression

$$f^w = (n_w^2 + 2)/3$$

but in the case of liquid crystal materials, the equation must be modified to take into account the shape of the molecules and the difficulty in reorienting these molecules. The equation

$$f_{I\omega} = 1 + (n_\omega^2 - 1)L_I \quad I=1,2,3$$

where $L_1+L_2=1/2$ and $L_3=0$ has been found to be a good approximation. The dipole in the presence of the local poling field can be described by the Onsager expression

$$f^o = \frac{\epsilon(n_\infty^2 + 2)}{n_\infty^2 + 2\epsilon}$$

where ϵ is the d.c. field dielectric constant and n_∞ is the optical refractive indices.

In an isotropic system $\langle P_2 \rangle$ and $\langle P_4 \rangle \rightarrow 0$ and so equations A8 and A9 give the nonlinear susceptibilities as

$$\chi_{333} \approx \frac{NFE_p}{kT} \beta_{zz} \mu_z \frac{1}{5}$$

$$\chi_{113} \approx \frac{NFE_p}{kT} \beta_{zz} \mu_z \frac{1}{15}$$

where the local field factors are collected under a common term F. The nonlinear susceptibility along the poling direction is a factor of three higher than the transverse component. It is also assumed that the poling field is small in the condition $\mu E < kT$ so that there is no induced order in the material to significantly increase $\langle P_2 \rangle$ and $\langle P_4 \rangle$. This is known as the low field approximation.

For a perfectly ordered system (the Ising limit) then $\langle P_2 \rangle$ and $\langle P_4 \rangle \rightarrow 1$ and equations A8 and A9 become

$$\chi_{333} \approx \frac{NFE_p}{kT} \beta_{zz} \mu_z$$

$$\chi_{113} = 0.$$

The potential for a fivefold increase in the susceptibility along the poling direction exists if one moves from an isotropic system to a perfectly ordered system. Of course liquid crystal phases are not perfectly ordered - in a typical nematic phase $\langle P_2 \rangle \approx 0.6$ and $\langle P_4 \rangle \approx 0.25$ which gives approximately a three fold increase in $\chi^{(2)}$. For more highly ordered smectic phases then $\langle P_2 \rangle \approx 0.9$ and $\langle P_4 \rangle \approx 0.8$ giving an increase of 4.5.

References.

Nye J. F., (1964), *Physical Properties of Crystals*, Oxford University Press, London .

Meredith G.R., Vandusen J. G., Williams D. J., (1985), in *Nonlinear Optical Properties of Organic and Polymeric Materials*, ed. Williams D. J., ACS series, Washington D.C..

Singer K. D., Kuzyk M. G., Sohn J. E., (1987), *J. Opt. Soc. Am. B*, **4**, p968.

Mohlmann G.R., van der Vorst C. P. J. M., (1989), in *Side Chain Liquid Crystal Polymers*, ed McArdle, C. B. Blackie, Glasgow.

Appendix B.

Theory for Electro-Optic Experiment.

Consider a uniaxial material which is aligned homeotropically in a glass cell of thickness h . The material has an optic axis defined by the extraordinary refractive index n_e and an ordinary refractive index n_o . Light was introduced into the material at an angle θ_x to the normal of the cell along a direction defined by the unit vector s . Figure 2.2 shows the refractive index ellipsoid for the material and defines axes. Refraction must also be taken into account at the boundaries of the cell structure, and so from Snell's Law

$$n_x(\theta_x) \sin \theta_x = \sin i \quad \text{B1}$$

$$n_o \sin \phi_o = \sin i \quad \text{B2}$$

where $n_x(\theta_x)$ is the refractive index seen by the extraordinary ray at an angle θ_x from the optic axis, θ_x is the angle of refraction for the extraordinary ray, ϕ_o is the angle of refraction for the ordinary ray, and i is the angle of incidence at the cell surface.

Eliminating n_x from equations B1 and B2 gives

$$\tan \theta_x = \frac{n_e \sin i}{n_o (n_e^2 - \sin^2 i)^{1/2}}. \quad \text{B3}$$

From *Principles of Optics* Born and Wolf p697, the phase delay between the extraordinary ray and ordinary ray, after travelling through a uniaxial material of thickness h , when light is incident at an angle i , is

$$\delta = \frac{2\pi h}{\lambda} (n_x \cos \theta_x - n_o \cos \phi). \quad \text{B4}$$

If the phase delay is increased up to $\pi/2$ by including a Babinet Soleil compensator, so that the resultant light is circularly polarised, then the extra phase delay introduced Δ is given by

$$\delta + \Delta = \pi/2. \quad \text{B5}$$

Eliminating θ_x and rearranging for n_e gives

$$n_e = \frac{\sin i}{\left[1 - \frac{1}{n_o^2} \left(\frac{\delta \lambda}{2\pi h} + n_o \cos \phi_o \right)^2 \right]^{1/2}}. \quad \text{B6}$$

Using equation B2 to eliminate ϕ_o gives

$$\delta_v = \frac{\pi r_{eff} n_o V_s}{\lambda} \left(1 - \frac{\sin^2 i}{n_e^2} \right)^{-1/2} \sin^2 i . \quad \text{B14}$$

The experiment was designed so that plane polarised light is coupled into its orthogonal component by using the sample and Babinet Soleil compensator as a quarter wave plate combination. Any small modulation in the retardation of one component can then be converted into an intensity variation by using a polariser.

The fraction of light coupled into the orthogonal polarisation, T , is

$$T = \sin^2 \left(\frac{\delta + \Delta}{2} \right). \quad \text{B15}$$

Differentiating with respect to δ gives

$$\frac{\partial T}{\partial \delta} = \frac{\sin(\delta + \Delta)}{2}. \quad \text{B16}$$

The experiment was arranged to have circularly polarised light out when the light source is linearly polarised light at an angle of 45° to the vertical. From equation B5, $T=0.5$ and equation B16 is also equal to 0.5. For small modulations, then

$$\frac{\partial T}{T} = \frac{V_m}{V_a} = \delta_v. \quad \text{B17}$$

The modulation amplitude from the detector was measured using a lock-in amplifier. This was calibrated against a known signal to obtain the conversion factor to give peak to peak (ptp) values. Rearranging equation B14 and substituting equation B17 gives

$$r_{eff} = \frac{\lambda}{\pi n_o V_s \sin^2 i} \frac{V_m}{V_a} \left(1 - \frac{\sin^2 i}{n_e^2} \right)^{1/2}. \quad \text{B18}$$